Technische Universität München

Institut für Organische Chemie und Biochemie

Targeting the p53-MDM2 and p53-MDMX interaction as a therapeutic strategy for anticancer treatment

Siglinde Guillermina Morelia Wolf

Vollständiger Abdruck der von der Fakultät für Chemie der Technischen Universität München zur Erlangung des akademischen Grades eines

Doktors der Naturwissenschaften

genehmigte Dissertation.

Vorsitzender:	Univ.-Prof. Dr. St. J. Glaser
Prüfer der Dissertation:	1. Apl. Prof. Dr. Dr. h.c. R. Huber (i.R.)
	2. Univ.-Prof. Dr. M. Groll

Die Dissertation wurde am 09.02.2012 bei der Technischen Universität München eingereicht und durch die Fakulät für Chemie am 18.06.2012 angenommen.

Corpora non agunt nisi fixata

„A substance will not work unless it is bound“

Paul Ehrlich (1913)

For Victor and my parents

Acknowledgements

I want to thank Prof. Dr. Robert Huber for being my Ph.D. supervisor, Prof. Dr. Groll and Dr. Glaser for being my second assessor and chairman, respectively.

I also want to thank Prof. Alexander Doemling and his students for the fruitful cooperation on the development of p53-MDM2/X antagonists.

I want to thank all my Max-Planck family:

- My boss and supervisor Prof. Tad Holak, who gave me the opportunity to work in his group, his always open manner, his advises and the long and funny conversations.

- All my lab-colleagues: Kaja, Weronka, Michal, Grzegorz, Arkadiusz, Sohee and Ola for the great conversations and the funny evenings in the glasshouse. Especially I want to thank Ania, Tomek and Marcelino for all their support.

- All the other Max-Planckos, especially to Valeria, Sandrita, Ganesh, Vaibhao, Johannes and Igor for the great talks and the awesome evenings playing Volleyball.

Very special thanks go to all my family (Wolf, Torres and Gomezes):

- I want to thank my cousin Maya for awaking my interest in science in my early ages. Her dedication to science was a big inspiration for me.

- Most of all I want to thank my Mom and Dad for all their support, advices and help throughout my whole life but most importantly for their never ending love and faith in me.

- I want to express my love and gratitude to my beloved husband Victor, who never stopped encouraging and supporting me in all possible ways but mostly with his love and affection.

Publications

Publications describing the work discussed in the Dissertation:

- M. Bista, **S. Wolf**, K. Khoury, Y. Huang, M. Castro, K. Kowalska, A. Dömling, T.A. Holak and G.M. Popowicz, Discovery of an unusually ligand-induced binding pocket in MDM2. *In preparation*.

- **S. Wolf**, Y. Huang, G.M. Popowicz, S. Goda, T.A. Holak, A. Dömling: Ugi Multicomponent Reaction Derived p53-Mdm2 Antagonists. *In preparation*.

- W. Wang, C. Haiping, **S. Wolf**, C. Camacho, T.A. Holak, A. Dömling, Benzimidazol-2-one: A Novel Anchoring Principle for Antagonizing p53-MDM2. Bioorg Med Chem., *In press*.

- D. Koes, K. Khoury, Y. Huang, W. Wang, M. Bista, G.M. Popowicz, **S. Wolf**, T.A. Holak, A. Dömling, C. Camacho: Enabling large-scale design, synthesis and validation of small molecule protein-protein antagonists. *PLoS One* 2012, 7(3): e32839.

- Y. Huang, **S. Wolf**, D. Koes, G.M. Popowicz, C. Camacho, T.A. Holak, A. Dömling: Exhaustive Fluorine Scanning toward Potent p53-Mdm2 Antagonists. *ChemMedChem* 2012, 7:49-50.

- A. Czarna, B. Beck, S. Srivastava, G.M. Popowicz, **S. Wolf**, Y. Huang, M. Bista, T.A. Holak, A. Dömling: Robust generation of lead compounds for protein-protein interactions by computational and MCR chemistry: p53/Hdm2 antagonists. *Angew Chem Int Ed Engl* 2010, 49:5352-6.

- Y. Huang, **S. Wolf**, M. Bista, L. Meireles, C. Camacho, T.A. Holak, A. Dömling: 1,4-Thienodiazepine-2,5-diones via MCR (I): synthesis, virtual space and p53-Mdm2 activity. *Chem Biol Drug Des* 2010, 76:116-29.

- G.M. Popowicz, A. Czarna, **S. Wolf**, K. Wang, W. Wang, A. Dömling, T.A. Holak: Structures of low molecular weight inhibitors bound to MDMX and MDM2 reveal new approaches for p53-MDMX/MDM2 antagonist drug discovery. *Cell Cycle* 2010, 9:1104-11.

- A. Czarna, G.M. Popowicz, A. Pecak, **S. Wolf**, G. Dubin, T.A. Holak: High affinity interaction of the p53 peptide-analogue with human Mdm2 and Mdmx. *Cell Cycle* 2009, 8:1176-84.

Table of Contents

1. Introduction

1.1. The cell cycle and the role of p53

The cell cycle is the essential mechanism which regulates the cell proliferation in all living organisms. The detail of the mechanism varies between organisms, but the core mechanism by which the genetic information is passed to the next generation stays the same. The sequence of stages in the cell cycle is outlined in Figure 1. In S-phase the chromosomes are been duplicated. Chromosome segregation and cell division occur in the M-phase. Between M- and S-phases and between S- and M-phases are the G1- and G2-phases, respectively. These two Gap-phases, not only provide the cell with more time for cell growth, but more importantly, they provide time for monitoring the internal and external environment to ensure that the conditions are suitable and preparations are complete before committing itself to major upheavals of the S-phase and mitosis. Especially the G1-phase is important in this respect. The switches are generally binary and launch events in a complete and irreversible fashion. And only if the previous process finished successfully, subsequent processes can take place. The control mechanisms monitor the correct progression (chronologically and statically) and the coordination within the cell cycle and the correction of errors. The stages at which the cell cycle is controlled are called checkpoints (Hartwell, L.H. *et al.*, 1989). If extracellular conditions are unfavorable, the cells can delay their progress in the G_1-phase or they can arrest in the specialized resting state G_0, in which they can remain even for years before resuming proliferation. However, if extracellular conditions are favorable and growth- and division-signals are present, the cells in early G1- or G0-phases will progress through the first checkpoint, the so-called restriction point at the end of the G1-phase. Reaching this state the cell is committed to DNA replication. In case of DNA damage the G1 checkpoint will lead cell cycle arrest, ensuring that the DNA damage is not replicated during the S-phase. In response to damaged and/or unreplicated DNA the G2 checkpoint leads also to cell cycle arrest ensuring the proper completion of S-phase. The M-checkpoint leads to the arrest of chromosomal segregation in response to misalignment on the mitotic spindle.

The arrest of the cell cycle at these checkpoints allows for (i) the cell to repair cellular damage, (ii) external stress signals to disappear or (iii) essential growth factors, hormones, or nutrients to appear. If the damage cannot be repaired properly, the checkpoint will give a signal leading to apoptosis. Defects in cell cycle checkpoints can result in gene mutations, chromosome damage, and aneuploidy, all of which can contribute to tumorgenesis (Paulovich, A.G. *et al.*, 1997).

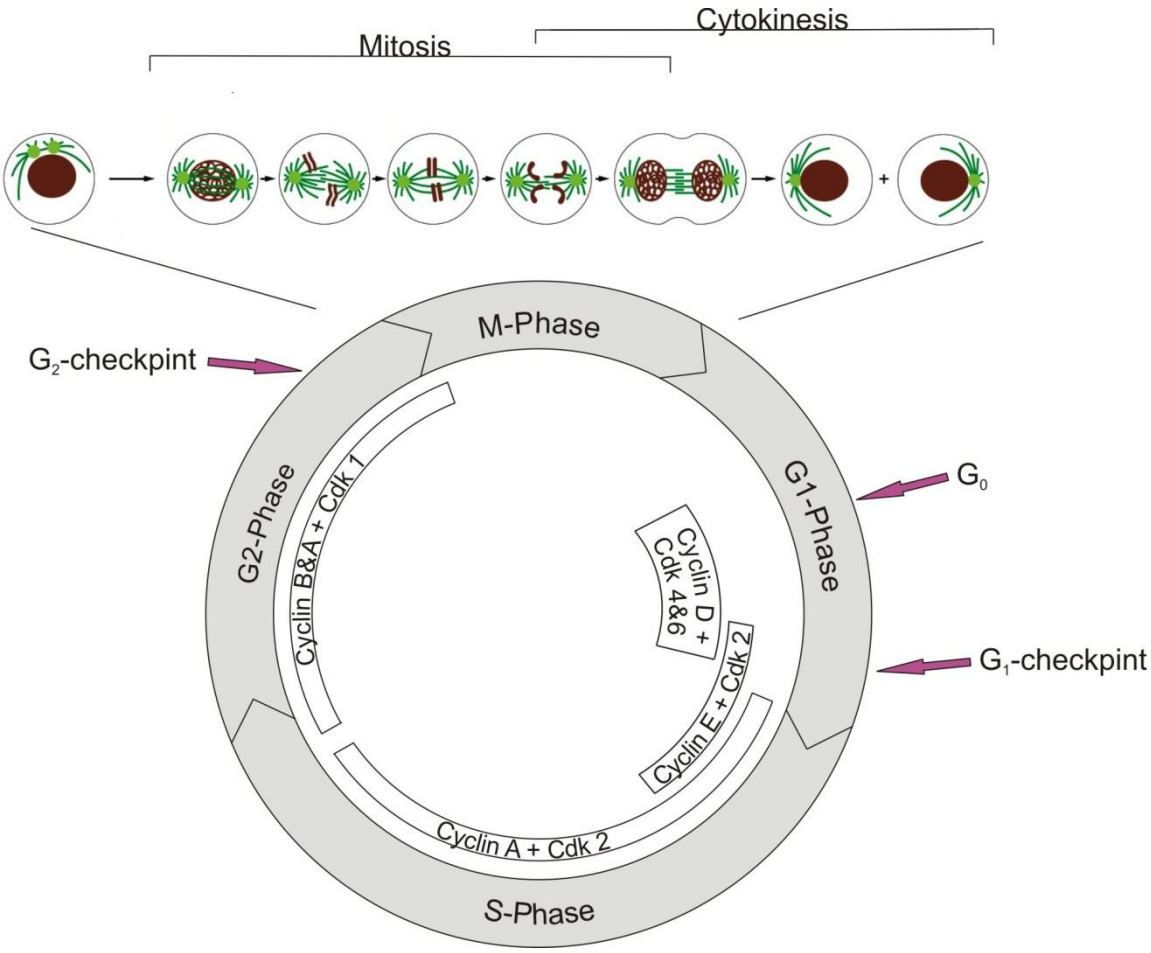

Figure 1. A schematic representation of the generic cell cycle. Picture modified from Alberts, B. *et al.*, 2008.

The cell cycle is carefully monitored by cyclin dependent kinases (Cdks) (Xiong, Y., 1996). The activity of the Cdks is in turn controlled by cyclins, regulatory proteins whose protein level changes in a cyclical manner. Only the cyclin-Cdk complex is able to trigger cell-cycle events. The Cdk activity is also regulated by two families of inhibitors: p16ink4a and p21 and the phosphorylation and dephosphorylation of Cdks. In addition, the master regulator and the “so-called” guardian of the genome is p53. This transcription factor mediates the G1/S cell cycle checkpoint and is

necessary for maintaining a G2 arrest: Cells in the G1-phase that are exposed to genotoxic agents activate p53, which then transcriptionally up-regulates the Cdk inhibitor p21 (el-Deiry, W.S. *et al.*, 1993). p21 inactivates the cyclin-Cdk complexes and binds to the proliferating cell nuclear antigen (PCNA), which inhibits the elongation step in the DNA replication (Waga, S. *et al.*, 1994; Waga, S. *et al.*, 1998).

Cells that have incurred DNA damage in previous phases, or have not correctly completed the S-phase will arrest at the G2 checkpoint before entering the M-phase. The DNA damage activates either of two kinases ATR or ATM. These phosphorylate and activate the Chk1 and Chk2 kinases, respectively, which inactivate Cdc25 responsible for activating Cdks. ATM and ATR also directly phosphorylate human p53 (Banin, S. *et al.*, 1998; Canman, C.E. *et al.*, 1998; Hall-Jackson, C.A. *et al.*, 1999; Tibbetts, R.S. *et al.*, 1999). It was also shown that Chk1 and Chk2 mediate phosphorylation and stabilization of p53 after DNA damage (Chehab, N.H. *et al.*, 2000; Hirao, A. *et al.*, 2000; Shieh, S.Y. *et al.*, 2000). A more detailed role of p53 signaling at the G2 checkpoint is still not well understood.

1.2. Structure of the p53 protein

The human *p53* gene, located on chromosome 17p13, contains 11 exons that encode a 393 amino acid long and 53 kDa heavy transcription factor. The active p53 protein is a homotetramer. The tetramerization and core domains are folded and are flanked by intrinsically disordered domains at the N- and C- termini (Figure 3) (Wells, M. *et al.*, 2008).

The protein is divided into seven domains (Figure 2). Each domain playing an essential role in the regulation of p53 functions. The transactivation domain I of p53 becomes fully helical upon binding MDM2 (Wells, M. *et al.*, 2008). The intrinsically disorder of the transactivation domain is possibly an essential structural feature that facilitates promiscuous binding to many partner proteins, for example, the transcription machinery, enhancers and many other proteins that regulate the ability of p53 to function as a transcription factor (Fields, S. *et al.*, 1990), and may also be a feature to be readily accessible for posttranslational modification that modulates binding. (Wells, M. *et al.*, 2008).

The proline rich domain exhibits enhanced stiffness relative to the transactivation domain, projecting the transactivation domain away from the surface of the p53 protein (Wells, M. *et al.*, 2008). Toledo *et al.* (2007a) suggest that the proline rich domain has a predominantly structural role, while (Walker, K.K. *et al.*, 1996) suggest, that this domain is necessary for an efficient p53-mediated growth suppression, dictating p53 specificity for transcriptional activation of downstream genes (Venot, C. *et al.*, 1998).

The p53 tetramer binds to a DNA response element consisting of two copies of the 10 base pair motif 5'-PuPuPuC(A/T)(T/A)GPyPyPy-3' separated by 0-13 base pairs (Pu stands for purine, Py for pyrimidine). Eight of the ten bases are degenerated, which may account for the selective activation of the downstream targets of the stimuli. The human genome is estimated to contain 200-300 p53 consensus sites (el-Deiry, W.S. *et al.*, 1992).

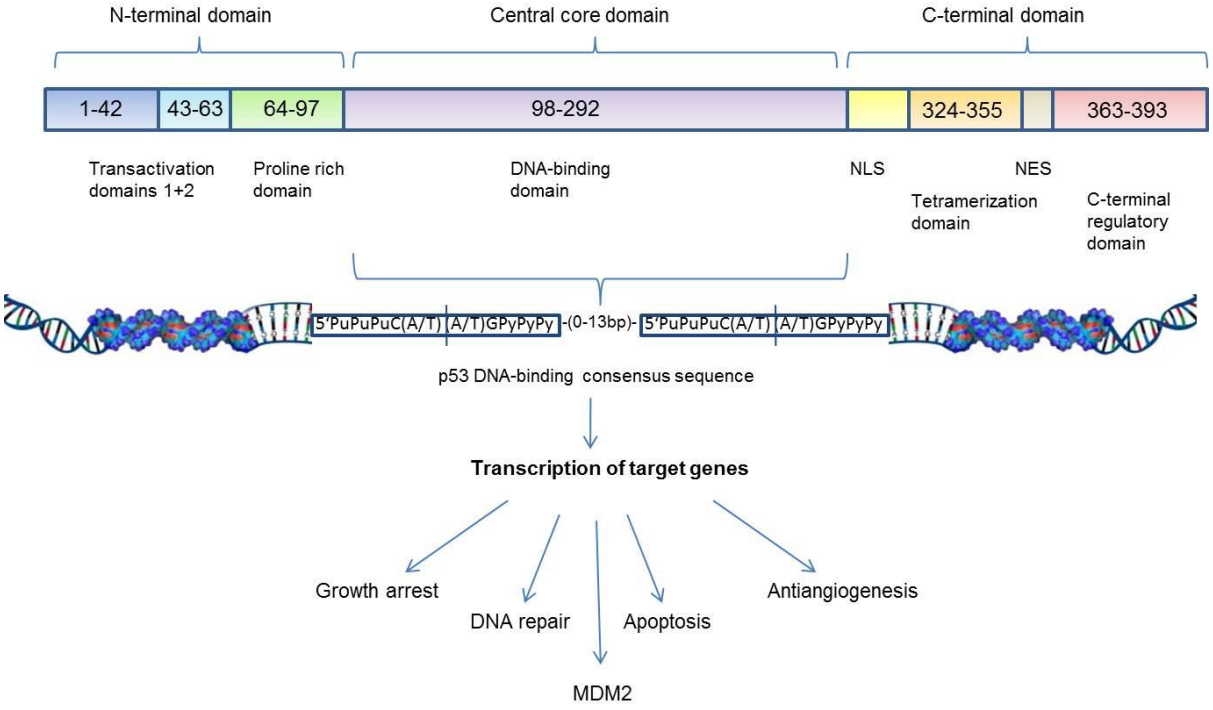

Figure 2. Scematic representation of the primary structure of p53 and the DNA binding site for p53.

The carboxy-terminal domain of p53 contains a nuclear localization signal, an oligomerization domain, a nuclear export signal and a regulatory domain. The nuclear localization and nuclear export signals regulate the subcellular localization of p53 (Oliner, J.D. *et al.*, 1993). The oligomerization domain is an amphipathic helix

that permits p53 to form transcriptionally active homodimers or homotetramers (Sturzbecher, H.W. *et al.*, 1992; Pietenpol, J.A. *et al.*, 1994). Tetramerization of p53 masks the nuclear export to the cytoplasm where it is subject to degradation (Stommel, J.M. *et al.*, 1999).

The C-terminal domain of p53 is subjected to extensive posttranslational modifications, including acetylation, ubiquitination, phosphorylation, sumoylation, methylation, and neddylation, that regulate p53 function and cellular protein levels. The function of the C-terminus and the role of individual modifications are only partly understood, and there is some controversy in the literature with regard to their exact role in vivo.

1.3. Quaternary structure of p53

The structure determination of p53 was difficult to solve because of its low solubility, its tendency to aggregate and its property of having a mixture of ordered and disordered domains. The combination of X-ray, NMR, SAXS, and electron microscopy data, leaded to the following quaternary p53 structure model. The free p53 protein in solution forms an elongated cross-shaped tetramer (Figure 3a). The core domain dimers are only loosely coupled and thus can interact with regulatory proteins. The N- and C-termini are extended and flexible, which is consistent with their biological functions. Upon DNA binding, p53 wraps around the DNA helix (Figure 3b). This process is facilitated by the flexible linker between the core and tetramerization domain, and the overall structure becomes more rigid (Joerger, A.C. *et al.*, 2008). Four p53 core domains bind to DNA, with one symmetrical core domain dimer bound to each DNA half site (superdomain I). The tetramerization domain (superdomain II) is located on the distal site of the core domain DNA complex. According to Joerger and Fershts model (Joerger, A.C. *et al.*, 2008) the two superdomains are only loosely connected, allowing relative change in their orientation depending on the presence of additional protein binding partners. The flexible linker region between the two folded domains contains a bipartite basic nuclear localization signal, which is accessible in both the DNA-free and DNA-bound form. In contrast, one of the two Leucine-rich nuclear export signals is concealed

within the tetramerization domain, thus requiring dissociation of the tetramer as part of the recognition process involved in nuclear export. The N-termini are extended in both the free and DNA-bound p53 models, in agreement with the facts that they are targeted by a myriad of signaling proteins and subject to extensive posttranslational modifications. Apart from providing binding promiscuity, the natively unfolded regions in p53 also provide flexible linkers to allow for structural reorganization upon formation of higher-order complexes. All four N-termini point away from one face of the core domain-DNA complex.

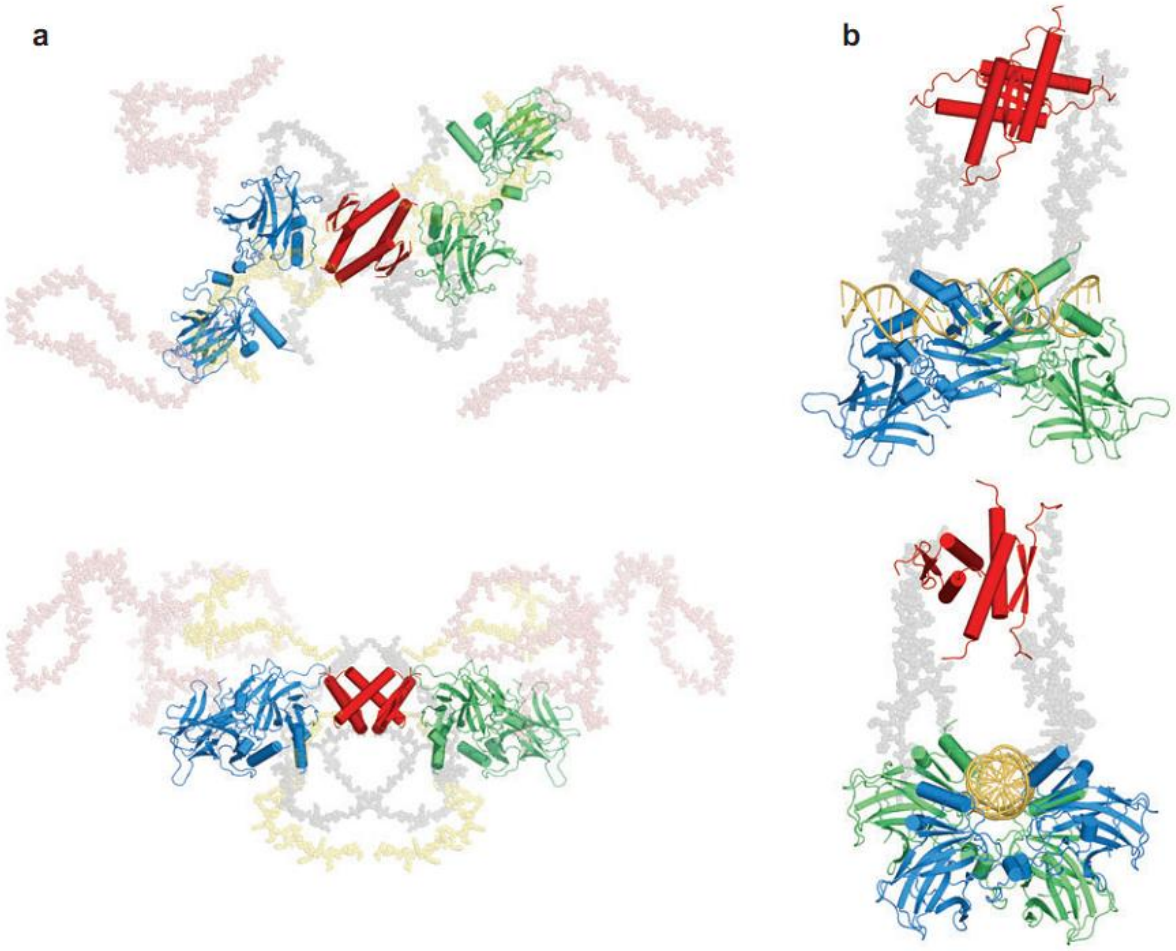

Figure 3. Rigid body models of free **(a)** and DNA-bound **(b)** p53 in solution from small-angleX-ray scattering data. Both models are shown in two different orientations. Core and tetramerization domains are shown as cartoon representations, with core domains binding to the half-site in the same color. Flexible connecting linkers (gray), N-termini (pink), and C-termini (yellow) are shown as semitransparent space-filled models. Models of N- and C-termini in the free protein are approximations to illustrate the space occupied by these flexible regions, rather than representing defined conformations (Joerger, A.C. *et al.*, 2008).

1.4. The p53 pathway

At the absence of cellular stress low levels of p53 induce antioxidant activity, which decreases the levels of reactive oxygen species (ROS) and subsequent DNA damage (Sablina, A.A. *et al.*, 2005). The low p53 level is regulated at the level of protein degradation, carried out by COP1, PIRH2, JNK, MDMX and the pivotal p53 regulator MDM2 (Wang, L. *et al.*, 2011). In normal cells most of the negative regulator genes are up-regulated by p53, leading to an auto regulatory feedback loop, that will keep the p53 level very low.

In case of cell stress, DNA damage, or oncogene activation, different pathways are induced that prevent p53 degradation by MDM2. The main proteins that are involved in the stress signal cascade are the Kinases ATM and ATR. ATM is phosphorylated under stress and phosphorylates p53, MDM2 and MDMX amongst others. The phosphorylation of these proteins leads to an active p53 protein, with a reduced affinity for MDM2 and MDMX. Additionally it inhibits the nuclear export of p53. In MDM2 and MDMX the phosphorylation leads to a rapid degradation of these proteins, a reduced affinity for p53 and a lost in their ability to inhibit p53. Kinase ARF stabilizes p53 by sequestering MDM2 in the nucleus, thus inhibiting the E3-ligase activity of MDM2 and by blocking its nuclear export (Perry, M.E., 2010).

A plethora of proteins have been found to bind and regulate the specificity of p53. Some proteins function as coactivators, others appear to dictate the nature of p53´s downstream response, determining whether p53 induces a cell cycle arrest, DNA repair, apoptosis, or inhibition of angiogenesis (Braithwaite, A.W. *et al.*, 2006). In order to induce programmed cell death, it is necessary that the p53-dependent apoptotic target genes activate apoptotic pathways in parallel (Burns, T.F. *et al.*, 1999). Due to the central role of p53 as guardian of the genome, mutations in the p53-pathway are linked to tumor formation. Cells lacking p53 show a high incidence of tumor development. The Li-Fraumeni cancer susceptibility syndrome for example, is an autosomal dominant hereditary disorder caused by a germ line mutation of one of the p53 allele. About 50% of all human cancers are derived from mutations in the *p53* gene. Most of these mutations are missense mutations, specially six codons located in the DNA binding domain are affected and are therefore referred to as “hotspots”. In the other ~50% of human cancers the wildtype p53 protein is

expressed, but it is inactivated by deregulations in the p53 pathway, mostly by overexpression of its negative regulators MDM2 and MDMX.

1.5. MDM2 and MDMX

MDM2 and MDMX have been studied intensively because of its association with p53 and its implication in human cancer. Mice lacking the *MDM2* or the *MDMX g*ene die during embryogenesis. However, mice lacking both the *p53* and *MDM2* gene are viable as with the *p53* and *MDMX* gene loss (Jones, S.N. *et al.*, 1995) (Parant, J. *et al.*, 2001). It is therefore indispensable to understand the role of MDM2 and MDMX in the p53 pathway.

The *MDM2* gene possesses two promoters, which trigger the expression of different types of MDM2 proteins. Additionally several MDM2 variants are generated by alternative splicing. Some of these short MDM2 splice products functions as negative MDM2 regulators, inhibiting the function of the full-length MDM2 protein and thus activating the p53 activity.

The 491 and 490 amino acid long full-length human MDM2 and MDMX protein, respectively, are structurally related (Figure 4). The N-terminal p53 binding domain binds p53 at the amino terminal transactivation domain of p53 and is well conserved in both proteins, especially the residues required for the interaction with p53 (Shvarts, A. *et al.*, 1996). Conversely, the same residues in p53 are required for both MDM2/p53 and MDMX/p53 interactions (Bottger, V. *et al.*, 1999). The RING finger is a conserved region located at the C-terminal end of both proteins, essential for the heterodimerization of MDM2 and MDMX or homodimerization of MDM2 (Sharp, D.A. *et al.*, 1999; Tanimura, S. *et al.*, 1999). Unlike MDMX, MDM2 also possesses a E3-ligase activity present in Ring finger domain . Both proteins possess a Zinc-finger domain with unknown function. A central acidic domain, with a high content of acidic amino acids, is present in both proteins, although no significant similarity between these two domains is observed (Marine, J.C. *et al.*, 2005). A nuclear localization signal is present in the RING domain of both proteins. Additionally, MDM2 possesses a nuclear localization and a nuclear export signal, responsible for shuttling MDM2 back and forth between the cytoplasm and the nucleus. Last two

domains are not found in MDMX, suggesting that the subcellular localization of MDMX is determined by interaction with other proteins, like MDM2 (Marine, J.C. *et al.*, 2004). This theory is supported by the fact, that MDM2 is primary acetylated in the RING finger domain, particularly on the two lysines K466 and K467, localized within the NLS and which modification affects the cellular distribution, while in MDMX these residues are not conserved Marine, J.C. *et al.*, 2004).

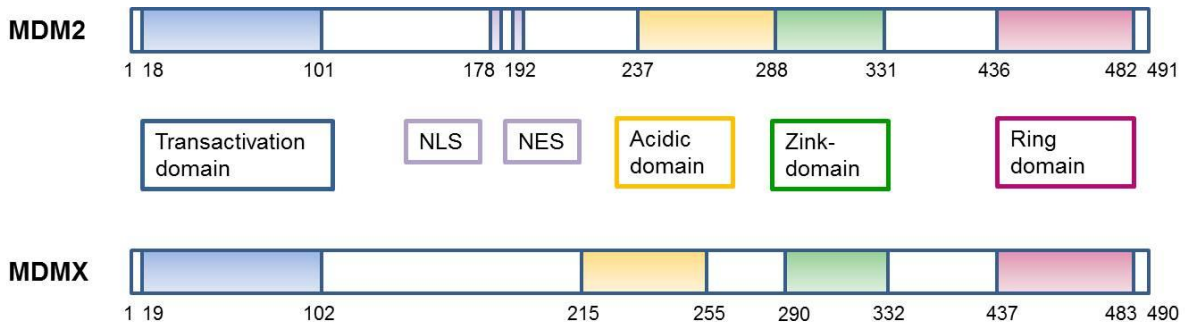

Figure 4. Scematic representation of the primary structure of the MDM2 and the MDMX proteins.

Studies indicate that MDM2 and MDMX have distinct but complementary roles in p53 regulation: MDM2 mainly regulates p53 stability, while MDMX has a major role in regulating p53 activity (Francoz, S. *et al.*, 2006; Toledo, F. *et al.*, 2006; 2007b).

MDM2 represses p53 by several means: First MDM2 binds to the transactivation domain of p53 thereby blocking its transcriptional ability preventing the recruitment of essential cofactors. Second MDM2 favors the recruitment of histone deacetylases to the p53 transcriptional complex, thus decreasing transcriptional activity and inducing p53 degradation. Finally, p53 is regulated by the ubiquitination activity of MDM2, which goes together with the nuclear export and the proteolytic degradation by the proteosome (Haupt, Y. *et al.*, 1997; Honda, R. *et al.*, 1997; Kubbutat, M.H. *et al.*, 1997; Stad, R. *et al.*, 2001). Three proteins are necessary for ubiquitination: E1-enzyme, which binds ubiquitin and activates it, the conjugating E2-enzyme, which accepts the activated ubiquitin and transfers it to MDM2, which in turn serves as the ubiquitin-E3-ligase and ubiquitinates p53 at several lysine residues (Nakamura, S. *et al.*, 2000; Rodriguez, M.S. *et al.*, 2000). Lai, Z. *et al.*(2001) showed that MDM2 only

mediates monomeric ubiquitination on multiple p53 residues, suggesting that MDM2 does not mediate p53 degradation. Thrower, J.S. *et al.* (2000) suggest that at least four ubiquitin molecules are necessary for efficient proteosomal degradation. Other proteins have to aid for polyubiquitination of p53 to be degraded by the proteosom. Additionally, MDM2 also ubiquitinates itself, thereby inducing its own degradation, regulating this way the MDM2 level in the cell (Fang, S. *et al.*, 2000; Honda, R. *et al.*, 2000).

Like MDM2, MDMX binds to the transactivation domain of p53 inhibiting its transcriptional ability. MDMX also possesses a RING-finger domain but lacks the E3-ligase function present in MDM2. Although the role of MDMX in the p53 pathway has to be further elucidated, it is known that high levels of MDMX stabilize p53. This is achieved by competing for the p53 binding site with MDM2 and this way inhibiting the degradation of p53 (Jackson, M.W. *et al.*, 2000; Stad, R. *et al.*, 2000; Stad, R. *et al.*, 2001; Migliorini, D. *et al.*, 2002) The main mechanism by which MDMX stabilizes p53 is through sequestration of ubiquitinated p53 in the nucleus, as the nuclear export of ubiquitinated p53 is essential for its degradation (Roth, J. *et al.*, 1998; Tao, W. *et al.*, 1999; Boyd, S.D. *et al.*, 2000; Geyer, R.K. *et al.*, 2000). According to Stad *et al.* (2000); (2001), a possible mechanism by which relocalization of p53 into the cytoplasm would be avoided is the formation of a trimeric complex of p53, MDM2 and MDMX The presence of MDMX, lacking a nuclear export signal in this complex may interfere with the nuclear export of p53 (Stad, R. *et al.*, 2001). Moreover, MDMX stabilizes MDM2. This is accomplished by binding MDM2 over their RING-finger domains and inhibiting the autoubiquitination of MDM2 (Marine, J.C. *et al.*, 2004). As poly-ubiquitination of MDM2 is required for the p53-MDM2 complex export, the inhibition of MDM2 poly-ubiquitination by MDMX results in stabilization of p53 (Stad, R. *et al.*, 2001).

The cocrystal structure of the MDM2 protein (residues 17-125) with a wildtype p53 peptide (aminoacids 15-29) was solved by Kussie, P.H. *et al.* (1996) (**Error! eference source not found.** A). The structure reveals a hydrophobic cleft at its N-terminal domain composed of two helices forming the sides, two shorter helices that make up the bottom, and a pair of three-strand β- sheets that cap each end. The p53 peptide forms an amphipathic α-helix of about 2.5 turns, followed by an extended

region of three residues. The primary contacts from p53 are made by its α-helix, which binds the MDM2 cleft with its hydrophobic face and buries all but one of its five hydrophobic amino acids at the interface. The key of this interface is a triad of hydrophobic and aromatic amino acids of p53 - Phe19, Trp23 and Leu26 – which inserts deep into the MDM2 cleft. The interface relies extensively on van der Waals contacts and the steric complementary between the MDM2 cleft and hydrophobic face of the p53 helix as these interactions are augmented by only two intermolecular hydrogen bonds: one between the amide group of Phe19 located in the backbone of p53 and the carbonyl group of the Gln72 side chain of MDM2; the second bond is formed by indole nitrogen of Trp23 of p53 and the carbonyl group of Leu54 in MDM2 located deep inside the cleft (Kussie, P.H. *et al.*, 1996). The dissociation constant measured by isothermal titration calorimetry by Kussie et al (1996) was calculated to be 600nM and 420nM for peptides corresponding to residues 15 to 29 and 1 to 57, respectively.

The cocrystal structure of human MDMX (residues 15-129) with p53 (residues 15-29) was solved by Popowicz, G.M. et al. (2008) (5B). Similar to the p53-MDM2 structure the p53-MDMX structure features a central hydrophobic cleft. The primary contacts of the p53 peptide to MDMX are made by same triad as with MDM2. The hydrophobic cleft of MDMX is smaller and differently shaped, compared to that of MDM2. This is derived from the sidechains of Met53 and Tyr99 of MDMX, which protrude into the binding pocket and block part of the cleft on its opposite sides. The Met53 sidechain has the same orientation as the corresponding Leu54 of human MDM2, but the larger Met53 sidechain makes the p53-binding smaller. While the Tyr99 in the p53-MDMX structure is in a “closed conformation”, the corresponding Tyr100 sidechain in the p53-MDM2 structure of Kussie et al., is flipped way from the p53 binding pocket adopting the “open conformation” (Popowicz, G.M. *et al.*, 2008). However, later crystallized structures of MDM2 in complex with a short peptidic analogue showed the Tyr100 ring collapsed into the p53 pocket, adopting the closed conformation, though it never fully acquires the conformation seen in the MDMX structures. Popowicz *et al.* hypothesizes that the “closed” Tyr99 arrangement is the intrinsic property of MDMX that most probably arises from the differences between MDMX and MDM2 that are located in helix α2’. The K_D of the p53-MDMX binding is 210 nM (Popowicz, G.M. *et al.*, 2008).

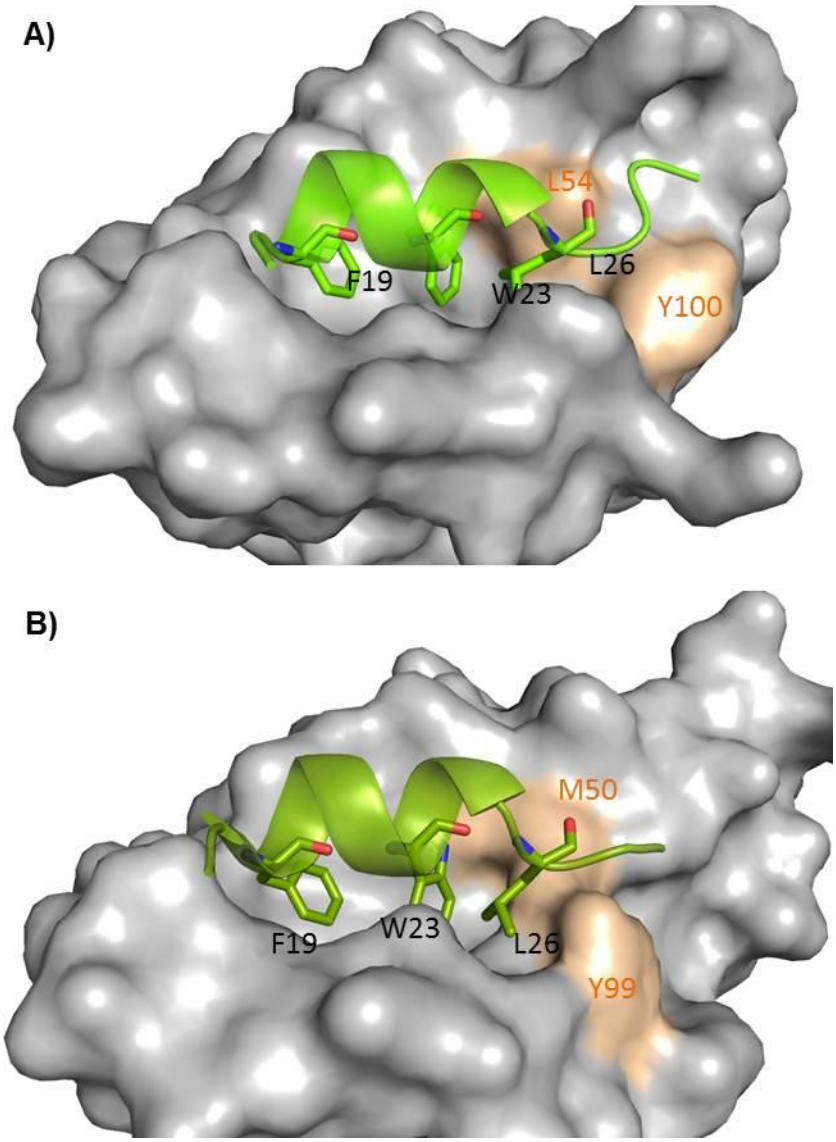

Figure 5. A) Structure of human MDM2 (residues 17-125) (gray surface), in complex with p53 (residues 15-29) (green cartoon, amino acids F19, W23 and L26 represented by sticks) PDB-ID: 1YCR. **B)** Structure of human MDMX (residues 23-109) (gray surface) in complex with p53 (residues 15-29) (green cartoon, amino acids Phe19, Trp23 and Leu26 are represented by sticks) PDB-ID: 3DAB. The amino acids Met53 and Tyr99 of MDMX are highlighted in light orange as these two amino acids protrude into the cavity making it smaller. For comparison the corresponding amino acids in MDM2 Leu45 and Tyr100 are also highlighted in orange.

1.6. p53-MDM2 and p53-MDMX disrupting small drug-like molecules

Many currently used genotoxic chemotherapeutics rely on DNA damage-dependent activation of p53 to mount an apoptotic response. However, high doses of genotoxic drugs can also induce p53-independent pathways and thus may cause severe

toxicities in normal tissues eventually leading even to secondary malignancies. Therefore, selective, non-genotoxic p53 activation, targeting the p53–MDM2 and p53-MDMX interaction, should be an important alternative to current cytotoxic chemotherapy. In addition, the combination of various drugs that target multiple p53 pathways may be a useful strategy to achieve synergistic drug efficacy (Popowicz, G.M. *et al.*, 2011).

Small molecules have been developed that compete with the p53 binding site of MDM2, inhibiting the binding and degradation of p53 by MDM2 and MDMX, thus preventing p53 degradation. Disrupting the interaction between p53 and MDM2 was shown to restore the wild type p53 activity and drive cancer cells selectively into apoptosis (Cheok, C.F. *et al.*, 2011). Investigations of small molecule p53-MDM2 antagonists in different cancer cell lines and animal models support their usefulness as potential anticancer agents with a novel mode-of-action (Vassilev, L.T., 2007). In fact recent interim results from the first-in-class clinical p53-MDM2 antagonist RG7112 in patients with relapsed/refractory acute myeloid and lymphoid leukemia and refractory chronic lymphocytic leukemia/small cell lymphocytic lymphomas are encouraging although not stellar. RG7112 was developed by Roche and is a member of the Nutlin-family. The problem of this compound may lay in its poor bioavailability.

While several classes of small molecule p53-MDM2 antagonists have been described in the past, only some are of sufficient potency and few have been structurally characterized (Vassilev, L.T. *et al.*, 2004; Marugan, J.J. *et al.*, 2006; Allen, J.G. *et al.*, 2009; Czarna, A. *et al.*, 2010; Popowicz, G.M. *et al.*, 2011). Protein-protein interaction antagonists are described to be challenging targets for small molecule drug discovery due to their often extended and rather flat interfaces (Wells, J.A. *et al.*, 2007). However, the interface between p53 and MDM2 is accessible to small molecule drug discovery due to its small dimension, concavity and hydrophobicity of the binding site (Fry, D.C. *et al.*, 2005).

MDM2 and MDMX antagonists may also be important in cyclotherapy: This therapy should prevent normal proliferating cells during antimitotic chemotherapy. Pre-treatment with the MDM2 and MDMX antagonists will lead to cell cycle arrest in normal cells with functional p53 and thus be protected from the toxicity of the

chemotherapy unlike the tumor cells expressing mutant p53 that will be insensitive to the MDM2 and MDMX antagonists and thus be selectively vulnerable to the mitotic poison.

Sur *et al.* (2009) showed that the combination of Nutlin-3 and the PLK inhibitor BI-2536 prevented neuropenia in a mouse xenograft model, a frequent dose-limiting toxic effect, during anticancer treatment and additionally achieved tumor-killing.

The search for efficient p53-MDM2 inhibitors has led to several small-molecule ligands. The first reported small molecule inhibitors were chalcones (Stoll, R. *et al.*, 2001). Several different scaffolds have been published since then: Nutlins, benzodiazepinedione, Mi's, imidazole-indoles, chromenotriazolpyrimidines, peptides, and peptide based miniproteins, among others.

A common way of action of several compounds like benzodiazepinediones, Nutlins and Mi's is by mimicing the three amino acids of p53: F19, W23 and L26.

Several of these compounds are currently in pre-clinical studies: Ascenta Therapeutics entered the clinical trials with a compound belonging to the Mi-familiy. The Mi scaffold is based on an oxoindole group. The affinity of Mi-219 and Mi-63 towards MDM2 is K_i 5 nM and 3 nM, respectively (Popowicz, G.M. *et al.*, 2011). As mentioned before Roche entered the clinical trials with compound RG7112 that belongs to the Nutlin-family. Nutlins are cis–imidazoline analogs and are the best studied small molecules so far. Nutlin-2 was the first published p53-MDM2 inhibitor with a crystallographic structure (Vassilev, L.T. *et al.*, 2004).. Nutlin-3 is the most potent p53-MDM2 antagonist with a K_i of 36 nM. In vivo experiments proved that Nutlin-3 induced cell cycle arrest in tumor cells, while not affecting healthy cells (Tokalov, S.V. *et al.*, 2010; Zheng, T. *et al.*, 2010), (Shangary, S. *et al.*, 2009) (Laurie, N.A. *et al.*, 2007).

Targeting MDMX for antitumor research has only recently found importance and finding a p53-MDMX antagonist has been a big challenge. Till now no high affinity p53-MDMX antagonist has been found. However, peptide and knockout studies confirm that such an inhibitor should possess a high therapeutic value (Marine, J.C. *et al.*, 2004; Marine, J.C. *et al.*, 2007).

2. Goal of study

The search for the p53-MDM2 and for p53-MDMX inhibitor has a high therapeutic value. The challenge is to find the compound, with high affinity to the target and having good pharmacokinetics. Only few compounds approach these properties, so far.

Goal of the investigations made during the thesis was to screen for small molecule inhibitors that could disrupt the p53-MDM2 and p53-MDMX interaction, determine their affinity by the FP-assay and nuclear magnetic resonance spectroscopy, crystallize the best binding compounds and solve the cocrystal structures.

I will present new p53-MDM2 and p53-MDMX inhibitor scaffolds, their affinity and several p53-MDM2 cocrystal structures in the following pages.

3. Materials and Methods

3.1. Materials

3.1.1. E-coli strains

Strain	Usage	Company
Bl21Codon Plus (DE3) RIL	Expression	Stratagene (USA)
Arctic Express (DE3) RIL	Expression	Stratagene (USA)
DH5α	Cloning	Novagen (Canada)
One Shot TOP 10	Cloning	Novagen (Canada)

3.1.2. Plasmids

Vector	Antibiotic	Tag	Company
pET 28a (+)	Kanamycin	6-His	Novagen (Canada)
pET 20b (+)	Ampicillin	-	Novagen (Canada)
pET46 Ek/LIC	Ampicillin	6-His	Novagen (Canada)
pET 11a	Ampicillin	-	Novagen (Canada)

3.1.3. Cell-growth media and stocks

For 1 liter of the Luria Bertani (LB) medium:

10 g peptone from casein

5 g yeast extract

10 g sodium chloride

For preparation of agar plates the medium was supplemented with 15 g agar per liter.

For 1 liter of the minimal medium (MM) for uniform enrichment with ^{15}N:

0.5 g NaCl

1.3 ml trace elements solution

1 g citric acid monohydrate

36 mg ferrous citrate dissolved in 120 µl concentrated HCl

4.02 g KH_2PO_4

7.82 g K_2HPO_4 x $3H_2O$

1 ml Zn-EDTA solution

1 g $^{15}NH_4Cl$

pH was adjusted to 7.0 with NaOH, the mixture was autoclaved, upon cooling separately sterilized solutions were added: 25 ml glucose, 560 µl thiamine, antibiotics, 2 ml of the $MgSO_4$ stock (see below).

Stock solutions:

Ampicillin: 100 mg/ml of ampicillin in deionized H_2O, sterilized by filtration, stored in aliquots at -20°C until usage. Working concentration: 100 µg/ml.

Chloramphenicol: 34 mg/ml of chloramphenicol in ethanol, stored at -20°C until usage. Working concentration: 34 µg/ml.

Kanamycin: 100 mg/ml of kanamycin in deionized H_2O, sterile filtered and stored in aliquots at -20°C until used. Working concentration: 100 µg/ml.

Streptomycin: 60 mg/ml of streptomycin in deionized H_2O, sterile filtered and stored in aliquots at -20°C until usage. Working concentration 60 µg/ml.

Isopropyl-β-thiogalactopyranoside (IPTG): A sterile filtered 1 M stock of IPTG in deionized water was prepared and stored in aliquots at -20°C until used.

Glucose: 20% (w/v) in deionized H_2O, autoclaved.

Thiamine: 1% in deionized H_2O, sterilized by filtration.

$MgSO_4$: 1 M in deionized H_2O, sterilized by filtration.

Zn-EDTA solution:

5 mg/ml EDTA

8.4 mg/ml zinc acetate

Trace elements solution:

2.5 g/l H_3BO_3

2.0 g/l $CoCl_2 \times H_2O$

1.13 g/l $CuCl_2 \times H_2O$

9.8 g/l $MnCl_2 \times 2H_2O$

2.0 g/l $Na_2MoO_4 \times 2H_2O$

pH adjusted with citric acid or HCl.

3.1.4. Solutions and Buffers

3.1.4.1. Solution used for competent cells preparation

Buffer A: 100 mM $MgCl_2 \times 6H_2O$

Buffer B: 100 mM $CaCl_2$ - 15% glycerol

3.1.4.2. Buffer for DNA agarose gel electrophoresis

50 x TAE buffer (for 1 l):

40 mM Tris-acetate	242 g of Tris base
1 mM EDTA	100 ml of 0.5 M EDTA (pH 8.0)
Glacial acetic acid	57.1 ml

3.1.4.3. Reagents and buffers for SDS-PAGE

Anode buffer (+):

200 mM Tris pH 8.9

Cathode buffer (-):

100 mM Tris pH 8.25

100 mM Tricine

0.1% SDS

Separation buffer:

1 M Tris pH 8.8

0.3% SDS

Stacking buffer:

1 M Tris pH 6.8

0.3% SDS

Separation gel:

1.675 ml H_2O

2.5 ml separation buffer

2.5 ml acrylamide solution

0.8 ml glycerol

25 µl APS (10% Stock)

2.5 µl TEMED

Intermediate gel:

1.725 ml H_2O

1.25 ml separation buffer

0.75 ml acrylamide solution

12.5 µl APS (10% Stock)

2.5 µl TEMED

Stacking gel:

2.575 ml H_2O

0.475 ml stacking buffer

0.625 ml acrylamide solution

12.5 µl 0.5 M EDTA, pH 8.0

37.5 µl APS (10% Stock)

1.9 µl TEMED

Coomassie-blue solution:

45% ethanol

10% acetic acid

0.25% (w/v) Coomassie Brilliant Blue R

Destaining solution:

5% ethanol

10% acetic acid

Acrylamide solution:

Rotiphorese® Gel 30 (37, 5:1), Roth (Germany)

3.1.4.4. Protein Purification Buffers

PBS:

140 mM NaCl

2.7 mM KCl

10 mM Na_2HPO_4

1.8 mM KH_2PO_4

0.05% NaN_3

pH 7.3

NMR buffer:

50 mM KH_2PO_4

50 mM Na_2HPO_4

150 mM NaCl

5 mM DTT

pH 7.4

Crystallization buffer:

50 mM NaCl

5 mM Tris-HCl

10mM β-mercaptoethanol

pH 8.0

Buffers for the immobilized metal-chelate chromatography (IMAC) under native conditions:

Binding buffer:

50 mM NaH_2PO_4

300 mM NaCl

10 mM imidazole

pH 8.0

Wash buffer:

50 mM NaH_2PO_4

300 mM NaCl

20 mM imidazole

pH 8.0

Elution buffer:

50 mM NaH_2PO_4

300 mM NaCl

250 mM imidazole

pH 8.0

Buffers for protein purification under denaturing conditions:

Solubilizing buffer:

6 M guanidinium chloride

100 mM Tris HCl

1 mM EDTA

10 mM β-mercaptoethanol

pH 8.0

Dialysis buffer:

4 M guanidinium chloride

10 mM β-mercaptoethanol

pH 3.5

Refolding buffer:

10 mM Tris-HCl

1 mM EDTA

10 mM β-mercaptoethanol

pH 7.0

Elution buffer:

100 mM Tris

10 mM β-mercaptoethanol

pH 7.0

3.1.4.5. Fluorescent polarization (FP) buffer

20 x FP buffer:

200 mM Tris

20 mM EDTA

1 M NACl

pH 7.3

3.1.5. Peptides used for FP-assay

Name	Sequence	
Zondlo	CPPLSQETFSDLWKLLSENN	Coupled to 5-carboxyfluorescein
P4	LTFEHYWAQLTS	Coupled to 5-carboxyfluorescein
P6	ETFEHWWSQLLS	Coupled to 5-carboxyfluorescein

3.1.6. Kits

QIAprep Spin Miniprep Kit	Qiagen (Germany)
Complete Protease Inhibitor Cocktail	Roche (Germany)

3.1.7. Protein, nucleic acids markers and sample loading dyes

Markers:

Page Ruler^{TM} Prestained Protein Ladder	Fermentas (Lithuania)
Gene Ruler^{TM} DNA Ladder	Fermentas (Lithuania)

Sample loading dyes:

5x protein loading dye:	0.225 M Tris-HCl, pH 6.8
	50% glycerol
	5% SDS
	0.05% bromophenol blue
	0.25 M DTT
5x Gel Plot Loading Dye	Qiagen (Germany)

3.1.8. Chromatography equipment, columns and media

ÄKTA basic	Qiagen (Germany)
ÄKTA explorer 10	GE Healthcare (UK)
Peristaltic pump P-1	
Fraction collector RediFrac	
Recorder REC-1	
UV flow through detector UV-1	
BioLogic LP System	
HiLoad 26/60 Superdex S75pg	
HiLoad 16/60 Superdex S75pg	
HiLoad 16/60 Superdex S200pg	
NTA Superflow	
Buthyl Sepharose 6 Fast Flow	
GE Healthcare (UK)	
GE Healthcare (Germany)	
Amersham Pharmacia (Sweden)	
Amersham Pharmacia (Sweden)	
Amersham Pharmacia (Sweden)	
Amersham Pharmacia (Sweden)	
Biorad (USA)	
GE Healthcare (UK)	
GE Healthcare (UK)	
GE Healthcare (Germany)	

3.1.9. Fluorescent polarization equipment

384 well assay plate	(Corning)
96 well assay plate non-binding surface	(Corning)
384 well black assay plate non-binding surface	(Corning)
Ultra Evolution 384-well plate reader	(Tecan)

3.2. Laboratory methods and principles

3.2.1. Preparation of plasmid DNA

The isolation of plasmid DNA from *E. coli* was carried out using dedicated plasmid purification kits from Qiagen. The kits employ a standard alkaline lysis of the precipitated bacteria in the presence of RNAse and a strong ionic detergent, SDS, followed by neutralization/DNA renaturation with acetate. For purification, a crude cell lysate is loaded onto a silica gel column, washed with an ethanol-containing buffer, and eluted in a small volume, yielding up to 20 μg of the plasmid DNA.

3.2.2 Transformation of E. coli

3.2.2.1 Making chemically competent cells

A single colony of an overnight grown bacterium from a LB agar plate was inoculated into 100 ml of the LB media. The culture was incubated at 37°C with vigorous agitation, monitoring the growth of cells. Cells were grown till the OD_{600} reached ~0.6. The bacterial culture was transferred to sterile, disposable, ice-cold 50 ml polypropylene tubes and centrifuged at 3000 g for 10 min at 4°C. The supernatant media was completely removed and the cell pellets were re-suspended by gentle pipetting in 30 ml of the ice-cold 100 mM $MgCl_2$ solution and incubated for 30 min on ice. Cells were centrifuged at 3000 g for 10 min at 4°C. The supernatant media was completely removed and the pellet re-suspended in 2,5 ml of ice-cold 100 mM $CaCl_2$ containing 15% glycerol by gentle pipetting. Cells were dispensed into aliquots of 100 µl, flash frozen in liquid nitrogen and stored at -80°C.

3.2.2.2 Transformation of chemically competent cells

3 µl of a ligation mix or ca. 50 µg of plasmid DNA was added to 100 µl of chemically competent cells. The mixture was incubated on ice for 15 min followed by a heat shock of 30 s at 42°C, and the addition of a 250 µl of LB medium. After 1 h of incubation at 37°C, 100 µl of the mixture was spread out on LB agar plates (supplemented with selective antibiotic) and incubated overnight at 37°C.

3.2.3 Protein chemistry methods & techniques

3.2.3.1 Protein expression

Optimization of the conditions is important for expressing proteins. The aim is to secure the maximum amount of a protein in the soluble fraction of the lysate. A number of parameters were checked to get the maximum yields of the protein, which include optimization of a type of culture media, temperature, induction duration, induction OD, concentration of inducer (IPTG), and cell type. All proteins were cloned in and expressed from the pET vectors, which are IPTG inducible.

3.2.3.1.1 Expression and purification of proteins from inclusion bodies

The vector pET-20b containing the MDM2 crystallization constructs (residues 18-111, 18-125 or 25-111), the MDMX crystallization construct (residues 23-111), as well as the pET-11a vector containing the MDM2 construct (residues 1-125) used for NMR-spectroscopy and FP-assay, were transformed into the Bl21Codon Plus(DE3) RIL or BL21 Arctic Express (DE3) expression cells (Stratagene). The cells were grown until the OD_{600} reached 0.8 and were then induced with 1 mM IPTG. After 4 h post induction the cells were harvested by centrifugation at 5500 g for 15 min. The pellets were re-suspended in the PBS buffer. Lysis was performed by sonication followed by centrifugation at 10000 g for 30 min. The pellets were re-suspended in 10 ml of the solubilization buffer and incubated for 2 h on a rotator at 4°C. Dialysis was performed overnight, followed by refolding at 4°C for 8 h. Ammonium sulfate was added to a final concentration of 2 M and incubated overnight at 4°C. The solution was

centrifuged at 11000 g for 30 min. Buthylsepharose 6 Fast Flow (GE Healthcare) was added to the supernatant and incubated for 2 h. The protein was eluted, concentrated and loaded onto the HiLoad 16/60 Superdex75 or Superdex 200 pg gel filtration columns (Amersham Biosciences). The purity and folding of the protein was confirmed by SDS-gel electrophoresis and NMR spectroscopy.

3.2.3.1.2 Expression and purification of soluble proteins

The p53-MDM2 protein complex, expressed in the pET-Duet-1 vector, and the MDMX protein (residues 1-134), expressed in the pET-46 vector, were transformed into the Bl21Codon Plus (DE3) RIL or BL21 Arctic Express (DE3) expression cells (Stratagene). The LB-media was inoculated with an overnight culture and grown at 37°C. At OD_{600} of 0.8. the cells were induced with 0,5 mM IPTG and the temperature was lowered to 20°C. After 14-16 h of protein expression the cells were harvested by centrifugation of 5500 g for 15 min. The pellets were re-suspended in the lysis buffer containing 0.5 mM PMSF and adequate concentration of benzamidine. The lysis was performed by sonication followed by centrifugation at 48000 g for 30 min. The supernatant, containing the 6His-tagged protein or protein complex, was purified by NiNTA agarose beads (Qiagen) followed by gel filtration on the HiLoad 16/60 Superdex75 or Superdex 200 pg gel filtration columns (Amersham Biosciences). The purity and homogeneity of proteins were confirmed by SDS-gel electrophoresis and NMR spectroscopy.

3.2.3.2 Sonication

Pulsed mode of operation was applied (output control 8, 60% duty cycle) and sonication was carried out on ice, in 5 repeats of 3 min each, with 5 min intervals in between, to avoid overheating of the sample.

3.2.3.3 SDS polyacrylamide gel electrophoresis (SDS-PAGE)

The SDS polyacrylamide gel electrophoresis was performed to verify the identity and purity of eluted proteins. For all expressed proteins, tricine gels were applied

(Schagger and von Jagow, 1987). The protein samples were prepared by mixing 20 µl of the protein solution with 5 µl of the sample buffer followed by 5 min incubation at 100°C. Due to the precipitation of SDS in contact with guanidinium, samples containing guanidinium were prepared as follows: 20 µl of the protein solution in a denaturing buffer were diluted with 400 µl 20% trichloroacetic acid (TCA). The samples were incubated for 5 min on ice followed by centrifugation for 5 min at 20000 g. The supernatants were removed and the protein pellets were washed by re-suspending them in 400 µl ethanol. The samples were centrifuged, the pellets re-suspended in 20 µl 2x Sample buffer and boiled for 5 min.

3.2.3.4 Visualization of separated proteins

For visualization of the protein bands, the gels were stained in a Coomassie-blue solution. Background was cleared by incubation of the gel in a destaining solution. Both processes were greatly accelerated by brief heating with microwaves of the gel submerged in an appropriate solution.

3.2.3.5 Determination of protein concentration

The concentration of proteins in solution was estimated by means of the Bradford colorimetric assay. 5 µl of the protein sample was added to 1 ml (10 x diluted stock) of Bradford reagent (BioRad) in a plastic cuvette. After gentle mixing, A595 was measured and converted to the protein concentration on the basis of a calibration curve prepared for known concentrations of BSA.

Determination of protein concentration was performed spectrophotometrically. Absorption A_{Prot} at 280 nm was measured and converted to a protein concentration on the basis of theoretical extinction coefficients. It has been shown that it is possible to estimate the molar extinction coefficient $\epsilon_{M,Prot}$ of a protein at a given wavelength λ from knowledge of its amino acid composition (Gill and Hippel, 1989). This can then be calculated using the equation:

$$\epsilon_{M,Prot}(\lambda) = \alpha \cdot \epsilon_{M,Y}(\lambda) + \beta \cdot \epsilon_{M,W}(\lambda) + \gamma \cdot \epsilon_{M,C}(\lambda)$$

where $\epsilon_{M,Y}$, $\epsilon_{M,W}$ and $\epsilon_{M,C}$ are the molar extinction coefficients of tyrosine, tryptophan and cysteine (cysteine residues do not absorb appreciably at wavelengths > 260 nm, while cystine does) respectively; and α, β and γ are the number of each type of residue per molecule of protein.

Protein concentration C_{Prot} can then be derived from the following formula of the absorption:

$$A_{Prot}(\lambda) = \epsilon_{M,Prot}(\lambda) \times C_{Prot} \times l$$

where l is the cuvette path length in cm.

3.2.4 Nuclear magnetic resonance spectroscopy (NMR)

All NMR experiments were carried out at 300 K on a Bruker DRX 600 spectrometer equipped with a ^{1}H,^{13}C and ^{15}N triple resonance, triple gradient 5 mm probehead. The samples contained between 0.05 and 0.2 mM protein in a NMR buffer. Water suppression was carried out using the WATERGATE 5 sequence (Piotto, M. *et al.*, 1992). NMR data were processed using the Bruker program Xwin-NMR 3.5.

50 µl of D2O is added to 450 µl of a protein complex or labeled protein for AIDA or 2D-HSQC, respectively. After having taken a reference spectrum, the compound is added in different ratios depending on the affinity. The AIDA experiments were performed according to Bista *et al.* (2009). The 2D-HSQC spectra were acquired using the fast-HSQC pulse sequence (Mori, S. *et al.*, 1995). Typically a total of 2048 complex points in t2 and 192 in t1 increments were acquired.

3.2.5. Fluorescence polarisation Assay

All FP experiments were performed as described by Czarna *et al.* (2009). The fluorescence polarization experiments were read on an Ultra Evolution 384-well plate reader (Tecan) with the 485 nm excitation and 535 nm emission filters. The fluorescence intensities parallel ($\mathrm{Int}_{\parallel}$) and perpendicular ($\mathrm{Int}_{\perp}$) to the plane of excitation were measured in black 384-well NBS assay plates (Corning) at room temperature (~20°C). The background fluorescence intensities of blank samples

containing the references buffer were subtracted and steady-state fluorescence polarization was calculated using the equation:

$$P = \frac{(\mathrm{Int}_{\parallel} - \mathrm{G} \cdot \mathrm{Int}_{\perp})}{(\mathrm{Int}_{\parallel} + \mathrm{G} \cdot \mathrm{Int}_{\perp})}$$

The correction factor G (G = 0.998, determined empirically) was introduced to eliminate differences in the transmission of vertically and horizontally polarized light. All fluorescence polarization values were expressed in millipolarization units (mP). The binding affinities of the fluorescent p53-derived peptide was determined in the FP-buffer containing 10% DMSO. Competition binding assays were performed using MDM2 and MDMX at a final concentration of 100 nM or 120 nM, respectively. Fluorescent-labeled peptides were dissolved in DMSO and used at 10 nM. Binding constant and inhibition curves were fitted using the SigmaPlot (SPSS Science Software).

3.2.6 X-ray crystallography

3.2.6.1 Protein crystallization

Purified MDM2 and MDMX were concentrated up to 5 mg/ml. Followed by the addition of the inhibitor in a 3 fold excess, the complex is then further concentrated to achieve the final protein concentration of about 15 mg/ml. The crystallization was carried out at both 4°C and 20°C in several crystallization conditions using the sitting drop vapour diffusion method. The 1-2 µl drops consisted of a 1:1 (vol/vol) mixture of protein and the well solution. All crystals grown in non-cryoprotectant conditions were soaked in cryo-solutions containing mother liquor supplemented with 20% MPD or glycerol and were flash frozen in liquid nitrogen.

3.2.6.2 Data collection and structure analysis

X-ray data sets were collected on the SLS beamline PXII at the Paul Scherrer Institut, Villigen, Switzerland.

The data sets were integrated, scaled and merged by XDS and XSCALE programs (Kabsch, W., 1993). The structures were determined by molecular replacement using the Molrep program from the CCP4 suite (Bailey, S., 1994). Model building and refinement were carried out with the program XtalViev/Xfit and REFMAC5 (Bailey, S., 1994; McRee, D.E., 2004). Water molecules were added using Arp/Warp (Perrakis, A. *et al.*, 1999).

4. Results and Discussion

4.1. Protein expression and purification

All MDM2 and MDMX constructs were expressed in *E. coli Bl21Codon Plus (DE3) RIL.* For the biophysical and biochemical studies, the proteins were purified. The MDM2 constructs and the $MDMX_{23-111}$ were obtained from inclusion bodies, while the $MDMX_{1-134}$ construct and the MDM2/p53 complex was expressed and purified in their native form by means of their His-tag.

Table 1. Protein constructs used in this thesis.

construct	vector	Tag	purpose	purified
$MDM2_{1-125}$	pET-11a	T7-tag	FP-analysis and HSQC-NMR	From inclusion bodies
$MDM2_{1-125}$ / $p53_{1-321}$	pET-Duet-1	His-tag	AIDA-NMR	Native conditions
$MDM2_{25-111}$	pET-20b	-	Crystallization	From inclusion bodies
$MDM2_{18-111}$	pET-20b	-	Crystallization	From inclusion bodies
$MDM2_{18-125}$	pET-20b	-	Crystallization	From inclusion bodies
$MDMX_{23-111}$	pET-28a	-	Crystallization	From inclusion bodies
$MDMX_{1-134}$	pET-46	His-tag	FP-analysis	Native conditions

The constructs used for crystallization do not contain any tag in order to avoid interference with the crystallization process. No influence of the tag was observed for the constructs used in the NMR- or FP-assays.

The last purification step was performed by gel filtration (**Error! Reference source ot found.Error! Reference source not found.**, left side). Fractions containing the proteins were collected and the purity was confirmed by SDS-PAGE (**Error! eference source not found.**, right side). Generally a high yield of the pure protein was achieved. Finally, the protein was concentrated to the desired concentration.

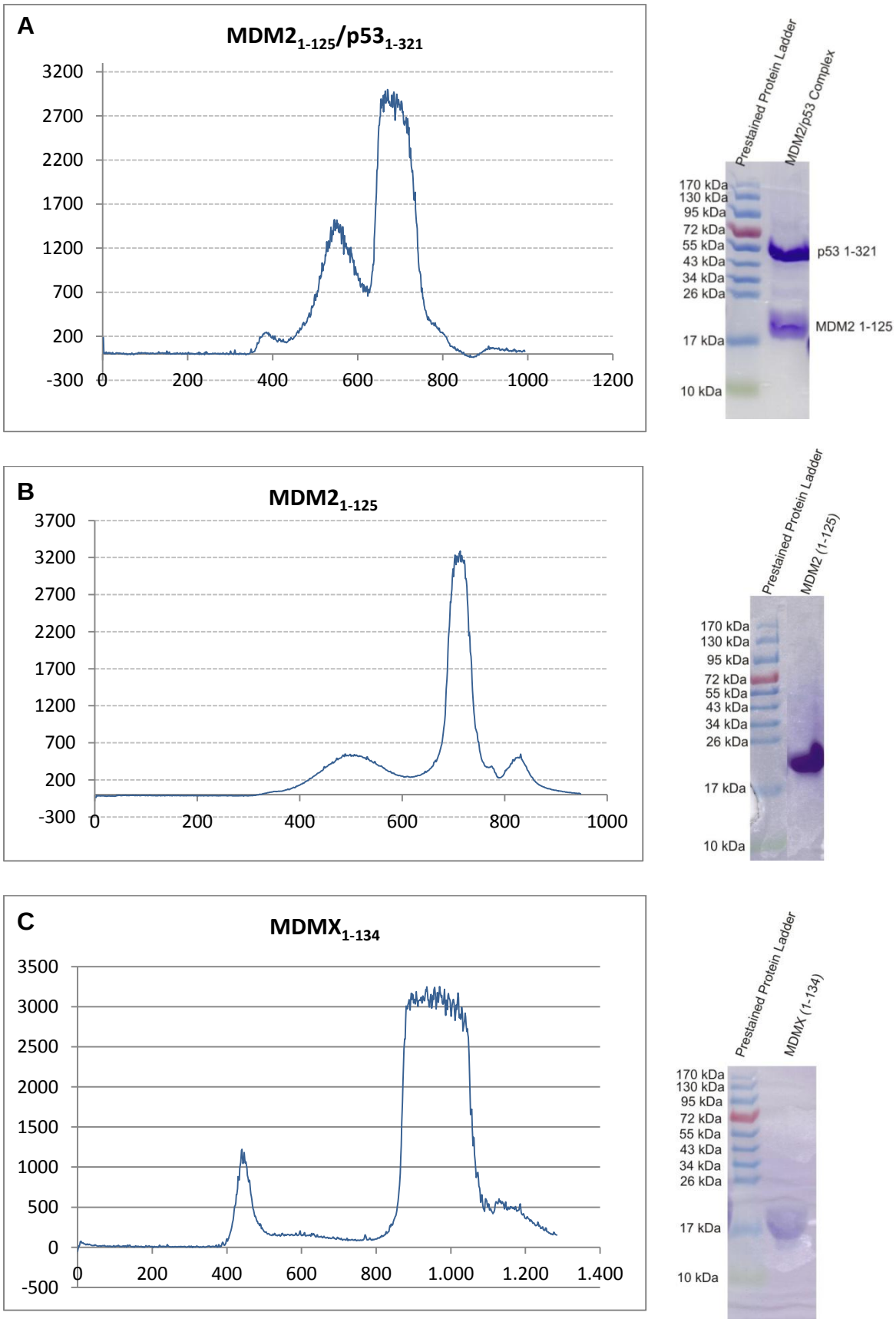

Figure 6. Gel filtration chromatograms (left side) and SDS-PAGE-gels (right side) of **A)** MDM2 (residues 1-125) in complex with p53 (residues 1-321). The first peak at ~500 ml corresponds to p53, the second peak at ~700 ml to MDM2. **B)** MDM2 (residue 1-125) **C)** MDMX (residues 1-134).

4.2. Anchor.Query

Anchor.Query is a virtual screening platform which is used for the rational design of small molecule antagonists. It was used to screen for scaffolds which are able to efficiently disrupt the p53-MDM2 interaction. Therefore ~5 million unique multicomponent reaction (MCR) compounds containing an indole anchor were aligned with the Trp23 anchor of p53 and screened for matching the anchor/pharmacophore model. The screening results were then sorted and ranked by molecular descriptors. For example, molecular weight ranking is important for the selection of the compounds to potentially achieve good ligand efficiency. The scaffold and individual compounds were chosen for synthesis according to the binding poses and the electrostatic complementarity of the molecules.

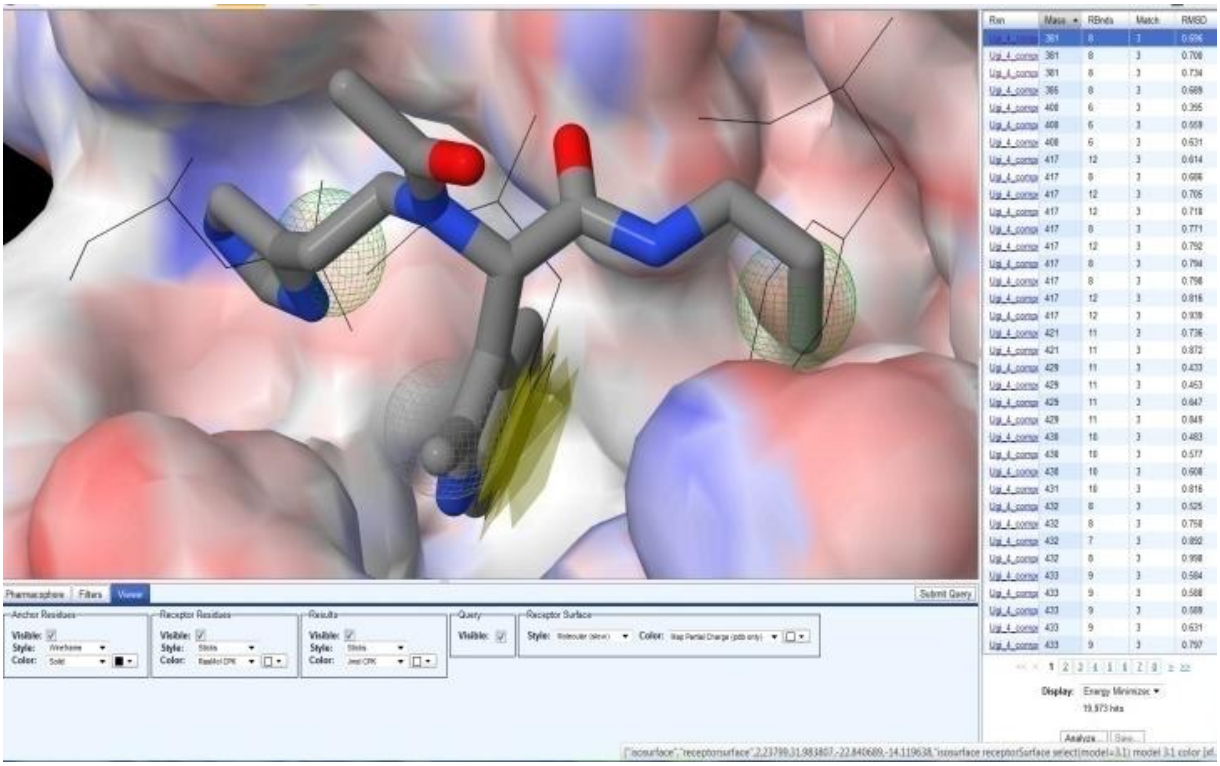

Figure 7. Screen shot of pharmacophore-based virtual screening platform ANCHOR.QUERY to discover MCR-derived MDM2 antagonists. The MDM2 receptor is shown in surface representation (PDB ID: 1YCR). The hot spot p53 derived amino acids Phe19 and Leu26 are shown as lines and green spheres and the Trp23 indol anchor as yellow disk. The virtual U-4CR product (grey sticks) with the lowest MW and matching with the pharmacophore model is depicted.

The proposed virtual molecule based on the Ugi multicomponent reaction (U-4CR) with the lowest molecular weight and matching the pharmacophore points is shown in

Error! Reference source not found.. This served as a starting point for validation nd optimization in the discovery of new p53-MDM2 antagonists. Different MDM2 inhibitor scaffolds were synthesized this way. The search for lead compounds started by analyzing small molecules by means of the fluorescent polarization (FP)-assay. This high-throughput-assay allows a fast and accurate selection of compounds. Hundreds of small molecules belonging to different scaffolds were screened this way. Some of the compounds were also checked by the NMR based assay AIDA. For the best binding compounds a NMR-HSQC spectrum was performed. Furthermore not only crystals of selected high affinity binding compounds could be obtained but also their structures of high scientific value could be solved.

4.3. AIDA-assay

The Antagonist Induced Dissociation Assay, AIDA, provides unambiguous information on whether an antagonist of a protein-protein interaction is strong enough to dissociate the complex and weather its action is through denaturation, precipitation, or release of a protein in its functional folded state. AIDA can also quantitatively characterize antagonist-protein and antagonist-protein-protein interactions in the form of K_D´s and fractions of the released proteins from their mutual binding (Bista, M. *et al.*, 2009). This assay requires a large protein fragment to bind a small protein, which in the case of MDM2 and p53 are the 14 kDa and 35,5 kDa fragments, respectively. The 1D AIDA-assay uses the p53 tryptophanes as amino acid reporters to monitor the binding of a compound (Figure 8). p53 has three tryptophanes: Trp91, Trp23, and Trp53. The $^{N}H^{\varepsilon}$ groups of Trp23 and Trp53 make sharp peaks in the NMR spectrum because of the their location in the highly flexible N-terminal domain of p53. Conversly the $^{N}H^{\varepsilon}$ group of Trp91 makes a broad peak, because it is in the rigid DNA-binding domain (Lee, H. *et al.*, 2000; Ayed, A. *et al.*, 2001; Schon, O. *et al.*, 2002; Dawson, R. *et al.*, 2003; D'Silva, L. *et al.*, 2005a; Joerger, A.C. *et al.*, 2008). The inhibitory effect of the putative antagonist is monitored by the appearance or alternatively disappearance of the $^{N}H^{\varepsilon}$ Trp23 signal. Trp23 is a key residue for MDM2 recognition. It is buried in the MDM2 binding pocket, contacting 10 residues of MDM2 (Kussie, P.H. *et al.*, 1996; Ferreira, M.E. *et al.*, 2005). Due to the complex formation residues 17 to 26 of p53 are stabilized within the N-terminal domain, leading to the disappearance of the $^{N}H^{\varepsilon}$ Trp23 NMR signal

(D'Silva, L. *et al.*, 2005a; Krajewski, M. *et al.*, 2007a). Disruption of the complex by addition of an antagonist results in the release of free p53 and thus recovery of the $^{N}H^{\varepsilon}$ Trp23 signal. The dissociation constant can be calculated by estimation of the fraction of released p53 protein, which is in accordance with the fraction of recovered $^{N}H^{\varepsilon}$ Trp23 signal (Krajewski, M. *et al.*, 2007a).

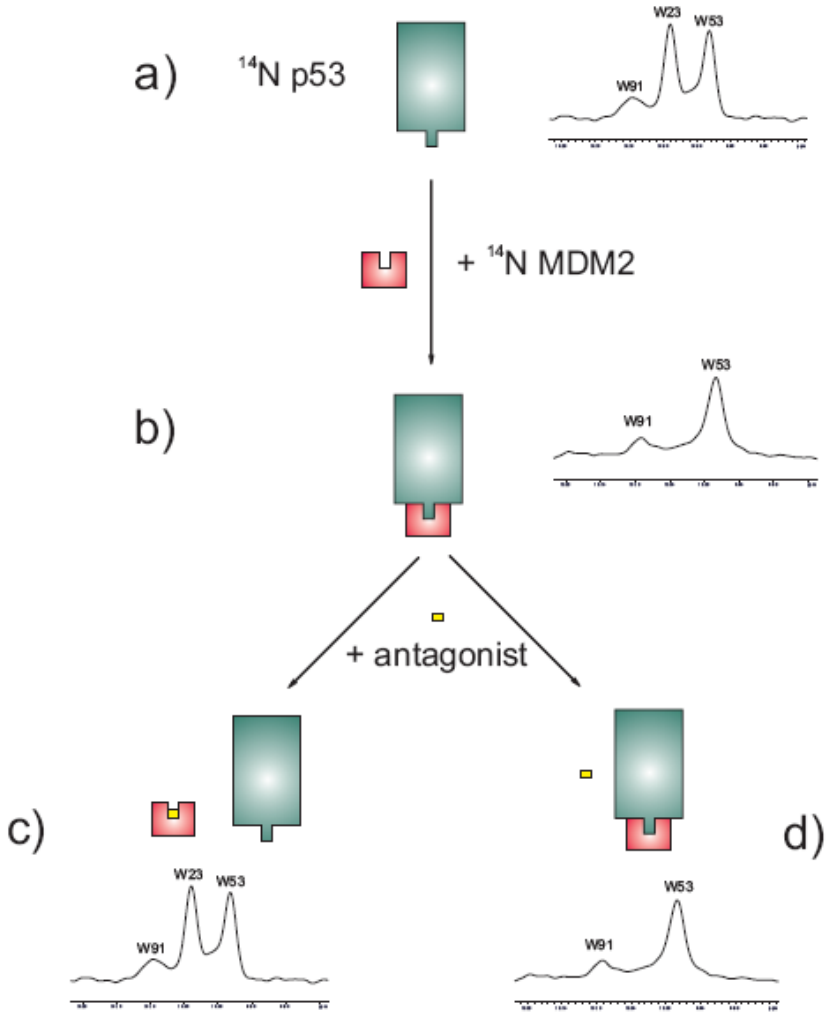

Figure 8. 1D NMR version of the AIDA assay. **(a)** The 1D proton NMR spectrum of the side chains of tryptophans (W) of free p53 (residues 1-321). The N-terminal domain of p53 contains three tryptophan residues: W23, W53, and W91. Because of a highly flexible nature of the very N-terminal segment of p53 between residues 1-73, the side chains of W23 and W53 give rise to sharp lines, because the very N-terminal segment of p53 comprising residues 1-73 has been shown to be very flexible(Lee, H. *et al.*, 2000; Ayed, A. *et al.*, 2001; Dawson, R. *et al.*, 2003). **(b)** Upon forming the complex with MDM2, the signal of W23 disappears. This is because W23, together with the p53 residues 17 to 26, comprise the primary binding site for MDM2. Upon binding, these residues participate in a well-defined structure of a large p53-MDM2 complex, whereas W53 is still not structured when p53 is bound to MDM2 (D'Silva, L. *et al.*, 2005b; Krajewski, M. *et al.*, 2007b; Rothweiler, U. *et al.*, 2008). Thus, the observed chemical shift is different and 1/T2 transverse relaxation rate of the bound W23 in the complexes increases thus significantly and broadening of NMR resonances results in the disappearance of this signal in the spectra (D'Silva, L. *et al.*, 2005a; Krajewski, M. *et al.*, 2007a; Rothweiler, U. *et al.*, 2008).

(c) Disruption of the p53-MDM2 interaction results in the release of free p53 and the recovery of the $W23^{p53N}$ H^{ε} signal. The height of W23 peak corresponds to the fraction of free p53 and thus, when total concentrations of the complex and the antagonist are known, the K_i of the MDM2-antagonist interaction can be determined from a single competition experiment (Wang, Z.X., 1995; Krajewski, M. *et al.*, 2007a). **(d)** A weak inhibitor does not dissociate the complex.

4.4. FP-assay

The FP-assay for the p53-MDM2 interaction was established at first by Zondlo *et al.* (2006). The same fluorescent peptide was used in the screenings of MDM2 inhibitors. The Zondlo peptide has an affinity of 15 nM towards MDM2. For screening MDMX inhibitors, the P4 peptide published by Hu *et al.* (2007) was used. Later, FP measurements with MDMX were performed with the P6 peptide published by Phan *et al.* (2010), because of its higher affinity.

Due to the fact that the range of the resolvable inhibitor potency measured in FP is determined by the solubility of an inhibitor and the affinity constant of the fluorescent labeled reporter peptide (Huang, X., 2003), it is important to make a binary titration of the protein with the peptide before measuring the affinity of putative Inhibitors. The binary titration was performed with a constant amount of a peptide and increasing amounts of MDM2 and alternatively MDMX. The affinities of the peptides to MDM2 or MDMX are listed in Table 2.

Table 2. Affinities of the peptides to their targets

Protein	Fluorescent peptide	K_D [nM]
MDM2	Zondlo	15
MDMX	Zondlo	>100
MDM2	P4	5.6
MDMX	P4	40.8
MDMX	P6	35

4.5. Novel Inhibitors following the 3-point pharmacophore model

4.5.1. Binding affinities of the alkaloid-like scaffold

One of the scaffolds designed with the Anchor.Query and synthesized by the Ugi multicomponent reaction was a scaffold with an alkaloid-like skeleton. The binding affinities of these compounds towards MDM2 and MDMX were measured by FP and AIDA and are shown in Table 3 and Table 4.

Table 3. Binding affinities of compound 8 derivatives.

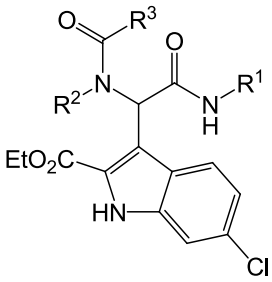

ID	R^1	R^2	R^3	FP K_i(μM)	FP plots	AIDA (μM)
8a	benzyl	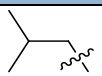	Me	n.i.		> 50
8b	benzyl	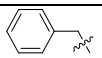	Me	n.i.		30
8c	benzyl		Me	4	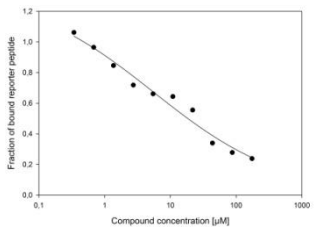	1.8
8d	benzyl		Me	6	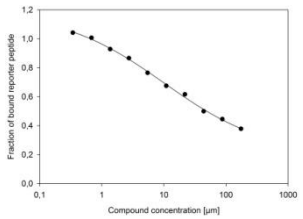	17
8e	cyclohexyl		Me	2	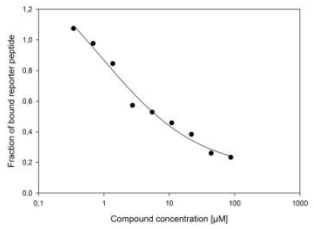	1.7

8f	cyclohexyl	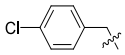	Me	22	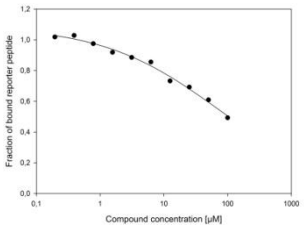	
8g	cyclohexyl	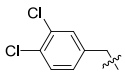	Me	9	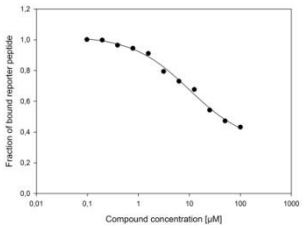	
8h	cyclohexyl		^{n}Pr	25	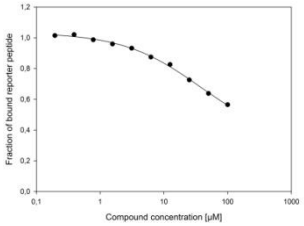	
8i	cyclohexyl		H	14	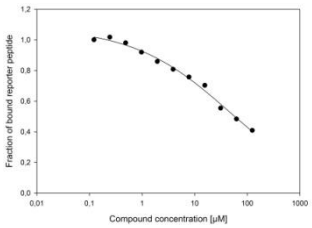	
8j	cyclohexyl	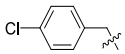	H	50		
8k	cyclohexyl	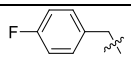	H	30		
8l	*tert*-butyl	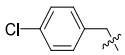	H	1.8	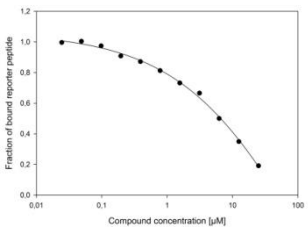	

8m	*tert*-butyl	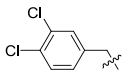	H	4	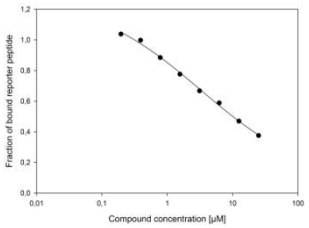	
8n	*tert*-butyl	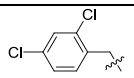	H	10		
8o	*tert*-butyl	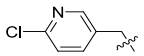	H	2.7	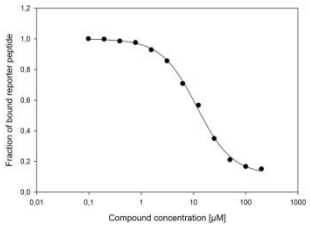	
8p	*tert*-butyl	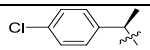	H	n.i.		
8q	*tert*-butyl	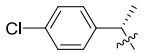	H	8	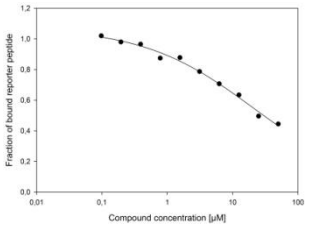	
8r	*tert*-butyl	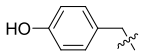	H	11	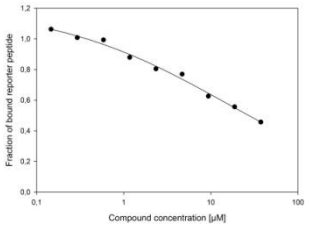	
8s	*tert*-butyl	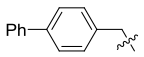	H	n.i.		
8t	*tert*-butyl	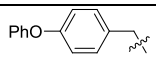	H	n.i.		

* The abbreviation n.i. stands for “no interaction”.

Table 4. Binding affinities of compound 9 derivatives.

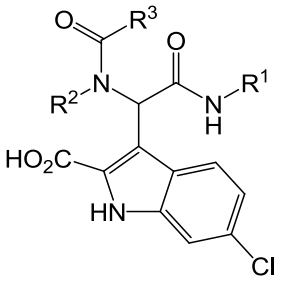

ID	R^1	R^2	R^3	FP K_i(μM)	FP plots	AIDA (μM)
9e	cyclohexyl		Me	1.6	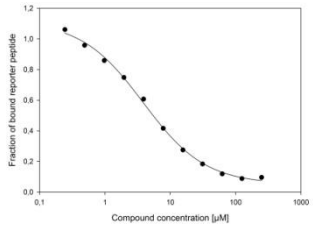	1.7
9i	cyclohexyl		H	1.6	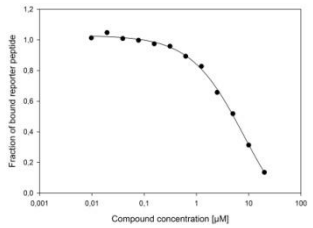	
9j	cyclohexyl	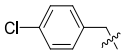	Me	2.3	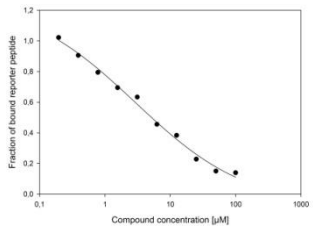	
9k	cyclohexyl	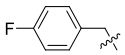	H	n.d.		
(±)9l	*tert*-butyl	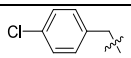	H	0.4		0.4
(+)9l	*tert*-butyl	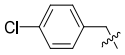	H	0.4	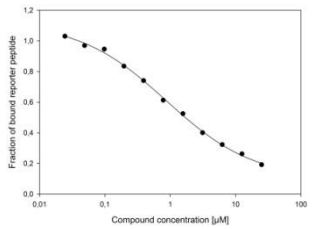	0.3
(-)9l	*tert*-butyl	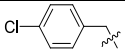	H	0.4		0.7

9m	*tert*-butyl	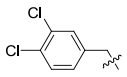	H	0.6	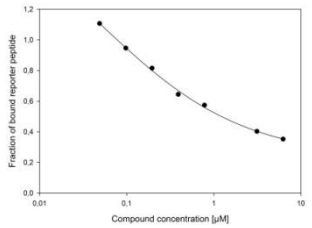	
9n	*tert*-butyl	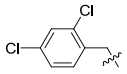	H	0.5	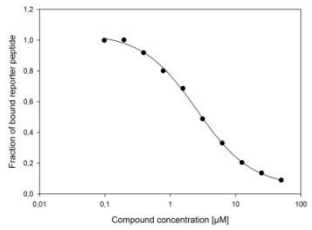	
9o	*tert*-butyl	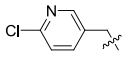	H	4	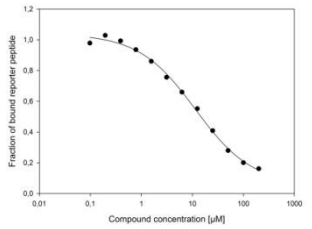	
9p	*tert*-butyl	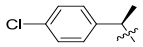	H	10.5	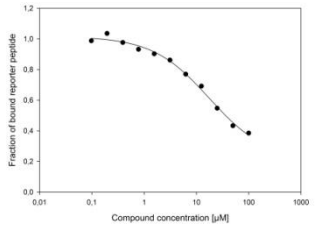	
9q	*tert*-butyl	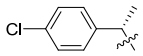	H	0.9	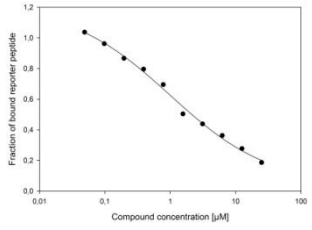	
9r	*tert*-butyl	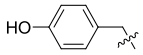	H	11	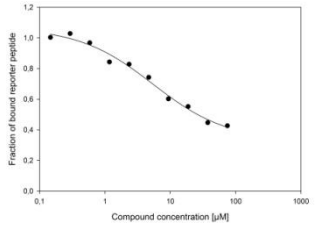	
9s	*tert*-butyl	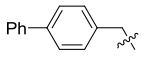	H	2.5	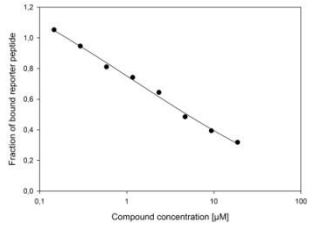	

9t	*tert*-butyl	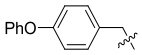	H	4.4	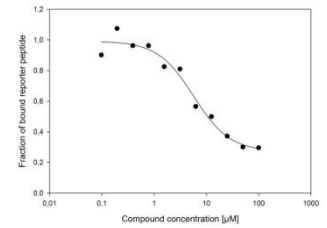	

* The abbreviation n.d. stands for “not determined”.

The exhaustive analysis on this scaffold by FP and NMR led to the following conclusion: In contrast to compound 8a (AIDA K_D>50 µM), compound 8b (AIDA K_D of 30 µM) was identified as a hit with weak binding affinity to MDM2. Based on this result compounds 8c-g were synthesized. The introduction of 6-Cl to the indole fragment seems to increases the binding affinity towards MDM2 (Garcia-Echeverria, C. *et al.*, 2000). Compound 8e (AIDA K_D of 1.7 µM and FP K_i of 2 µM) showed low micromolar binding affinity towards MDM2. Encouraged by these results, compounds 8h-t were synthesized with different substitutions. The R1-rest (benzyl, cyclohexyl, and tert-butyl) was designed to occupy the Phe19 pocket of MDM2. However, the binding is more sensitive to the hydrophobic fragment introduced by the amine (R2), which was designed to occupy the Leu26 pocket of MDM2. The binding is also influenced by the fragment introduced by the acid component (R3); small substituents (H and Me) were well tolerated. Compound 8l was found to be the most potent one in this series (Table 3).

As the introduction of solubilizing substituents can improve the water solubility of imidazolines and imidazoles while retaining or improving p53-MDM2 antagonistic activity (Srivastava, S. *et al.*, 2009; Huang, Y. *et al.*, 2010; Popowicz, G.M. *et al.*, 2010a), the ethyl esters were exchanged for the more soluble carboxylic acid. The binding affinities of these compounds, referred as compounds 9, improved overall compared to the parent ethyl ester. Compound 9l was found as the most potent inhibitor in this series (Table 4).

In order to explore the role of the fragment introduced by acid (R3) in the protein binding, the compounds 10, 11a, and 11b were synthesized. Compound 10 (K_i of 12µM) and 11a (K_i of 0.9 µM), as well as compound 11b (K_i of 0.7 µM), which was derived from compound 9l (K_i of 0.4 µM), have similar affinities suggesting that the formyl group is not necessary for the interaction with MDM2 (Figure 9).

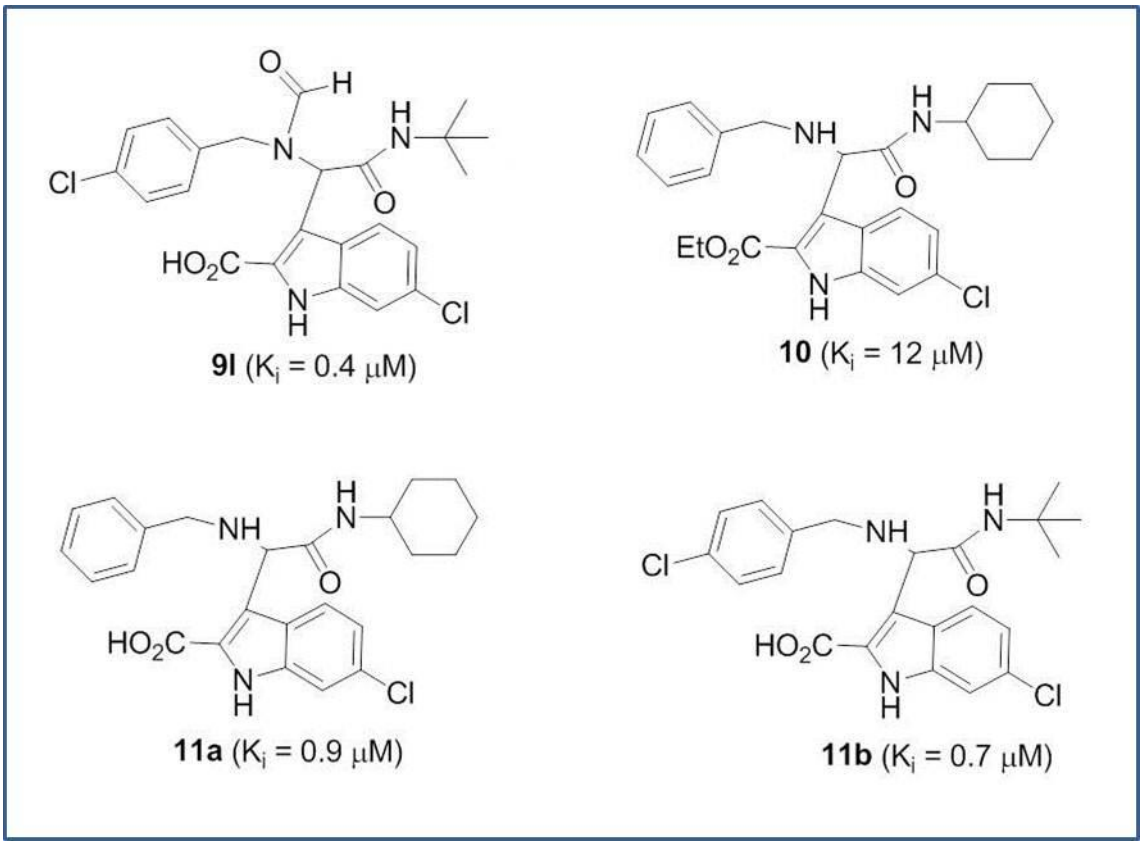

Figure 9. Chemical structures of compounds: 9l, 10, 11a and 11b.

Compounds 13a and 13b were synthesized by amine coupling with compound 8e (Figure 10) (Srivastava, S. *et al.*, 2009; Huang, Y. *et al.*, 2010). However, these compounds showed that the introduction of an amide in this class of compounds leads to a decrease in the binding affinity by 2-3 fold.

Interestingly, none of the compounds 8 or 9 showed comparable binding affinity towards MDMX, although MDMX shows significant overall sequence and very close shape similarity to the p53 binding site.

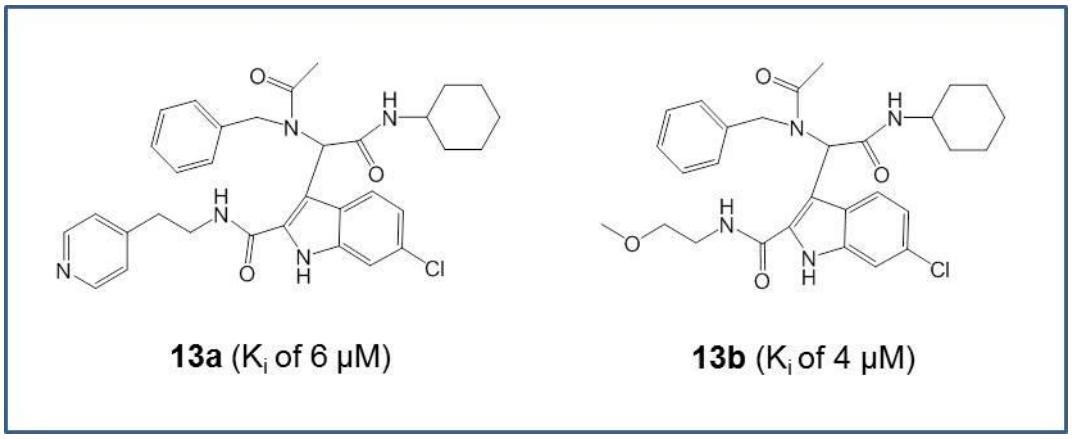

Figure 10. Chemical structures of compounds: 13a and 13b.

4.5.2. Binding affinity of compound 9l measured with HSQC

The most active compound 9l was separated into the enantiomers. NMR experiments, using [^{1}H, ^{15}N] HSQC spectra were performed with ^{15}N-labeled MDM2. The more potent enantiomer (+)-9l (K_i of 300 nM) was titrated against MDM2 (Figure 11). The Spectrum maps the backbone amide groups of the MDM2 Protein according to their proton and nitrogen frequencies. As every proton bound directly to nitrogen shows a peak in the HSQC spectrum, each signal corresponds to an amino acid residue in the protein (excluding Proline, as it is devoid of a proton bound nitrogen and residues like Tryptophan that have nitrogen containing side chains) (Rehm, T. *et al.*, 2002).

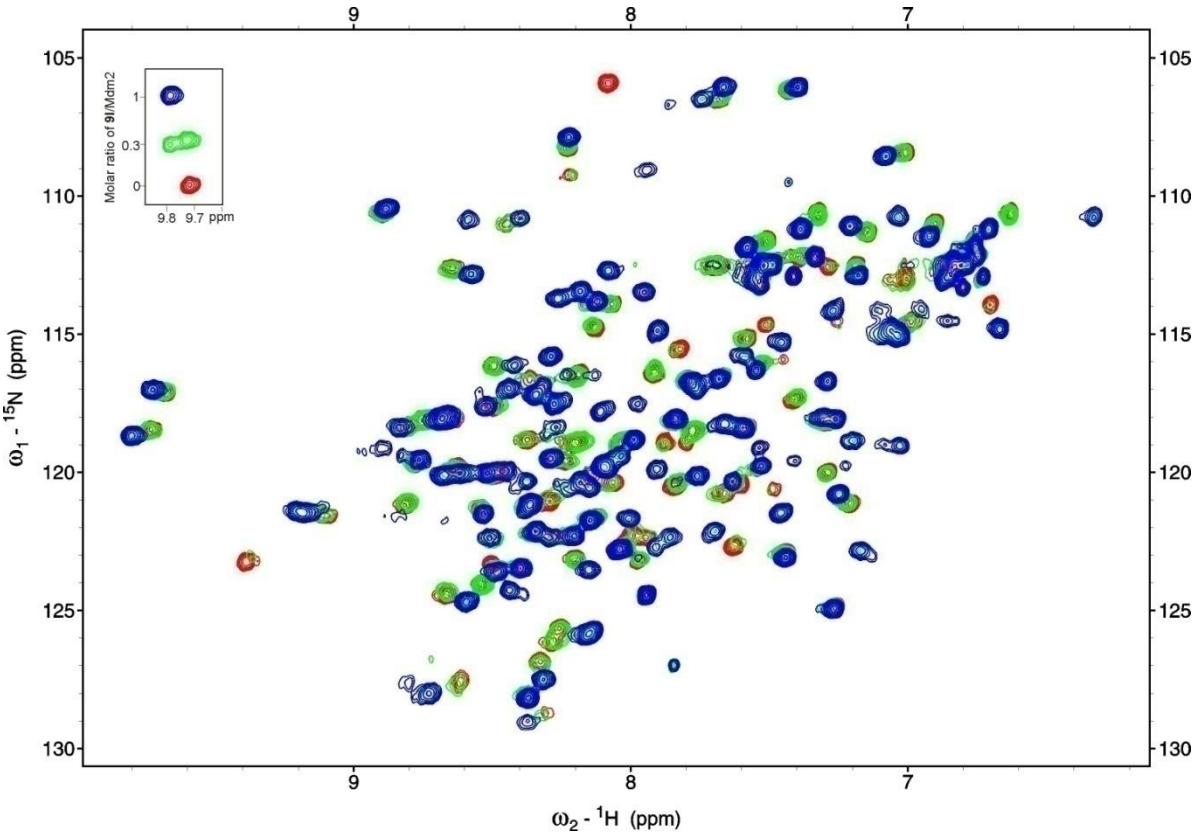

Figure 11. Superposition of NMR HSQC spectra of ^{15}N-labeled MDM2 titrated against the stronger binding enantiomer (+)-9l. The spectrum of free MDM2 is shown in red. The spectrum of (+)-9l-MDM2 (intermediate ratio, 3:10) is shown in green, and the spectrum of (+)-9l-MDM2 (final ratio, 1:1) is shown in blue. The inset shows the cross-peaks at ca. 118.5 ppm in the 15N dimension and 9.7 ppm in the 1H dimension, which demonstrates tight binding of (+)-9l to MDM2.

Changes in the chemical shifts were observed comparing the HSQC spectra of the free protein with the spectra after ligand titration. The here observed “slow” chemical exchange – two peaks originating from the “bound” and “free” form of the protein are present – indicate that the K_D is in submicromolar range, assuming that the bimolecular association is limited only by diffusion for interactions of the small molecule with the protein (Wüthrich, K., 1986; Fersht, A.R., 1998; Rehm, T. *et al.*, 2002).

4.5.3. Ligand Efficiency

Ligand efficiency reflects the aim of medical chemistry to keep the molecular weight of a ligand small to enhance chances of oral bioavailability. At the same time receptor affinities should be as high as possible to reduce the doses of the drug. Binding

efficiency index (BEI) describes the binding affinity of a given ligand to its receptor taking into account the molecular weight (MW) of the ligand.

$$BEI = \frac{pK_i}{MW} = \frac{-\log K_i}{MW} \frac{[M]}{[kDa]}$$

The lead compound (+)-9l (molecular weight: 475 Da.) has a binding efficiency index of 13.7, which indicates the best ligand efficiency compared with other published and cocrystallized p53-MDM2 antagonists (Table 5, Figure 12). The water solubility of 9l was determined as 1.3 mg/mL (Wolf S., *et al*., submitted). These properties suggest reasonable drug-like properties of a lead compound serving for further optimization.

Table 5. Ligand efficiency.

	Ligand	PDB/ID	K_i (µM)	MW (Da)	BEI	
1	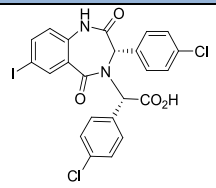	1T4E	0.067	566	12.7	(Grasberger, B.L. *et al.*, 2005)
2	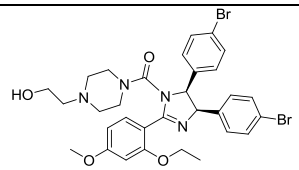	1RV1	0.09	581	12.1	(Vassilev, L.T. *et al.*, 2004)
3	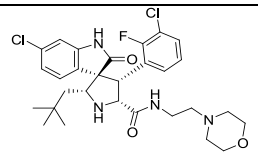	3LBL	0.036	577	12.9	(Popowicz, G.M. *et al.*, 2010a)
4	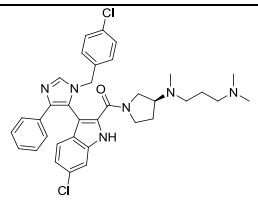	3LBJ	0.11	630	11.0	(Popowicz, G.M. *et al.*, 2010a)

5	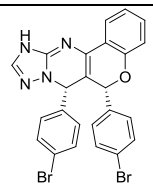	3JZK	11	536	9.3	(Allen, J.G. *et al.*, 2009)
6	 p53 residues 15-29	1YCR	0.6	1808	3.4	(Kussie, P.H. *et al.*, 1996)
7	 Stapled peptide	SAH-p53-8	0.055	2180	3.3	(Bernal, F. *et al.*, 2007)
8	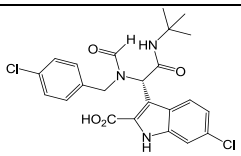	9l	0.3	475	13.7	

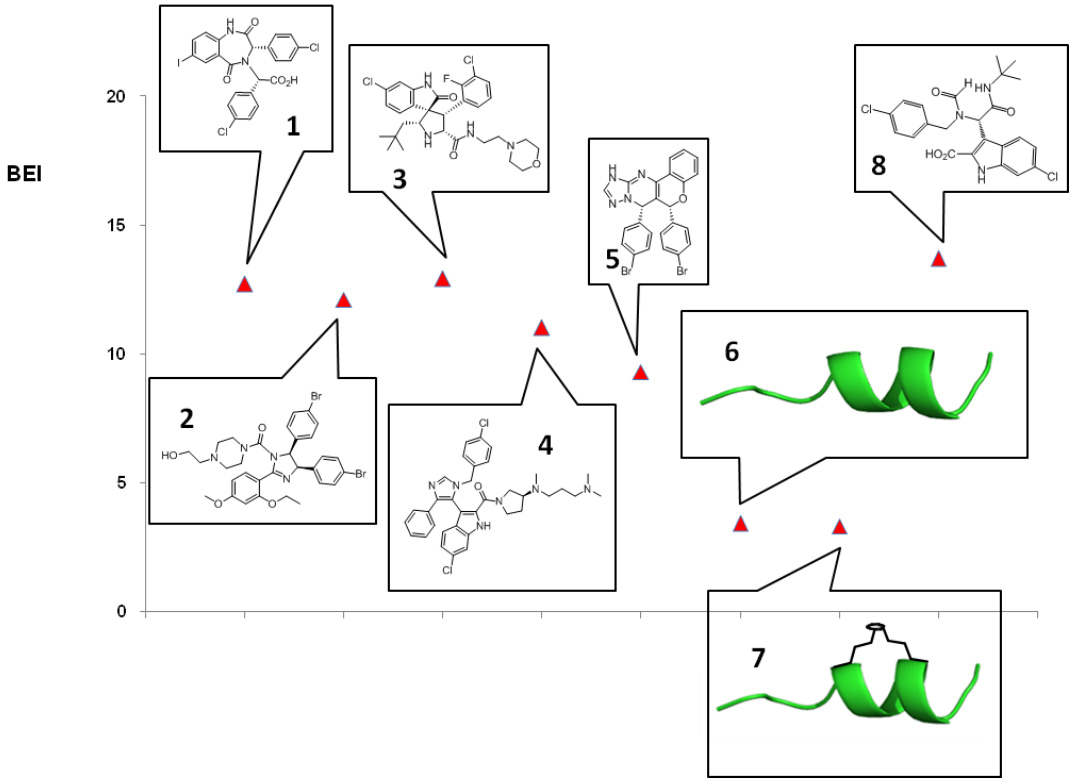

Figure 12. Analysis of ligand efficiency. Two classes of ligand efficiency can be observed. Whereas the small molecules show LE of 10-14, the peptide derived inhibitors tend to have low LE of ~3.4 due to their high molecular weight.

4.5.4. Crystal structure of the MDM2-9l complex

It was possible to cocrystallize compound 9l with $MDM2_{18-111}$. The crystal was grown in 0.15 M potassium bromide and 30% (w/v) polyethylen glycol monoethyl ether 2000 solution pH 8.0 at 4°C. After 2 weeks needles were observed. The crystals were frozen using 10 % of polyethylen glycol as cryoprotectant and measured in the Swiss Light Source (SLS) synchrotron in Villigen, Switzerland. The crystal diffracted up to 2.2 Å. The structure was solved using CCP4 and Mifit for molecular modeling, fitting, and refinement of the protein structure.

The enantiomer (*S*)-9l cocrystallized and binds into the well-established p53-MDM2 binding pocket (Figure 13) (Kussie, P.H. *et al.*, 1996). The indole anchor of (*S*)-9l binds in the Trp23 pocket of MDM2. The good alignment of the two indoles of (*S*)-9l and Trp23 (RMSD of 0.65 Å) is consistent with the prediction of the ANCHOR.QUERY approach.

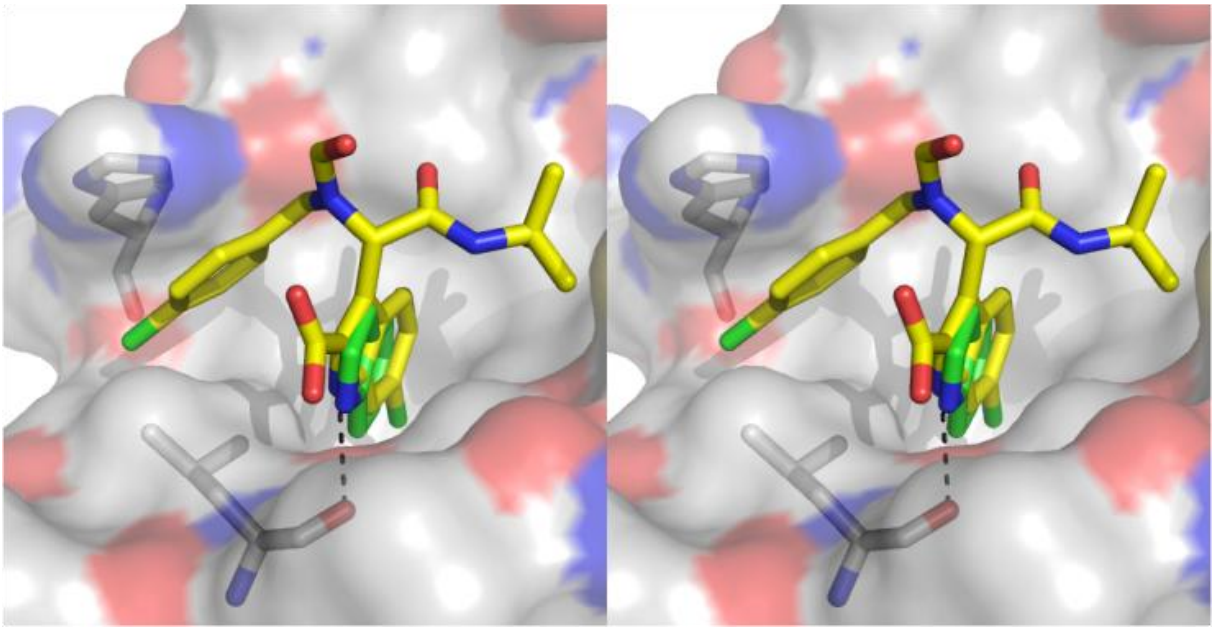

Figure 13. Stereo picture of the cocrystal structure of (*S*)-9l (yellow sticks) in MDM2 (grey, blue and red surface with the amino acids His96 and Leu54 shown as sticks). For comparison, the indole ring of Trp23 from the p53-MDM2 complex (PDB ID: 1YCR) is aligned and shown in green sticks. The hydrogen bond between the indole fragment and the carbonyl of Leu54 is indicated by a black dotted line (d = 2.95 Å).

The compound (*S*)-9l binds into the p53 binding site in MDM2. The different moieties of the molecule undergo mostly hydrophobic, π-stacking, few hydrophilic interactions

and one hydrogen bond contact (Trp23-Leu54) to the amino acids in the binding pockets which are exemplified in the following and should serve to understand the affinity of the molecule to its receptor:

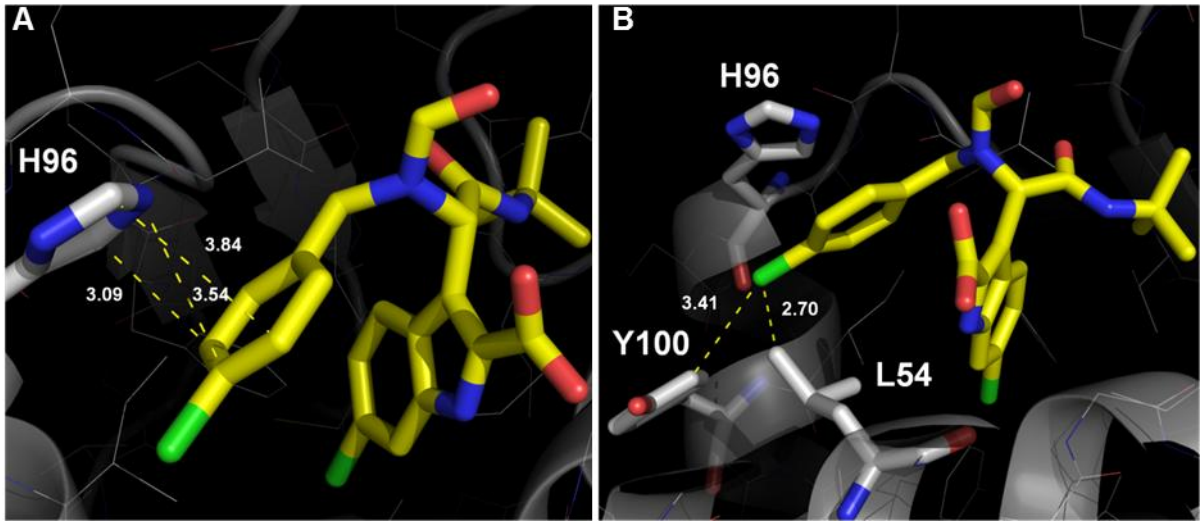

Figure 14. A) π-Stacking interactions of the benzyl group of (*S*)-9l with His96 (sticks). Selected distances are indicated as yellow dotted lines. **B)** 4-Chlorophenyl contacts.

The 4-chlorobenzyl group is penetrating deeply into the Leu26 pocket of MDM2. The 4-chloro substituent undergoes a variety of short contacts with Leu54 (2.7 Å) and Tyr100 (3.4 Å) (**Error! Reference source not found.**B). The shortest distance of the lolride to His96 imidazole is 4.1 Å. All crystallographically described MDM2 ligands have a halogen phenyl group in this pocket (Fry, D.C. *et al.*, 2004; Vassilev, L.T. *et al.*, 2004; Grasberger, B.L. *et al.*, 2005; Allen, J.G. *et al.*, 2009). It is aligned almost perfectly parallel to the π-electron rich imidazole ring of His96 (**Error! Reference ource not found.**A). The planes of the two aromates are shifted in a way that the center of the imidazole is approximately above the C-4 of the benzyl group. Representative short contacts are between 3.1 to 3.8 Å. These distances are well between what is observed with other π-π interactions (Meyer, E.A. *et al.*, 2003; Bissantz, C. *et al.*, 2010; Salonen, L.M. *et al.*, 2011). It is interesting to note that the parallel-displaced stacking arrangements are predominately found for two interacting π-systems. Short contacts between His and a phenyl ligand can be observed frequently in the PDB and a recently (06/12/2011) performed RELIBASE search for His-imidazol ligand-phenyl contacts <4Å resulted in 1.000 hits (Hendlich, M. *et al.*, 2003). All other small molecules binding to MDM2 feature a halogenated phenyl group in the same pocket and show parallel alignment with His96.

The two amide groups of (*S*)-9l do not undergo hydrogen bond contacts to the receptor. The formyl group rather points towards the solvent space, indicating that the introduction of solubilizing or affinity-enhancing groups at this position might be useful for further optimization.

The indole moiety of compound (*S*)-9l is a mimic of p53's Trp23. It is deeply embedded into a hydrophobic binding site but it also forms a hydrogen bond to the Leu54 carbonyl (2.95 Å) identical to Trp23. The reminder of the contacts is of hydrophobic nature. Short contacts to amino acids of the receptor are indicated in Figure 15A. Leu54 is making short contacts to both, the benzyl and indole portions of (S)-9l. Other contacting amino acids are Phe91, Val93, Ile99 and Ile61.

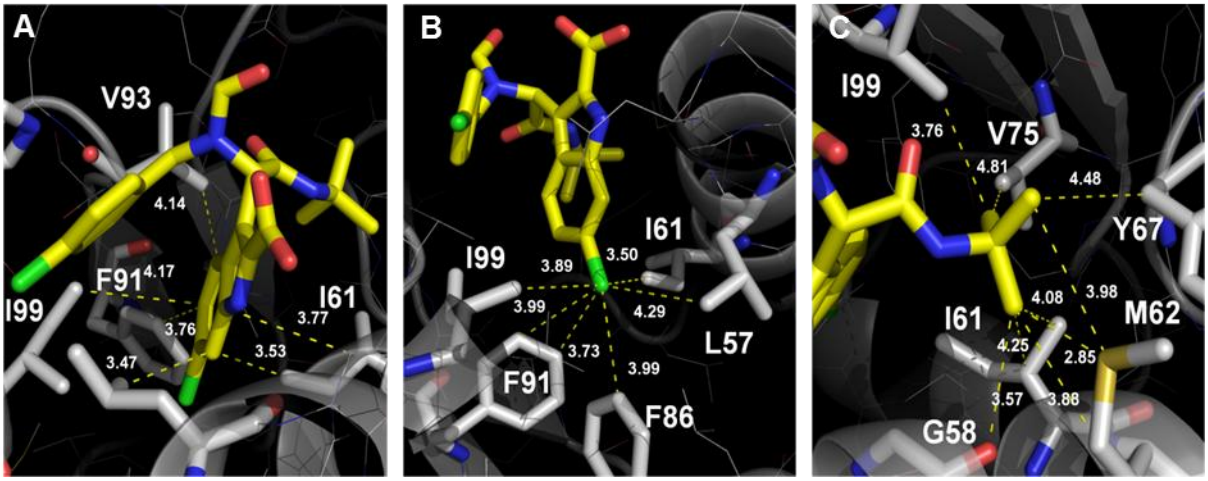

Figure 15. A) Hydrophobic indole contacts. **B)** 6-Chloroindole contacts. **C)** tert-Butyl contacts.

The 6-chloro substituent of the indole is at the very bottom of the pocket and fills a small but very hydrophobic portion which is void in the wild type p53 MDM2 structure (Figure 15B). All crystallographically described MDM2 ligands have a halogen phenyl group or halogen (ox)indole substructure in this pocket (Vassilev, L.T. *et al.*, 2004). Thus filling this hydrophobic part has been recognized early on to increase binding affinity (Garcia-Echeverria, C. *et al.*, 2000).

The bulky *tert*-butyl substituent, finally, occupies the Phe19 pocket in MDM2. Plenty of short contacts are made to the surrounding hydrophobic amino acids including Ile99, Ile61, Gly58, Met62, Tyr67 and Val75 (Figure 15C). Noteworthy, there is a very short CH_3-S contact of 2.85 Å involving Met62.

Table 6. Data collection and refinement statistics of compound 9l.

Data collection	
Space group	$P2_1$
Cell constants (Å)	a = 32.44
	b = 58.88
	c = 49.51
	β = 99.208
Resolution range (Å)	50 – 2.1
Wavelength (Å)	0.9786
Observed reflections	38681
Unique reflections	10740
Whole range	
Completeness (%)	98.8
R_{merge}	12.5
$I/\sigma(I)$	8.34
Last shell	
Resolution range (Å)	2.1 – 2.2
Completeness (%)	99.9
R_{merge}	31.6
$I/\sigma(I)$	4.48
Refinement	
No. of reflections	9155
Resolution (Å)	19 – 2.1
R-factor (%)	22.34
R_{free} (%)	30.8
Average B (Å^2)	14.4
R.m.s.d. bond length (Å)	0.015
R.m.s.d. angles (°)	1.707
Content of asymmetric unit	
No. of protein-ligand complexes	2
No. of protein residues/atoms	183/1508
No. of solvent atoms	150

4.6. Novel Inhibitors following the 4-point pharmacophore model

The analysis of compounds belonging to the peptidomimetic scaffold led to the discovery of the high affinity compound KK271.

4.6.1. Binding affinity of compounds KK271 and YH300

The binding affinities of the compounds KK271 and the later discussed YH300 towards MDM2 were measured by FP and are shown in Table 7.

Table 7. Binding affinities measured by FP-assay.

ID	K_i [µM]	FP plots
KK 271	1.2	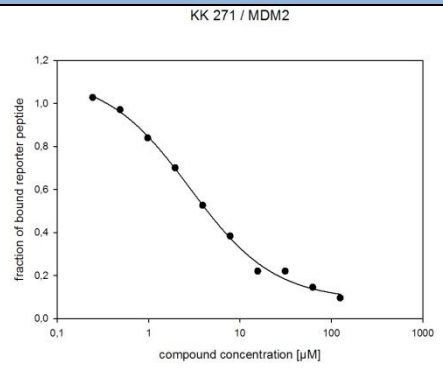
YH300	0.6	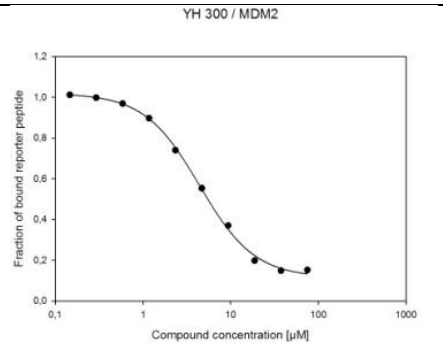

4.6.2. Crystal structure of the MDM2-KK271 complex

KK271 (Figure 16) was initially designed to mimic the critical p53 side chains: Phe19, Trp23, Leu26, thus complying with the “closed” MDM2 conformation and a 3-point pharmacophore model (Domling, A. *et al.*, 2010). The chloroindole moiety of KK271 was used as the “anchor” of the interaction to stably bind into the Trp23 cavity. The phenyl and isobutyl groups were introduced to mimic the Phe19 and Leu26 side

chains, respectively. Surprisingly, however, the cocrystal structure of the $MDM2_{18-111}$-KK271 complex revealed two inhibitor molecules bound to a single MDM2 protein chain (Figure 17). Cocrystallization of a protein with additional molecules of non-specifically bound inhibitors or buffer ingredients is observed frequently; however, this structure reveals that while the first molecule KK271A is specifically bound to the p53 pocket mimicking the native p53 amino acid triad, the second molecule, KK271B, is only partially bound and partially trapped by crystal contacts, using a new binding site that is easily accessible by the ligand. It induces a hydrophobic pocket outside the direct p53 interacting area, adding a fourth point to our pharmacophore model, thereby contributing significantly to the binding energy. The overall fold of MDM2 is similar to the native p53-MDM2 complex with the main-chain RMSD of 0.69 Å.

The binding mode of the first molecule KK271A is in good agreement with the Anchor.Query prediction and fulfills the predicted 3-point pharmacophore model.

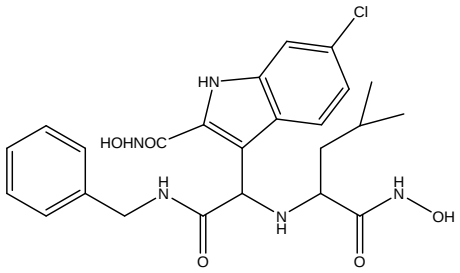

Figure 16. Chemical structure of compund KK271.

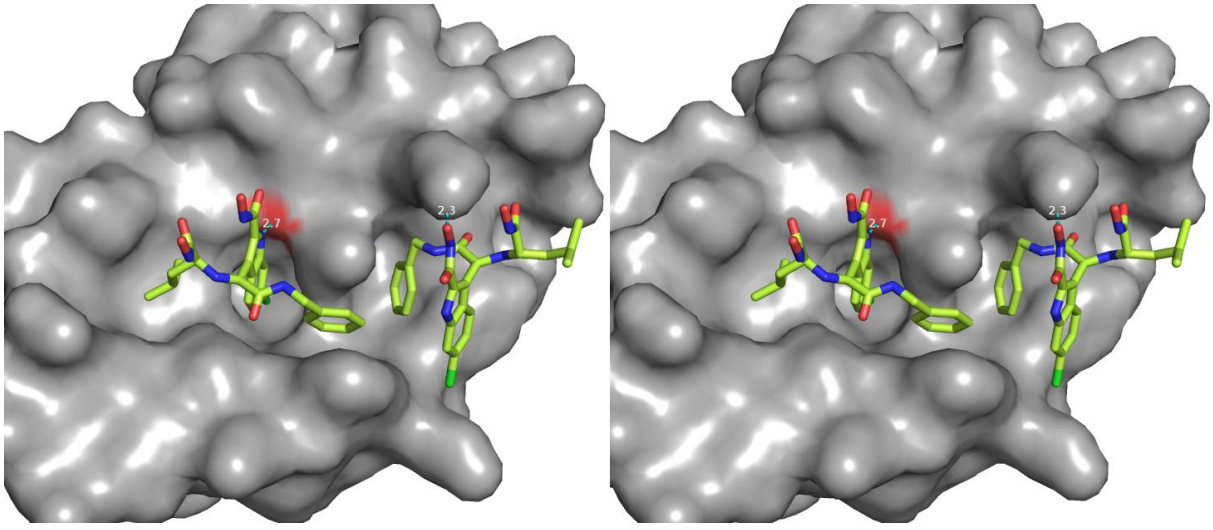

Figure 17. Stereopicture of two KK271 molecules (green sticks) bound to MDM2 (gray surface). Hydrogen bonds are shown as blue dotted lines.

The Trp23 pocket is filled with the 6-chloroindole-2-hydroxamic acid moiety in a way identical to the Trp23 indole moiety of p53 and forms hydrogen bond with the Leu54 carbonyl oxygen and extended hydrophobic contacts to Val93, Gly58, Leu54 (Figure 18A). The benzyl and isobutyl substituents of KK271 naturally resemble the p53 amino acids Phe19 and Leu26; however, the isobutyl side chain turns out to fill the Phe19 pocket and the benzyl moiety is binding within the Leu26 pocket. This represents a mirror image of the native p53 interaction with an indole moiety as a plane of symmetry. Such an rearrangement has been also described for another Mdm2 inhibitor (Popowicz, G.M. *et al.*, 2010a) .

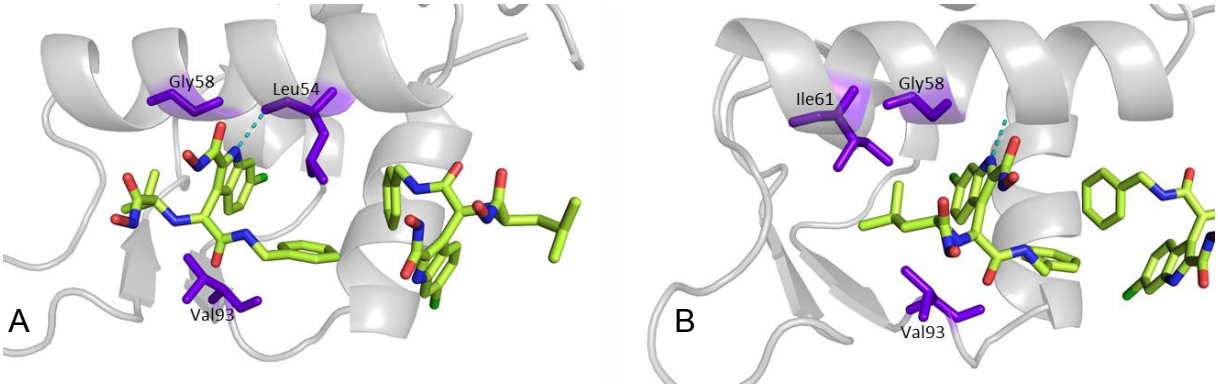

Figure 18. Picture of compound KK271 (green sticks) bound to the hydrophobic cleft of MDM2 (gray cartoon) **A)** The 6-chloroindole-2-hydroxamic acid moiety of the first inhibitor forms a hydrogen bond (blue dotted line) with the Leu54 carbonyl oxygen and undertakes extended hydrophobic contacts to Val93, Gly58, Leu54 (purple sticks). **B) The Isobutyl side chain of the first molecule undertakes** hydrophobic interactions to the MDM2 residues Ile61, Val93 and Gly58 (purple sticks).

The isobutyl side chain is filling the Phe19 pocket by forming hydrophobic contacts to Ile61, Val93 and Gly58 (Figure 18B). A loose fit of the inhibitor in this area suggests a way of improving the affinity by replacement of the isobutyl moiety by other branched hydrophobic groups. The mode of binding of the benzyl group to the Leu26 pocket substantially differs from other known inhibitors of the p53-MDM2 interaction; due to the length and flexibility of the scaffold; this part of the molecule binds close to helix IV (for helix numbering please refer to Figure 19) of MDM2 and is involved in a parallel aromatic stacking contact with His96 of MDM2, with a distance between the rings of 3.7 Å (Figure 20A). Similar π-stacking contacts are observed in a spirocyclic indolone and a chromenotriazolopyrimidine, but not in the imidazole, Nutlin and benzodiazepinedione structures (Vassilev, L.T. *et al.*, 2004; Huang, Y. *et al.*, 2011). The central and solvent-exposed peptidic core of the compound does not directly

contact the protein making it a good target for future modifications to improve the drug-likeness.

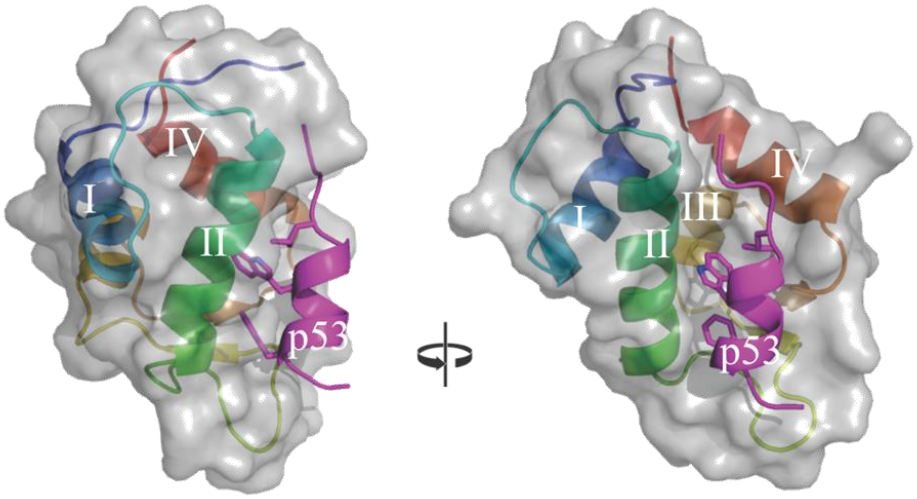

Figure 19. X-ray structure of the p53-MDM2 complex (PDB ID: 1YCR). Numbering of the secondary structure elements in agreements with labels used in the text and after Kussie *et al.* (1996).

While the binding mode of the first inhibitor molecule is analogous to other known antagonists of the interaction and could have been accurately predicted by pharmacophore modeling, the second inhibitor molecule is bound beyond the expected border of the Leu26 pocket. From other MDM2-cocrystal structures it is apparent that the region at the intersection of helices II and IV has hydrophobic character and tendency to be covered with the N-terminal “lid” helix or non-specifically bound inhibitor molecules that often also participate in crystal lattice formation. The benzyl group of the second inhibitor molecule is deeply inserted inside MDM2 forming numerous contacts with side chains of Tyr100, Leu54 and also with the S-methyl group of Met50 (Figure 20B). To accommodate the benzyl group contacts, the residues have to acquire different sidechain conformations. The remaining part of the inhibitor maintains scarce hydrophobic 6-chloroindole-helix IV contacts and a single hydrogen bond between the hydroxamate and the Lys51 side chain (**Error! Reference source not found.**). Analysis of the crystallographic B-actors of the second inhibitor molecule suggests that while the benzyl group is relatively stable bound inside the protein (avg. B = 33 $Å^2$), the remaining atoms of the molecule are to greater degree flexible (avg. B = 40 $Å^2$), and thus less likely to maintain steady contacts with the protein. Binding of the second inhibitor molecule is enabled by the rearrangement of the Tyr100 side chain to the “open” conformation

(χ_1 angle = -171°), that doubles the size of the Leu26 pocket. The flipping of the Tyr100 side chain constrains Tyr104 (χ_1 = -131°) in a parallel conformation to the Tyr100 side chain-ring-plane. The conformational selection of the second inhibitor molecules is completed by flipping the Leu54 side chain to the anti-conformation (χ_1 = -160°), maximizing the number of van-der-Waals contacts with the benzyl rings of both antagonist molecules.

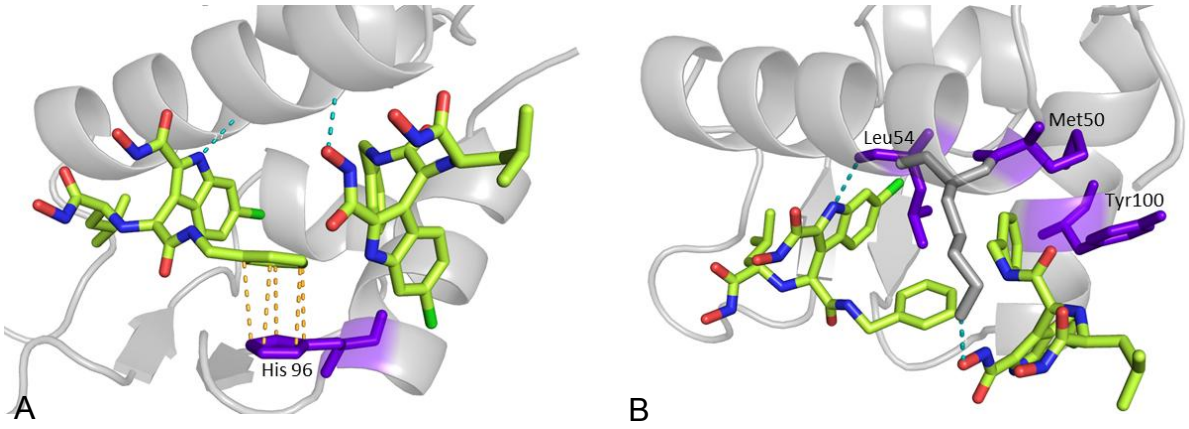

Figure 20. Picture of compound KK271 (green sticks) bound to the hydrophobic cleft of MDM2 (gray cartoon) **A)** The benzyl group of the first antagonist is involved in a parallel aromatic stacking contact (represented by the orange dotted lines) with His96 of MDM2, with a distance between the rings of 3.7 Å. **B)** The benzyl group of the second inhibitor molecule is deeply inserted inside MDM2, forming numerous contacts with side chains of Tyr100, Leu54 and also with the S-methyl group of Met50 (purple sticks). Hydrogen bonds are represented by blue dotted lines. The hydroxamate of the second inhibitor forms a hydrogen bond with the Lys51 side chain of MDM2.

The scale of the conformational rearrangements is best viewed after removing the inhibitor from the model (**Error! Reference source not found.**). The size of the DM2 cleft, which reaches far toward helix IV (Figure 19), is much larger than in other X-ray structures of the inhibitor-MDM2 complexes and is also larger than in the wt-p53-MDM2 complex. Consequently, the structure of the MDM2-KK271 complex represents the most profound example of conformational adaptability of MDM2 to various sizes of ligands.

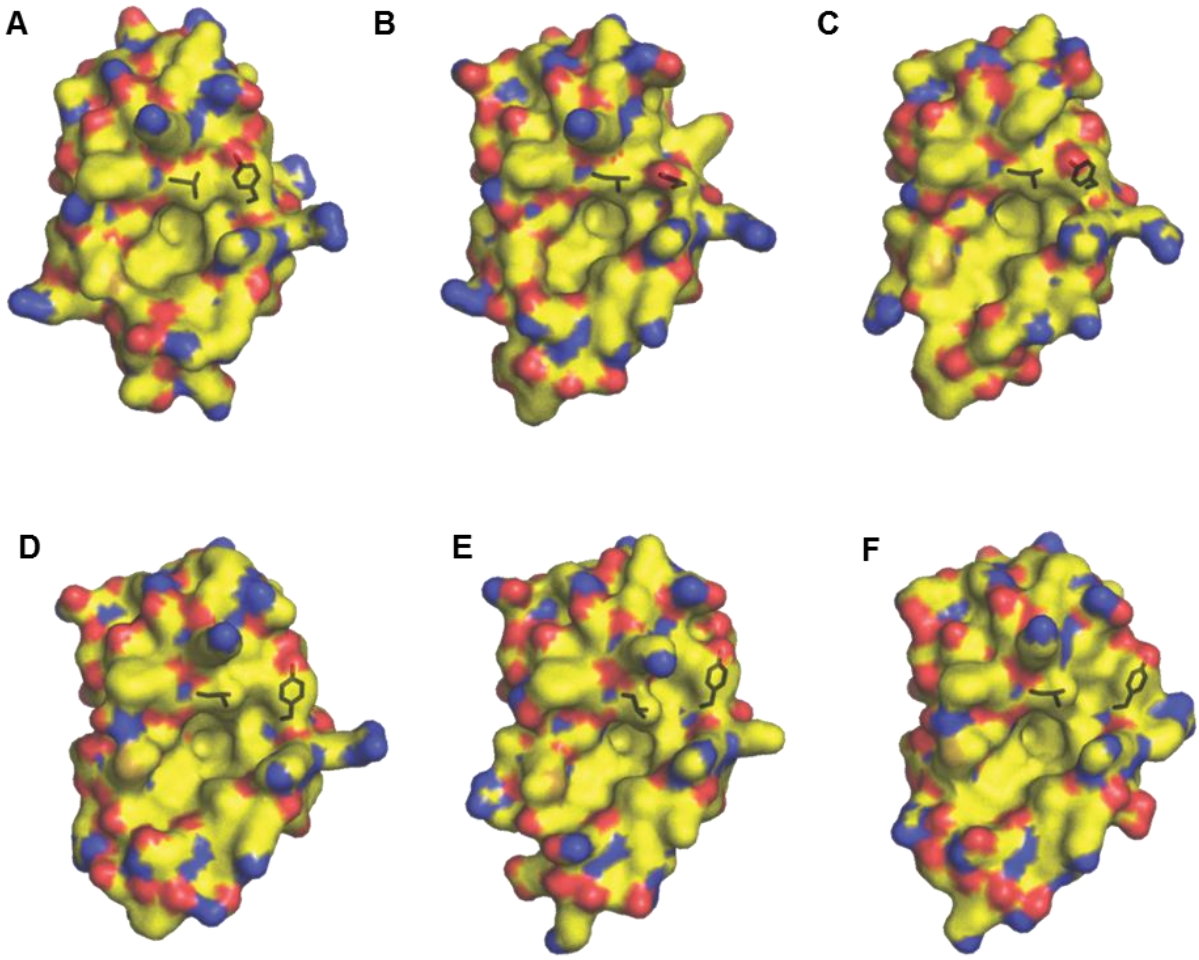

Figure 21. Conformational rearrangements of the N-terminal domain of MDM2 recognizing different ligand scaffolds: **A)**spirooxindole, **B)** cis-imidazoline, **C)** indolo-imidazoline inhibitros, **D)** wt-p53 (16-29), **E)** KK271 and **F)** YH300.

Table 8. Data collection and refinement statistics of compound KK271.

Data collection	
Space group	$P6_522$
Cell constants (Å)	a = 53.52
	b = 53.52
	c = 122.27
Resolution range (Å)	46.35 – 2.14
Observed reflections	63031
Unique reflections	11501

Whole range	
Completeness (%)	97.6
R_{merge}	2.6
$I/\sigma(I)$	32.03
Last shell	
Resolution range (Å)	2.24 – 2.14
Completeness (%)	84.2
R_{merge}	10
$I/\sigma(I)$	9.83
Refinement	
No. of reflections	10366
Resolution (Å)	18.5 – 2.14
R-factor (%)	20.42
R_{free} (%)	22.79
Average B (Å^2)	28.691
R.m.s.d. bond length (Å)	0.0098
R.m.s.d. angles (°)	1.317
Content of asymmetric unit	
No. of protein-ligand complexes	1
No. of protein residues/atoms	84/794
No. of solvent atoms	37

4.6.3. Molecular dynamics simulations of the Leu26 pocket of MDM2

The presence of the second molecule bound to MDM2 in an extended Leu26 pocket prompted us to further investigate the dynamics of this part of the molecule with different ligands bound. Molecular dynamics simulations were performed on the native p53-MDM2, the apo-MDM2, the KK271-MDM2 and the Nutlin-MDM2 structures. The χ_1 angles of His96 and Tyr100 were observed as indicators of the Leu26 pocket shape (**Error! Reference source not found.**). Interestingly only the 53-MDM2 and the later discussed p53-YH300 complex showed a stable conformation of these residues (Tyr100 $\chi_1 \approx -120°$, His96 $\chi_1 \approx -60°$). In the case of the apo-protein, as well as the protein bound to the KK271 and Nutlin inhibitor, the results indicate a flipping of the the sidechains of both residues between two

metastable positions: the “open” (Tyr100 $\chi_1 \approx -120°$) and “closed” (Tyr100 $\chi_1 \approx -90°$) conformations. Furthermore, we have analyzed if the N-terminal fragment of MDM2 that is not observed in most crystallographic structures has an influence on the behavior of the pocket. The molecular dynamics simulations of the complexes with an added N-terminal region showed that while His96 is stabilized by the N-terminal folding over the Leu26 pocket the Tyr100 is still able to switch between the two discrete conformations. Obviously such a situation is not optimal for the ligand binding: The discrete, metastable states have high entropic costs when compared to freely movable sidechains, while hydrophobic interactions are disrupted and do not fully contribute to the binding. We have therefore decided to extend our pharmacophore model by an additional hydrophobic center to fill the extended Leu26 pocket and constrain Tyr100 in a position beneficial for binding. The inhibitor designed on the basis of this extended model was named YH300 and had an improved affinity towards Mdm2.

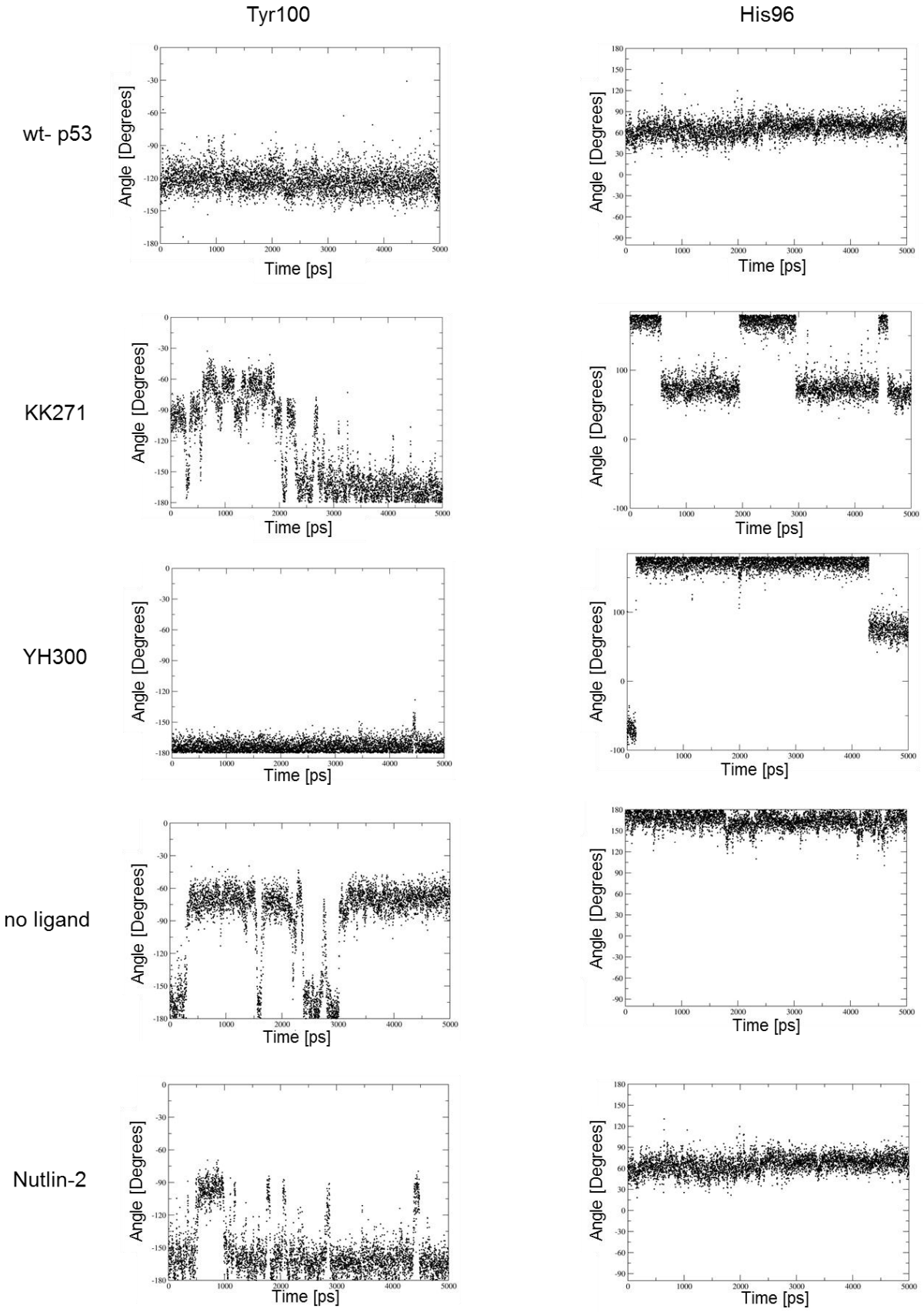

Figure 22. Conformational dynamics of the Tyr100 and His96 side chain upon binding different ligands: wt-p53, KK271, YH300, without ligand and Nutlin-2. The side chain is flipping between two metastable states. wt-p53 and YH300 are able to stabilize its conformation.

4.6.4. Compound YH300

Based on the results of the second molecule of the KK271 structure, which binds according to the 4-point pharmacophore model, compound YH300 (**Error! Reference ource not found.**) was synthesized. This closely related inhibitor, however, based on a different scaffold, exhibits an extended N-terminal region. Compound YH300 should give deeper insights to the N-terminal domain of MDM2, which is not visible in most of the crystallographic structures and show if the extended fragment of the compound could influence on the behavior on the binding pocket.

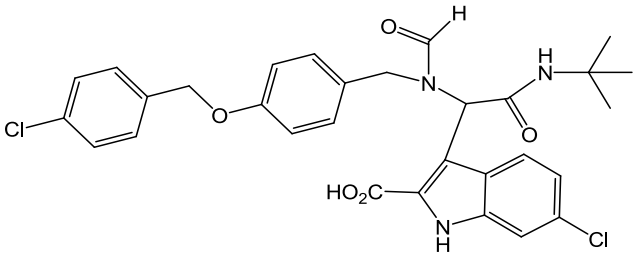

Figure 23. Chemical structure of compound YH300

YH300 was designed to bind and stabilize the “open” MDM2 conformation with higher affinity, due to increased van-der-Waals interaction energy and decreased entropic penalty. The binding affinity was measured by FP-assay (Table 7).

4.6.5. Crystal structure of the MDM2-YH300 complex

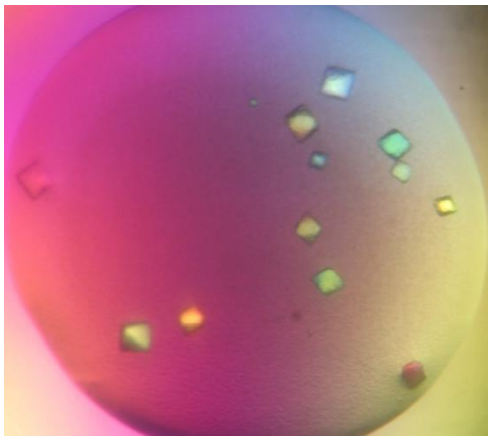

Figure 24. Cocrystals of MDM2 and YH300.

Compound YH300 was cocrystallized with $MDM2_{18\text{-}125}$. The crystals (**Error! Reference ource not found.**) grew at 4°C in 0.2 M dipotassium phosphate and 2,2 M ammonium sulfate. 10% glycerol was added as cryoprotectant.

The crystals turned out to have symmetry $P4_1$ with two protein-ligand complexes in the

asymmetric unit. Despite different crystal contacts between YH270 and KK300, both proteins have very similar structures (with all atom RMSD = 0.07 Å). Particularly the conformations of the inhibitors, as well as all the discussed residues around the inhibitor binding place, are identical in both models. One protein chain binds one single inhibitor molecule (

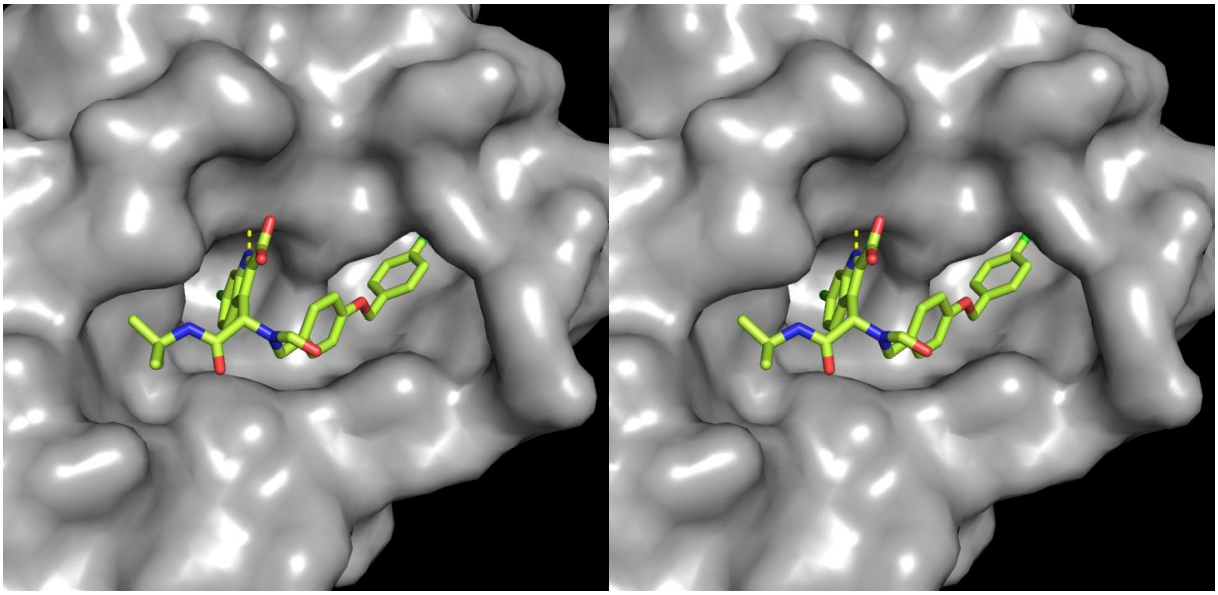

).

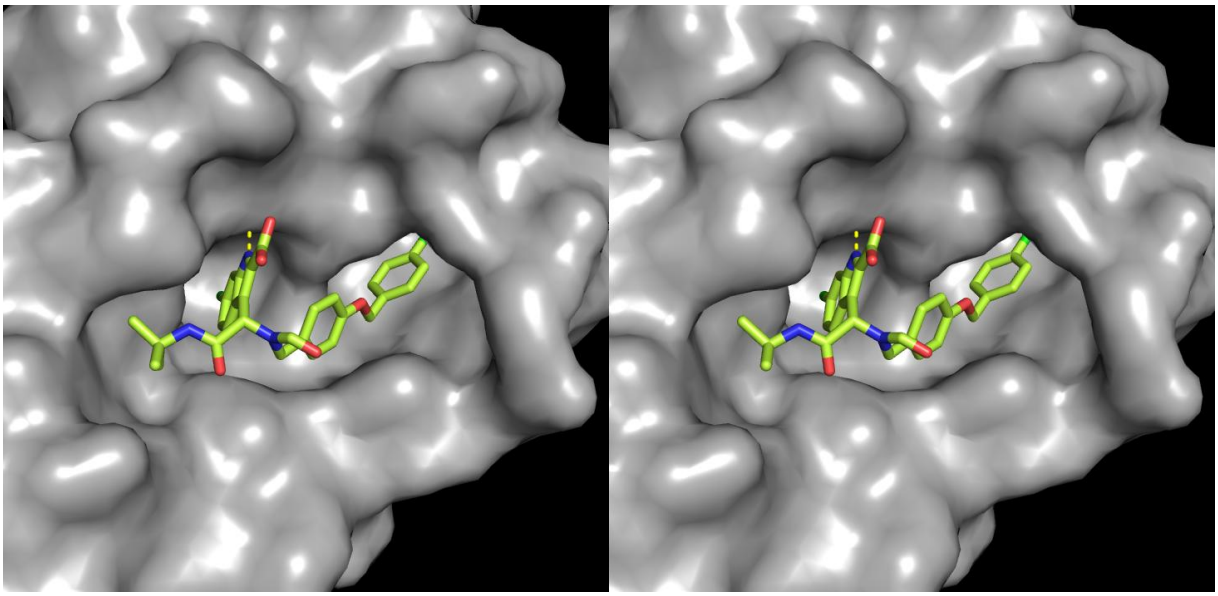

Figure 25. Stereo image of compound YH300 (pink sticks) in MDM2 (surface with lines). The hydrogen bond between the 6-chloroindole moiety and Leu54 is indicated by the yellow dotted line.

The space occupied by the 6-chloroindole ring of YH300 and its surroundings are similar to the structure of the KK271 complex, the depth of penetration of the Trp23 pocket in both structures is the same; however, the planes of the rings are tilted by ca. 18 degrees (**Error! Reference source not found.**). Conformations and positions f MDM2 amino acid side chains in both YH300 and KK271 complexes are the same, and thus, the protein-ligand contacts maintained within the Trp23 subpocket are identical: a hydrogen bond with Leu54 and numerous hydrophobic contacts to Val93, Gly58, Leu54 are seen (**Error! Reference source not found.**A). The Phe19 ubpocket is filled by the aliphatic, bulky and hydrophobic tert-butyl group. Compared to MDM2-KK271, the tert-butyl side chain of YH300 occupies the same space and maintains analogous van-der-Waals contacts to the Ile61 and Val93 side chains of MDM2 (**Error! Reference source not found.**B). The compact structure of the tert-utyl results in a better fit of this moiety to the Phe19 cavity and additional van der Waals contacts with Met62 side chain are gained. As expected, the large 4-chlorobenzyl phenyl ether is filling the enlarged Leu26 subpocket. The group forms an extended network of van-der-Waals contacts with Val93, Leu54, His96 and the Tyr100 in the “open” conformation (**Error! Reference source not found.**C). The ryl-imidazole π-stacking interaction with His96 is not kept in the X-ray lattice due to shift of the mid phenyl ring by ca. 2.3 Å toward the center of the pocket. The His96 side chain is, however, still keeping numerous van-der-Waals contacts to the internal aryl group and the methylenoxy linker fragment. The position of the terminal, 4-chlorophenyl ring partially overlays with the phenyl ring of the second KK271 molecule, however, the plane of the ring is perpendicular to the one in the KK271 complex, which results in slightly looser fitting of the pocket.

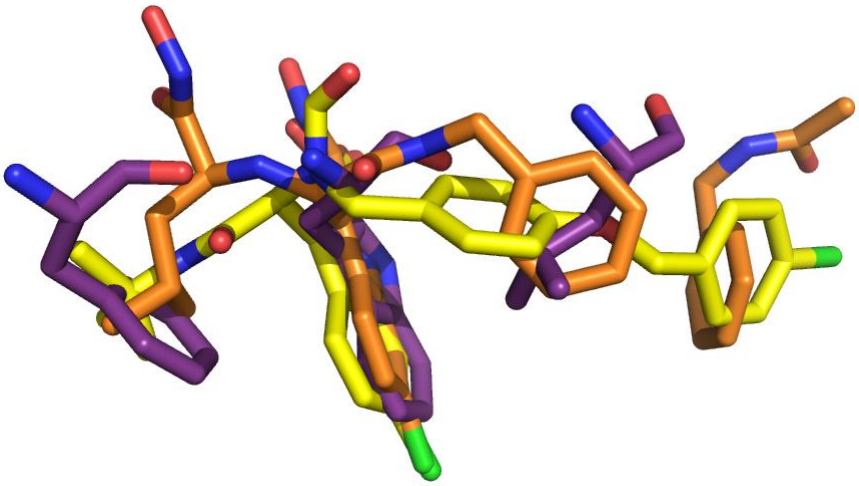

Figure 26. Comparison between wt-p53 (blue), KK271 (orange) and YH300 (yellow) inhibitors. The forth phenyl ring is filling the space used by benzyl moiety of second KK271 molecule. Remaining elements bind in similar fashion to their respective pockets.

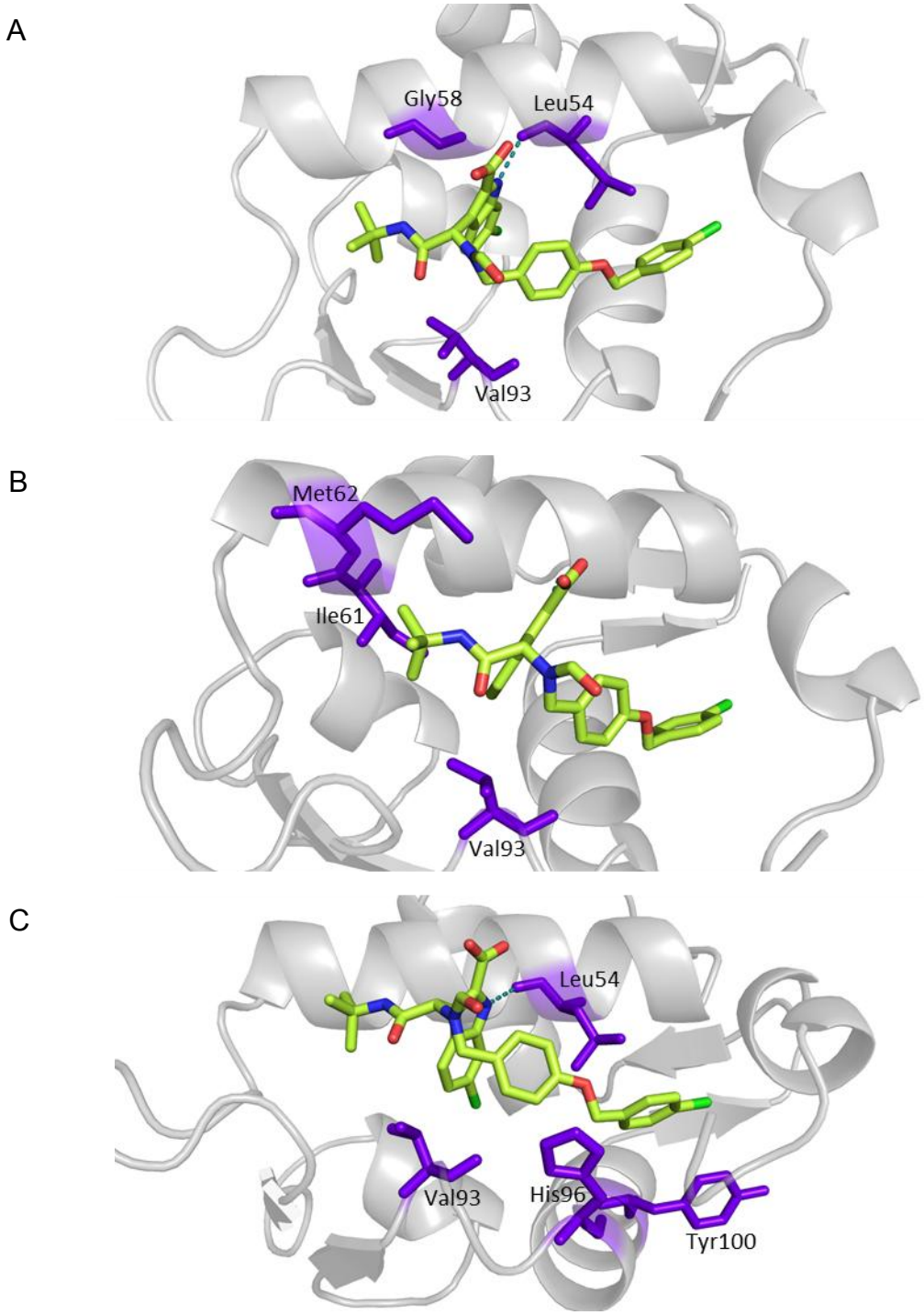

Figure 27. Stucure of MDM2 (gray cartoon) bound to YH300 (green).**A)** The 6-chloroindole submerged in the Trp23 pocket undergoes a hydrogen bond (blue dotted line) with Leu54 and numerous hydrophobic contacts to Val93, Gly58, Leu54. **B)** The tert-butyl side chain of YH300 forms van-der-Waals contacts to the Ile61, Val93, and Met 62 side chains of MDM2. **C)** The large 4-chlorobenzyl phenyl ether, whichfills the enlarged Leu26 sub-pocketforms an extended network of van-der-Waals contacts with Val93, Leu54, His96 and the Tyr100 in the “open” conformation.

The structure was subsequently used as a starting point for molecular dynamics simulations. The results met the expectations: The Tyr100 sidechain was stabilized

(**Error! Reference source not found.**) in a single conformation (χ_1 angle ≈ -171^{O}) imultaneously forming hydrophobic contact with the ligand molecule. The extended pharmacophore model resulted with an increase in affinity: K_i of 0.6 μM for YH300 compared to a K_i of 1.2 μM for KK271.

Table 9. Data collection and refinement statistics of compound YH270.

Data collection	
Space group	$P4_1$
Cell constants (Å)	a = 64.35
	b = 64.35
	c = 81.69
Resolution range (Å)	50 – 2.0
Wavelength (Å)	0.9793
Observed reflections	101912
Unique reflections	21419
Whole range	
Completeness (%)	95.1
R_{merge}	5.0
$I/\sigma(I)$	26.06
Last shell	
Resolution range (Å)	2.0 – 2.1
Completeness (%)	97.5
R_{merge}	31.4
$I/\sigma(I)$	4.55
Refinement	
No. of reflections	17744
Resolution (Å)	20 – 2.0
R-factor (%)	19.9
R_{free} (%)	23.9
Average B (Å^2)	28.4
R.m.s.d. bond length (Å)	0.01
R.m.s.d. angles (°)	1.535
Content of asymmetric unit	
No. of protein-ligand complexes	2
No. of protein residues/atoms	94/774
No. of solvent atoms	176

4.7. Fluorine

Fluorine has been valuable in the process of drug discovery to fine tune many different target and off-target related properties (Böhm, H.-J. *et al.*, 2004; Müller, K. *et al.*, 2007; Hagmann, W.K., 2008; Purser, S. *et al.*, 2008). For example, fluorine has been used to increase the binding affinity of small molecules to its target (Backes, B.J. *et al.*, 2007), to tune the pK_B and logD (Morgenthaler, M. *et al.*, 2007), to improve target selectivity (Su, H. *et al.*, 2011), to improve oral absorption and exposure (Kerekes, A.D. *et al.*, 2011), to prevent from metabolism (Park, B.K. *et al.*, 2001) or to increase the antibacterial spectrum (Percival, A., 1991). Not surprisingly, an estimated 20% of all pharmaceuticals contain fluorine (Böhm, H.-J. *et al.*, 2004). Additionally, ^{18}F is often used as a positron emission tomography (PET) active element to perform time and space resolved distribution studies of drugs in animals and humans (Le Bars, D., 2006; Cai, L. *et al.*, 2008). Last but not least, ^{19}F is very useful in NMR of complex biological systems due to its high sensitivity and zero natural background (Yanamala, N. *et al.*, 2010).

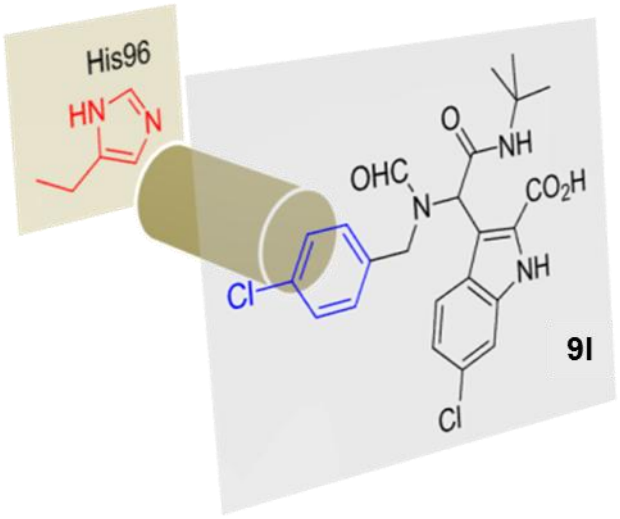

Figure 28. A cocrystal structure of p53-MDM2 antagonist 9l reveals a parallel alignment between the benzyl group of the Ugi scaffold and the imidazole ring of His96 (MDM2), which seems suitable for optimization of the π-π interaction.(Wolf, S. *et al.*, Submitted)

The previously discussed p53-MDM2 antagonist 9l showed a nice alignment with the three-finger pharmacophore model for MDM2 antagonists, in which key moieties fit into the Trp23, Phe19 and Leu26 binding pockets (Dömling, A., 2008). Notably, the benzyl substituent of the small molecule involves a stacking interaction with the

imidazole ring of His96 (**Error! Reference source not found.**). In an attempt to odulate the π-stacking interaction, all 19 isomers with different fluorine substitution pattern possible for the benzyl position were synthesized (Table 10).

By the nature of the Ugi reaction, all products were formed as racemic mixtures and screened as such.

4.7.1. Binding affinities of the fluorinated compounds measured by the FP- and AIDA-assays

The binding constants (K_i) of compounds 6 and 7 to MDM2 were measured using fluorescence polarisation assay (Table 9) (Popowicz, G. *et al.*, 2008). As a reference compound we used the well-known Nutlin-3a. The binding data compare well with the previously publised results (Popowicz, G.M. *et al.*, 2010b). The acid compounds 7 show overall improved potency compared with the corresponding parent ethyl ester compounds 6. The best compound 7m (K_i of 130 nM, molecular weight: 495 Da.) is amongst the most potent p53-MDM2 antagonists known, which has comparable affinity to the reference compound Nutlin-3a (K_i of 70 nM, molecular weight: 581.5 Da.) (Popowicz, G.M. *et al.*, 2010b). Compound 7m exhibits a binding efficiency index (BEI) of 13.9, which indicates a better ligand efficiency than Nutlin-3a (BEI of 12.3) (Popowicz, G.M. *et al.*, 2010b). The aqueous solubility and calculated lipophilicity of 7m is 0.85 mg/mL and cLogP of 3.69, which also is superior compared to Nutlin-3a (0.1 mg/mL, cLogP of 5.17).

Table 10. Inhibition constants [µM] of compounds 6 and 7.

Compounds 6

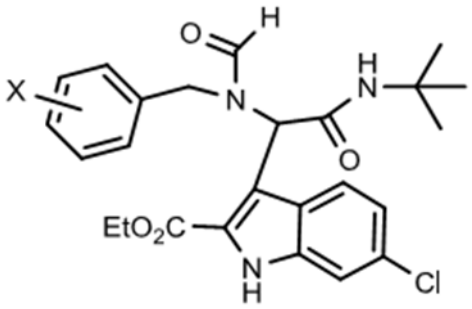

Compounds 7

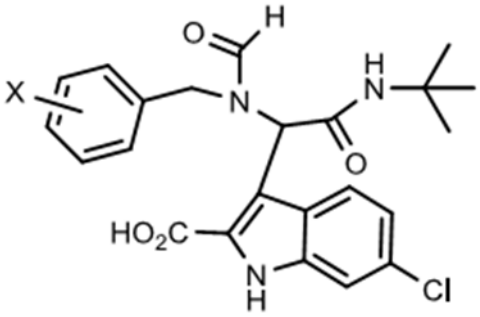

ID	X	K_i [µM] of compounds 6	K_i ([µM] of compounds 7	FP plots of compounds 7
a	H	1,5	1,8	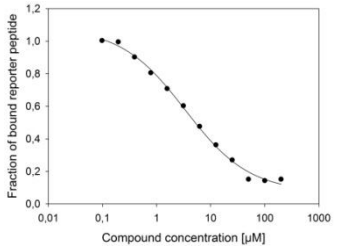
b	4-F	2,2	0,45	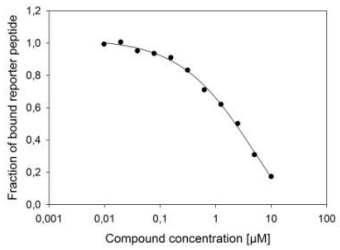
c	3-F	1,3	0,81	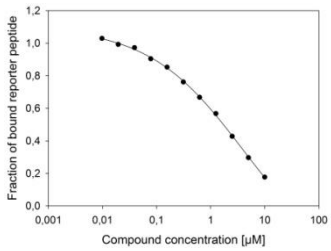
d	2-F	3,0	1,7	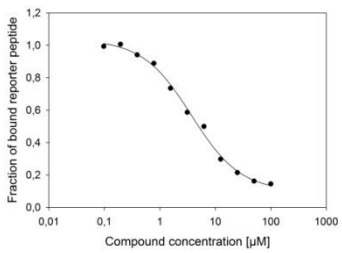

e	3,4-F	0,5	0,25	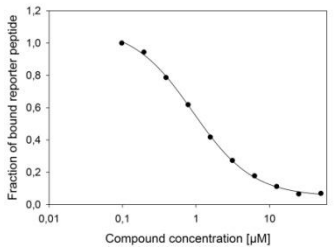
f	2,4-F	6,0	2,3	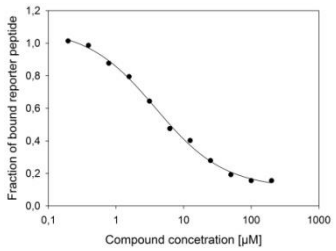
g	2,3-F	3,0	0,2	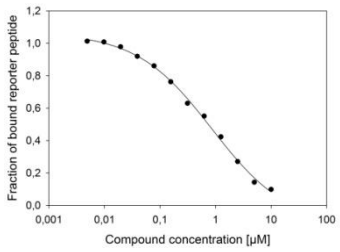
h	2,5-F	10,0	2,5	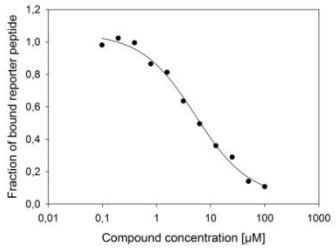
i	3,5-F	2,4	0,3	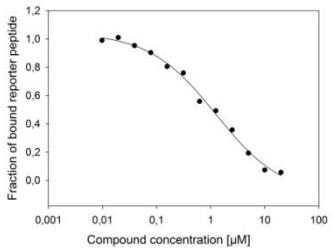
j	2,6-F	4,5	5,7	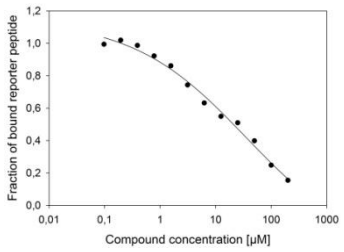

k	2,3,4-F	2,1	0,15	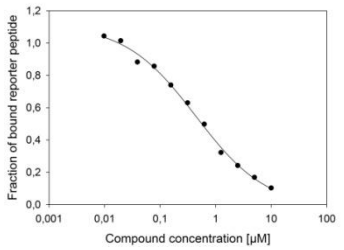
l	2,4,5-F	5,0	2,3	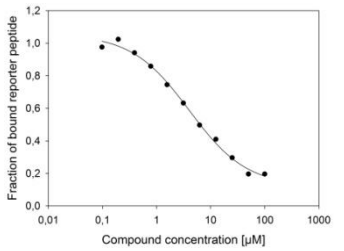
m	3,4,5-F	0,4	0,13	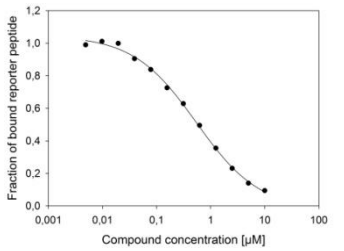
n	2,3,6-F	4,3	3,2	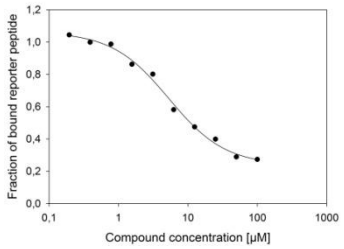
o	2,4,6-F	6,8	3,2	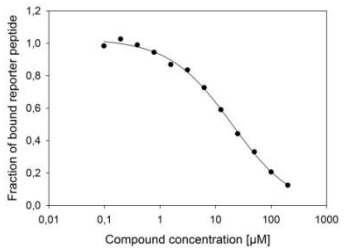
p	2,3,5-F	2,5	0,17	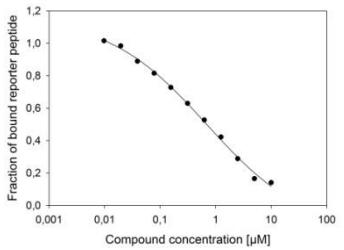

q	2,3,5,6-F	6,7	3,0	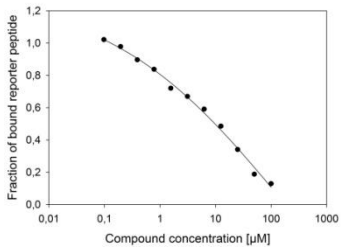
r	2,3,4,6-F	5,8	3,0	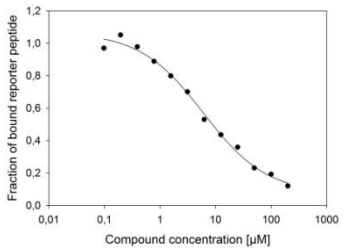
s	2,3,4,5-F	7,0	0,7	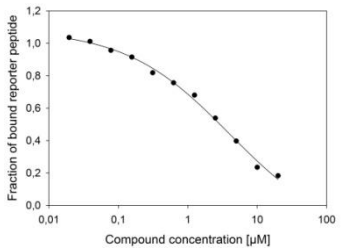
t	2,3,4,5,6-F	5,8	1,8	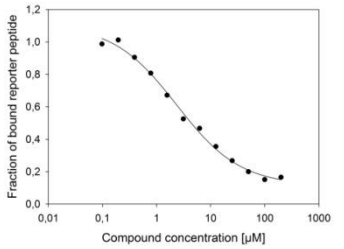
Nutlin-3A			0,07	

The enantiomers of 6e and 6m were efficiently separated by preparative supercritical fluid chromatography (SFC), and transformed to the corresponding enantiomers of 7e and 7m, respectively. The enantiomer (+)-7e (K_i of 200 nM) is more potent than (-)-7e (K_i of 400 nM). Similarly, the enantiomer (+)-7m (K_i of 100 nM) is more potent than (-)-7m (K_i of 280 nM).

4.7.2. Binding affinity of compound 7e measured by HSQC

Error! Reference source not found. shows a NMR HSQC experiment for 7e and DM2. A strong binding, with K_D of less than 1 μM, (and a slow chemical exchange) of 7e to MDM2 is indicated by signals doubling (Wüthrich, K., 1986; Rehm, T. *et al.*, 2002).

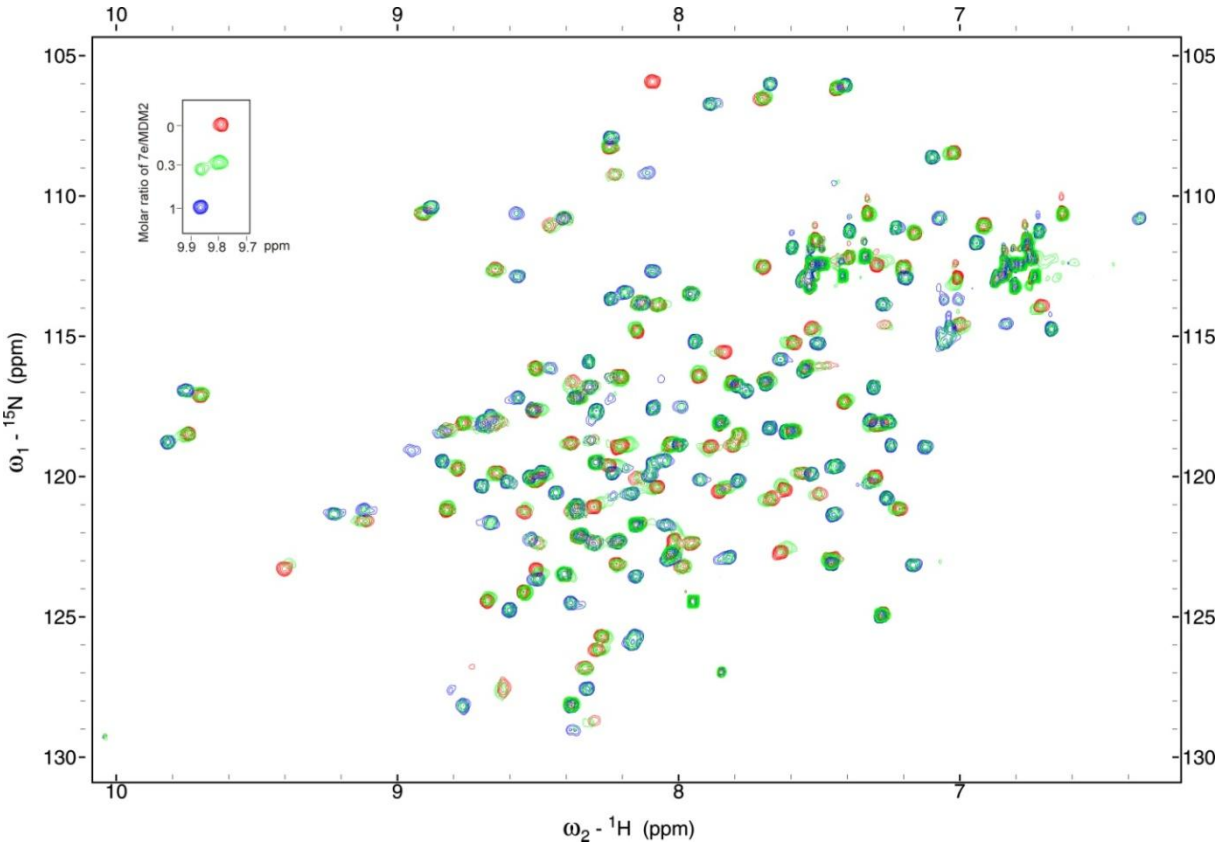

Figure 29. Superposition of NMR HSQC spectra of the ^{15}N-labeled MDM2 titrated against 7e. The spectrum of free MDM2 is shown in red. The spectrum of 7e-MDM2 (intermediate ratio, 3:10, respectively) is shown in green, and the spectrum of 7e-MDM2 (final ratio, 1:1) is shown in blue.

4.7.3. Crystal structure of the MDM2-7e complex

In order to better understand the structural basis of the interaction of 7e with MDM2, 7e was cocrystallized with $MDM2_{18-125}$. The crystal used for the structure determination grew at 4°C in 0.1 M sodium acetate pH 4,8 and 18% of PEG 4000 (**Error! Reference source not found.**). 10% of glycerol was used as cryoprotectant. he frozen crystals were taken to the SLS synchrotron in Villigen, Swiss.

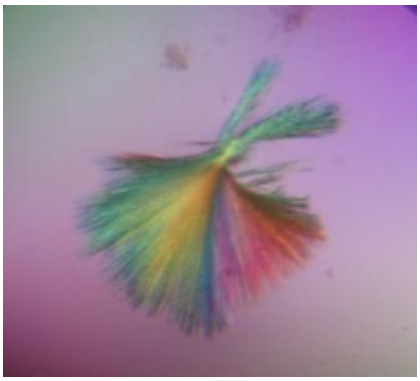

Figure 30. Cocrystals of MDM2 and compound 9l (racemic mixture).

The overall structure of the new scaffold bound to MDM2 and aligned with the native p53-MDM2 structure is shown in **Error! Reference source not found.**. Not urprisingly, the indole substructure of (*S*)-7e aligns very well with the indole side chain of Trp23 of p53, as this is a build-in due to the design principles of ANCHOR.QUERY (**Error! Reference source not found.**). Additionally, the small olecule (*S*)-7e nicely mimics the W23-L54 hydrogen bond. The difluorobenzyl and *tert*-butyl groups deeply intrude into the Leu26 and Phe19 binding sites, respectively.

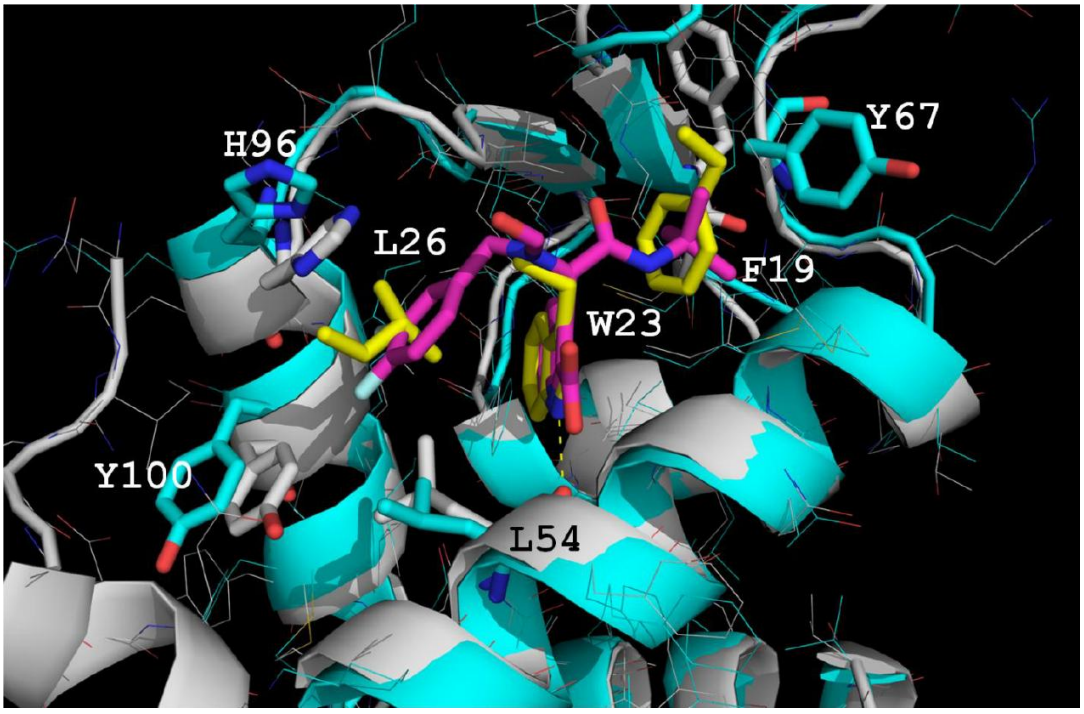

Figure 31. Alignment of the new cocrystal structure (grey cartoon, sticks and lines) with ligand (S)-7e (pink sticks) with the published p53-mdm2 structure (turquoise cartoon, sticks and lines; PDB ID: 1YCR; RMSD = 0.85) The p53 hot spot triad amino acids side chains Phe19, Trp23, and Leu26 are shown as yellow sticks. Amino acids showing considerable movements are highlighted as sticks and enumerated.

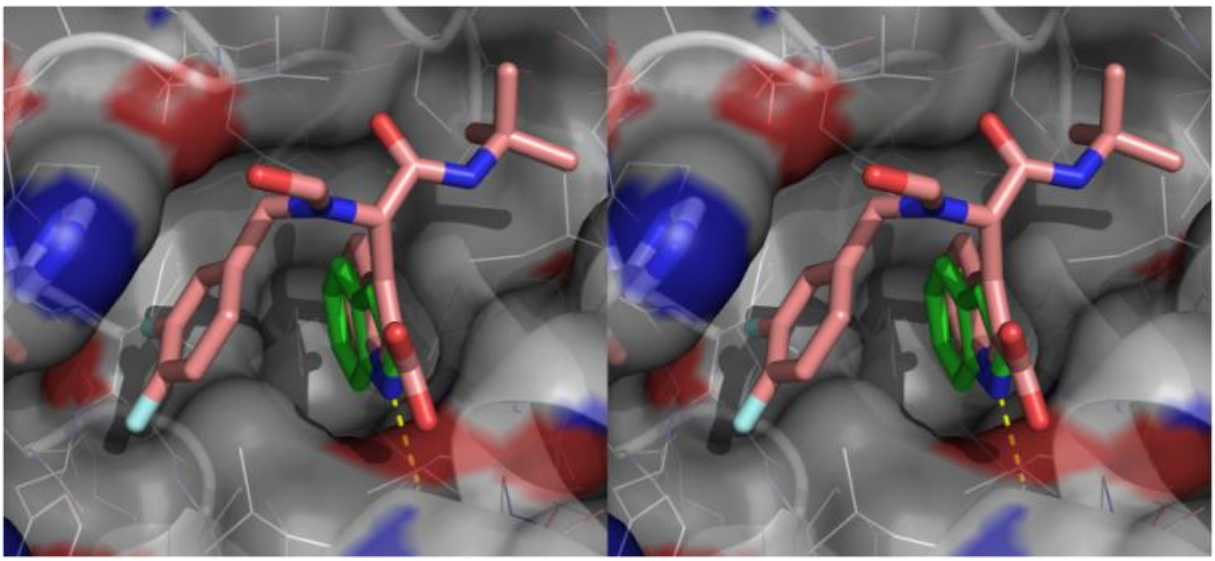

Figure 32. Stereo picture of compound (S)-7e (pink sticks) in MDM2 (surface with cartoon secondary structures and lines). His96, forming a π-stacking interaction with the 3,4-difluoro benzyl group of (S)-7e is highlighted as blue sticks. The indole fragment of (S)-7e aligns well with the anchor fragment Trp23 of p53 (green sticks, PDB ID: 1YCR; RMSD = 0.701 Å). The indole NH of (S)-7e also forms the characteristic conserved hydrogen bond with the carbonyl group of Leu54 (yellow dotted line).

Interestingly, the MDM2 receptor closes the binding site over (*S*)-7e considerably as compared to p53. Thus the two α-helices flanking the binding site encompassing p53 are much more open and a considerable replacement is observed. This has particular consequences for the Leu54 sub-binding site, and the flanking His96 and Leu26 clutch the benzyl portion of the small molecule. In fact, the comparison with the other small molecules cocrystallized in MDM2 reveal that in the current structure the Leu26 binding site is the most narrow (Fry, D.C. *et al.*, 2004; Vassilev, L.T. *et al.*, 2004; Grasberger, B.L. *et al.*, 2005; Allen, J.G. *et al.*, 2009). This might be a direct consequence of the optimized π–π interaction of the ligand with His96. Overall the interaction between (*S*)-7e and MDM2 is mostly governed by hydrophobic interactions. Key short interactions are highlighted below as follows. The 3,4-difluorbenzyl groups make short interactions to His96, Leu54 and Tyr100 (**Error! eference source not found.**). The planes of the His96 imidazole and the phenyl of (*S*)-7e are almost coplanar. However, the centers of the two rings are sided against each other (**Error! Reference source not found.**). The close distances between the wo rings vary between 3.4 and 3.9 Å, which is well in-between the π-π interaction distances described in the literature (Meyer, E.A. *et al.*, 2003; Bissantz, C. *et al.*, 2010; Salonen, L.M. *et al.*, 2011). The fluorine atom in para position undergoes a short contact to the 2-C of the phenol group of Tyr100 (3.5 Å).

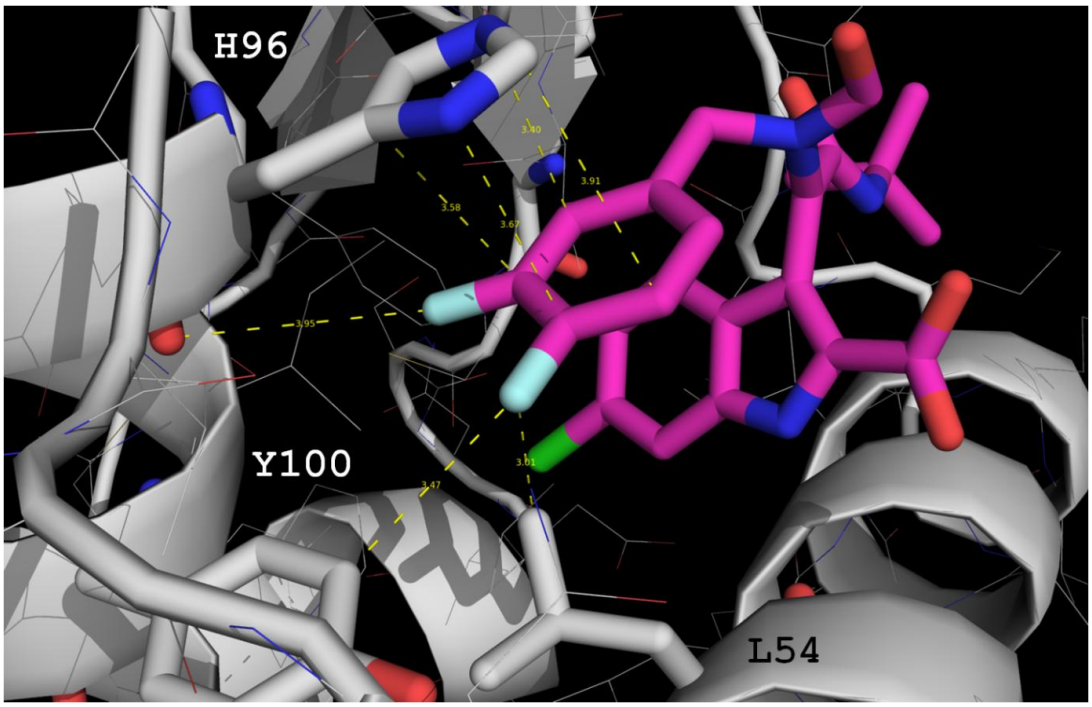

Figure 33. Short contacts of the (S)-7e benzyl group with the surrounding MDM2 residues.

Additionally, there is a short 3 Å contact to a Leu54 methyl group. In contrast, the fluorine atom in meta position makes short contacts to the His96 carbonyl oxygen (4 Å), the ipso-carbon of the His96 and the adjacent methylene group (3.5 and 3.7 Å).

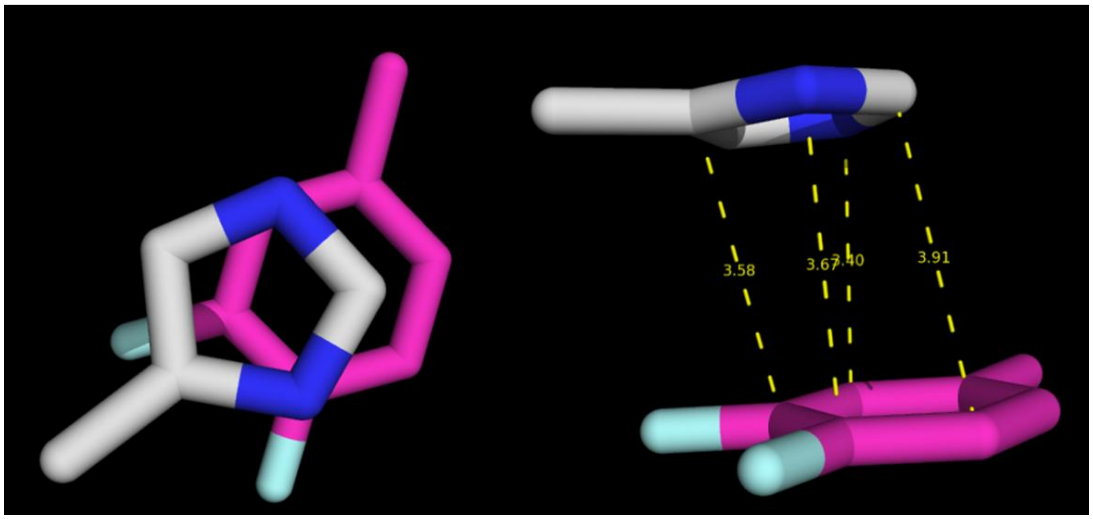

Figure 34. Relative orientation of the His96 imidazole and (S)-7e benzyl group viewed from top and side-on.

The 6-chloroindole substituent is a mimic of the p53 Trp23 indole group and aligning very well (**Error! Reference source not found.**). Analogously, the indole N-H of (*S*)-e undergoes a hydrogen bond to the Leu56 (2.8 Å). The remainder of contact of the indole substructure are of hydrophobic nature involving the amino acids Val75, Val93, Ile99, Leu54, Ile103, Leu57, Gly58, Phe86, Phe98 and Ile61 (**Error! Reference ource not found.**). Also worthwhile mentioning is the intramolecular π–π contact made in (*S*)-7e between the indole and the benzyl fragment. The close intramolecular distances between the benzyl and indole moiety vary between 3.3 and 4.9 Å.

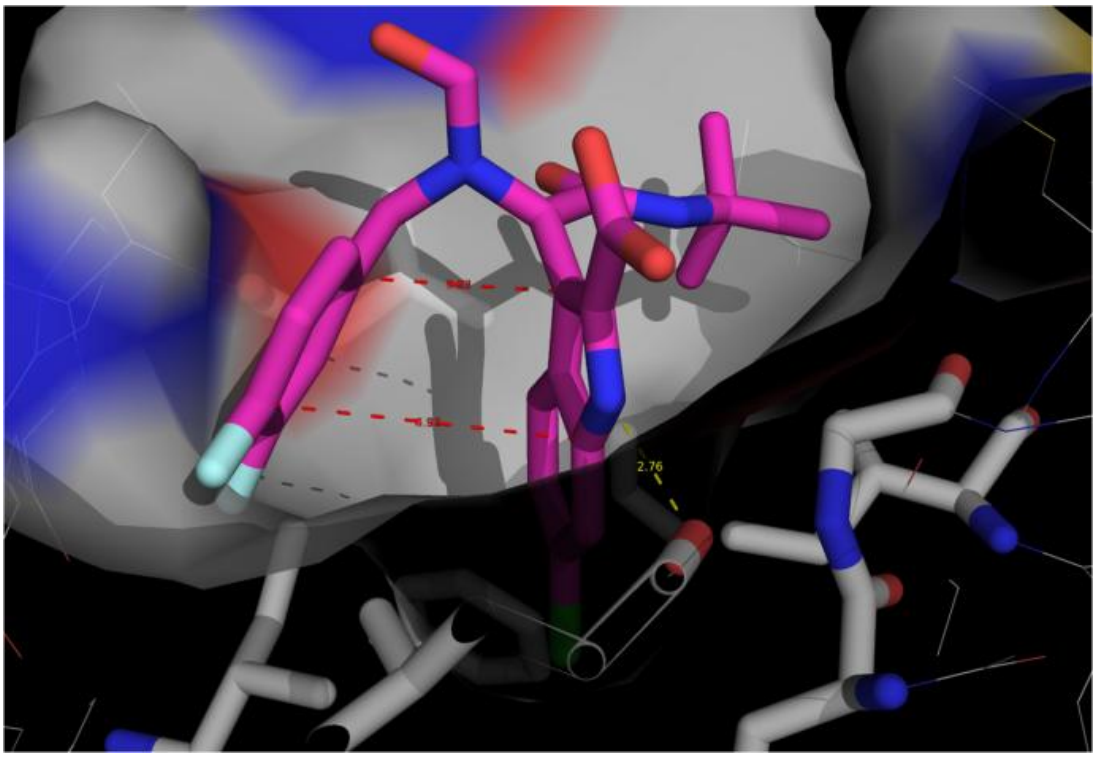

Figure 35. Cut away view of the hydrophobic indole receptor environment. Additionally short intra-molecular contacts are shown as red dotted lines.

The *tert*-butyl group mimics the Phe19 residue of p53. This bulky group makes short contacts to Gly58, Val75, Val93, Ile61, Met62 and Tyr67 (**Error! Reference source ot found.**). Interestingly, the Tyr67 side chain is skipped by ~100° towards Val75 whereas in most other structures the residue points to Met62. This is opening up a shallow but hydrophobic additional binding site, which might be addressed in future compound optimization strategies.

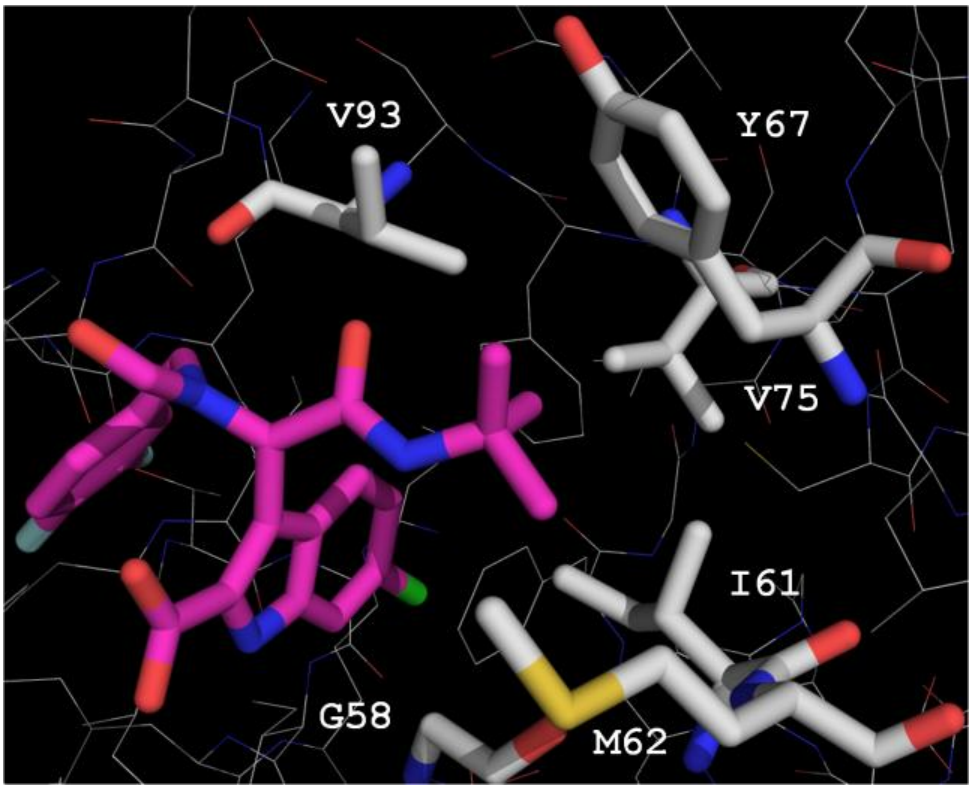

Figure 36. Hydrophobic embedding of the tert-butyl group into MDM2.

Table 11. Data collection and refinement statistics of compound 7e.

Data collection	
Space group	I222
Cell constants (Å)	a = 49.95
	b = 59.25
	c = 82.95
Resolution range (Å)	50 – 1.6
Wavelength (Å)	0.999
Observed reflections	113552
Unique reflections	16540
Whole range	
Completeness (%)	99.4
R_{merge}	9.5
$I/\sigma(I)$	13.27
Last shell	
Resolution range (Å)	1.6 – 1.75
Completeness (%)	97.5
R_{merge}	60.5
$I/\sigma(I)$	2.83
Refinement	
No. of reflections	11877
Resolution (Å)	1.6 – 2.0
R-factor (%)	20.5
R_{free} (%)	20.5
Average B (Å^2)	18.3
R.m.s.d. bond length (Å)	0.008
R.m.s.d. angles (°)	1.47
Content of asymmetric unit	
No. of protein-ligand complexes	1
No. of protein residues/atoms	93/1500
No. of solvent atoms	232

A key property of the C-F bond is the reversed polarization as compared to the C-H bond. Thus, the pattern of fluorine substitutions on the phenyl ring should be able to

modulate the aromatic interaction between the small molecule and its protein receptor (Kim, C.Y. *et al.*, 2000; Kim, C.Y. *et al.*, 2001). We have investigated this effect using docking models derived from the cocrystal structure by performing all possible fluorine substitution patterns in the benzyl group of compounds 7b-t. All the refined docked small molecules show only minor differences relative to the cocrystal structure. The models reveal that a C-H to C-F substitution at the buried ortho-position leads to a highly repulsive dipole-dipole interaction (**Error! Reference ource not found.**). In fact, the straightforward change in Coulomb energy due to the charge swap indicated in **Error! Reference source not found.** is ~4 kcal/mol. Not surprisingly, the fluorine in the buried ortho-position does not rank well wither in our models or in the experiments. Note that at least for the subset of compounds with symmetric fluorine patterns there in no ambiguity on the position of the fluorine atoms in the docked models based on the cocrystal structure.

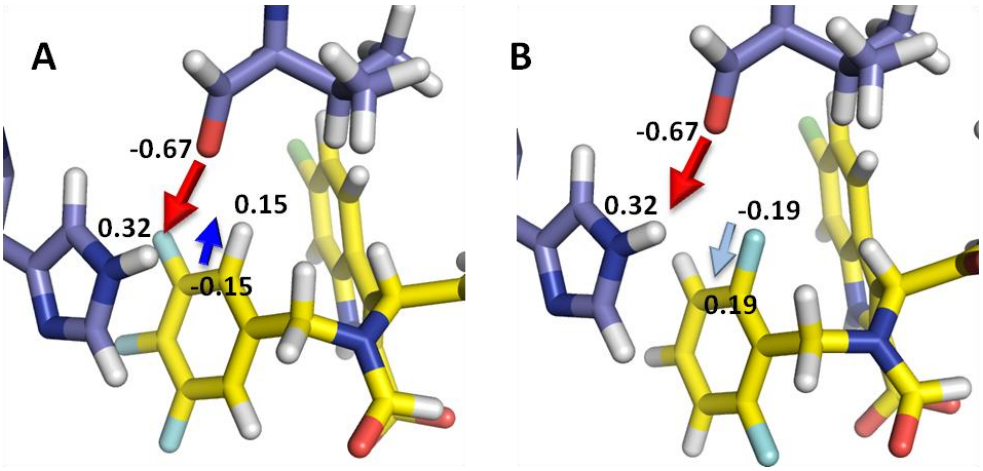

Figure 37. Dipole reversal by fluorine is the main determinant of binding affinity. Docking models (yellow sticks) of **A)** compound (*S*)-7m and **B)** compound (*S*)-7j are minimized structures of the superposition of the small molecules onto the ligand of the cocrystal structure shown in Figure 32. Arrows depict the dipole-dipole interaction between the His96···ε-Val93···O hydrogen bond (blue sticks, red arrow) and the C-H (A, blue arrow) and C-F (B, cyan arrow) dipoles that are attractive and repulsive, respectively. Also indicated are the Merck molecular force field (MMFF) partial charges.

Given the strong electrostatic coupling between the two rings, we expected the intermolecular component of the electrostatic free energy to be a main determinant of the binding affinity. Indeed, as shown in **Error! Reference source not found.**, the orrelation coefficient between the computed change in electrostatics and the experimentally determined affinity (pK_i) yielded a strikingly accurate R=0.96 value for compounds with symmetric fluorine substitutions. The analysis correctly ranks compounds with the best and worst K_i values among the benzyl rings with a

symmetric fluorine pattern. By itself, this result is quite impressive, as most physically based scoring functions do not recapitulate thermodynamic data (Warren G.L. *et al.,* 2006). The correlation of electrostatics with pK_i for the full set of compounds, including those with fluorine substitutions that form a symmetric patterns, sharply drops to R=0.58. An even lower correlation (R=0.22) is obtained by using the full binding affinities calculated by the software OpenEye Szybki, further emphasizing the key role of electrostatics in capturing changes in K_i for the different ligands. Refining the ligand protonation states by considering pK_a and tautomer enumeration with the AM1-BCC charge model of OpenEye QuacPac version 1.3.1 does not change the results (Wlodek, S. *et al.*, 2010). The conspicuous over-prediction of the electrostatic component of the binding free energy for a symmetric compound is likely to reflect the specificities of the internal energies for each rotamer of the benzyl ring. This effect is offset for symmetric compounds, but it should significantly affect the free energy of the unbound asymmetric ligands in ways that are ignored by the fixed ligand structures imposed by the Poisson Boltzmann calculations.

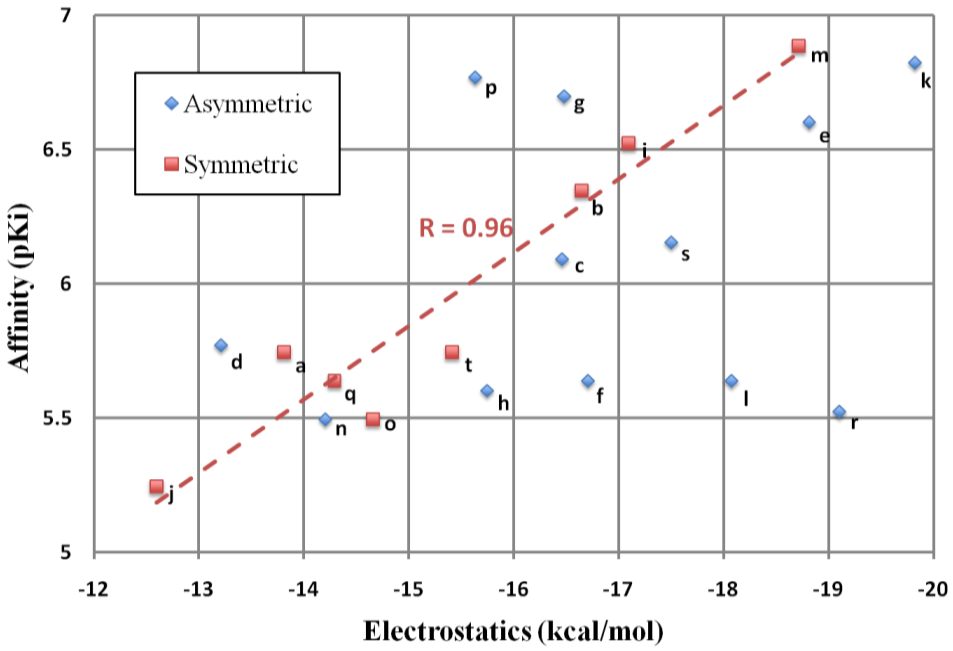

Figure 38. Correlation between the calculated change in electrostatics and the binding affinity (pK_i) for compounds (S)-7. Compounds with a symmetric arrangement of fluorine atoms in the benzyl group correlate closely (R=0.96) to the calculated electrostatics. The remaining asymmetric compounds are more difficult to characterize and decrease the overall correlation (R=0.58). Following Table 10, letters indicate the fluorine substitution pattern in the phenyl ring.

In summary, 40 derivatives of p53–Mdm2 antagonist 1 were efficiently synthesized via a one-pot Ugi-4CR including all possible fluorine substitutions on the benzyl group

in order to optimize aromatic interactions. The cocrystal structure of (S)-7e with Mdm2 reveals the structural basis of the potent interaction. The introduction of fluorine substitutions on the benzyl group can considerably improve the potency of p53–Mdm2 antagonists, due to the electrostatic interaction between the small molecules and the receptor. Although limited in scope, the computational analysis of docked configurations that are presumed to bind via the same binding mode shows that the electrostatics of unique rigid structures can be reasonably explained by current methods, whereas assessing the free energy of an unbound state with a variety of hard-to-evaluate internal states is quite detrimental to empirical estimates of the free energy. The findings underscore the principally known but often surprising effects that fluorine can exert on the biological activity of small molecules. The findings may also lead medicinal chemists to success in modulating molecular interactions with other types of targets.

4.8. p53-MDMX Inhibitors

Only few compounds have been reported to function as p53-MDMX antagonists. From all the hundreds of compounds scanned to disrupt the p53-MDMX interaction only one compound WK2-3 gave satisfactory results. WK2-3 is an optimized compound derived from a compound WK298 (also known as Novartis 101) synthesized by Boettcher, A. *et al*. (2008). WK298 is the first antagonist of the MDMX-p53 interaction with low µM K_i potency (Table 12). Compound WK2-3 differs only by an additional amide moiety (N,N-dimethylpropylamine) attached to the 2-position of the indole ring (Table 12). The affinity of both Inhibitors was measured by FP-assay and was compared to the strong p53-MDM2 inhibitors: Nutlin-3 and the spiro-oxindole compound Mi 63. Though Nutlin-3 and Mi63 reveal excellent binding affinities towards MDM2, they show only low inhibitory effect for the p53-MDMX Interaction, however the Imidazoyl-indole compounds WK298 and WK2-3 reveal the to date best binding compounds towards MDMX (Table 12 and **Error! Reference source ot found.**).

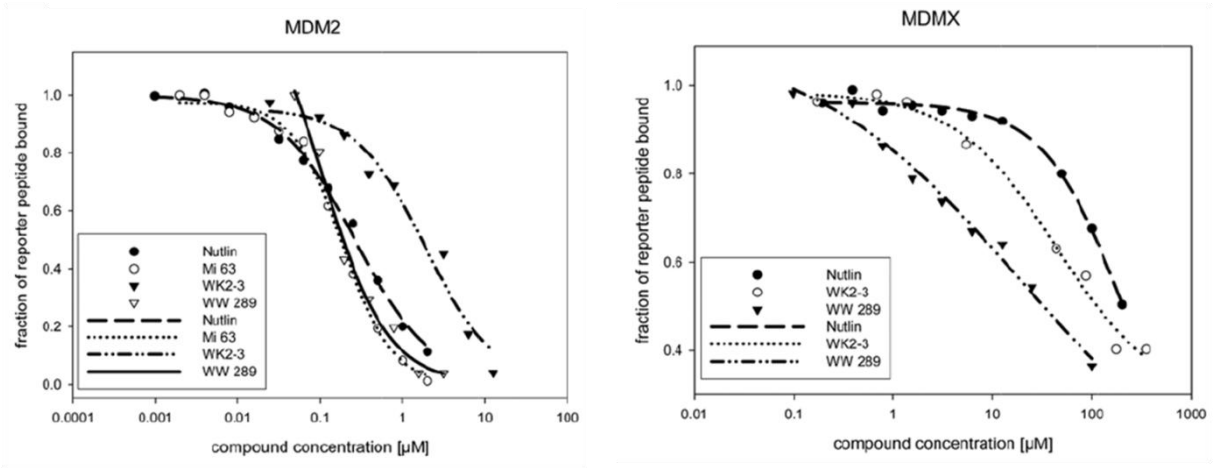

Figure 39. FP-plots of the p53-MDM2 and p53-MDMX Inhibitors.

Table 12. Binding affinities of the p53-MDM2 and p53-MDMX Inhibitors measured by FP-assay.

	structure	MDM2 K_i[nM]	MDMX K_i[µM]
Nutlin-3	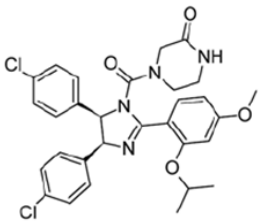	69	70
Mi-63	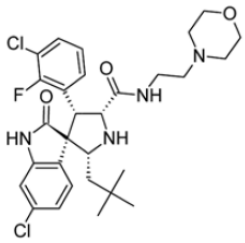	36	55
WK2-3	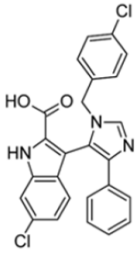	916	36
WK298	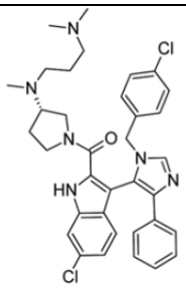	109	11

It is essential to have structural information of small molecular weight compounds in order to understand the binding mode and to be able to optimize these small molecular weight antagonists. It was found that small differences in the structures of MDM2 and MDMX lead to dramatic differences in their affinities to small binding molecules, thus making a crystallographic structure of MDMX bound to an Inhibitor very valuable issue (Popowicz, G.M. *et al.*, 2008; Czarna, A. *et al.*, 2009).

Popowicz *et al.* (2010a) published the first cocrystall structure of an MDMX-Inhibitor: Compound WK298 in complex with MDMX. Also the cocrystal structure of the similar compound WK2-3 bound to MDM2 was solved by Popowicz *et al.* (2010a). Comparing these two crystal structures, the differences between the MDM2 and MDMX binding modes can be compared. The two inhibitors differ by the presence of the ((3-(dimethylamino) propyl)(methyl)amino)pyrrolidin-1-yl tag in the WK298 compound. The portions of the two compounds that are responsible for the primary interaction inside the p53 binding pockets are identical (**Error! Reference source not ound.**).

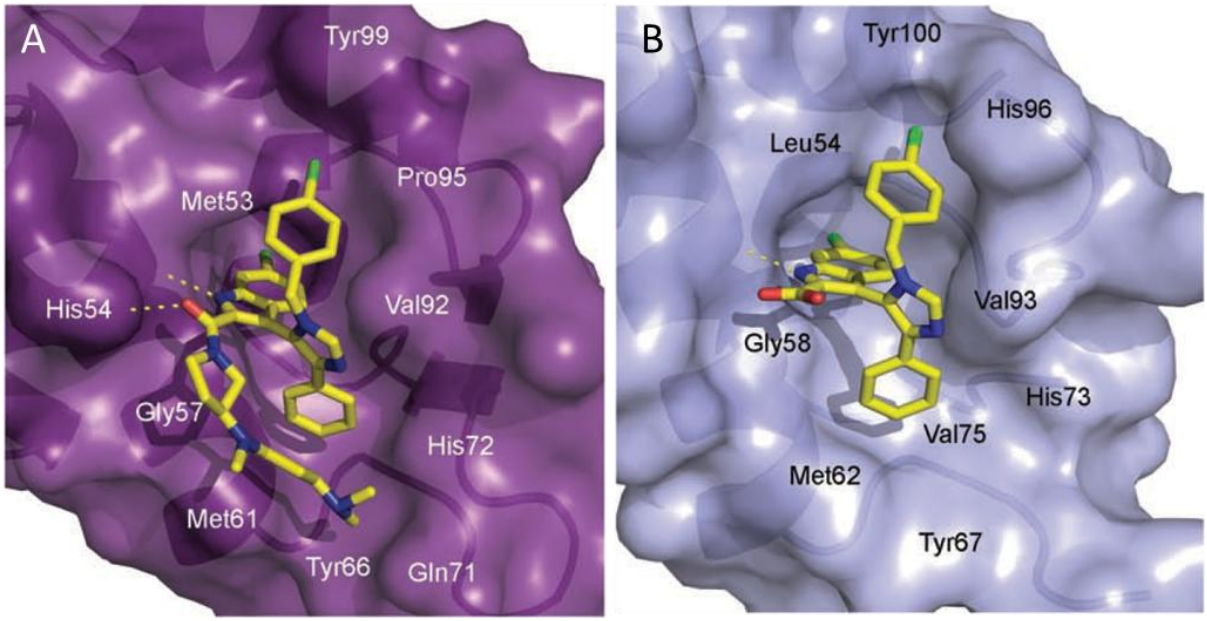

Figure 40. Inhibitors bound to MDM2 and MDMX proteins. The inhibitors are shown in stick models with carbon atoms colored yellow, nitrogen blue and oxygen red. Key side-chains of the proteins are labeled. Hydrogen bonds are depicted as yellow dashed lines. The numbering of substituents in WK2-3 and WK298 is provided in the Supporting Information. (A) Compound WK298 binds to MDMX by filling its Trp23 subpocket with the 6-chloroindole group. The 4-phenyl group is located in the Phe19 and 1-(4-chlorobenzyl) group in the Leu26 pockets, respectively. Two hydrogen bonds to Met53 and His54 are formed. The N,N-dimethylpropylamine part of the WK298 molecule folds over Gly57 and Met61, forming additional hydrophobic protection of the binding cleft. Tyr99 closes the Leu26 subpocket. (B) Similarly, the panel shows inhibitor WK2-3 bound to the MDM2 protein. A very similar binding pose as in (A) is formed despite of different shapes of the p53 binding sites in MDM2 and MDMX. The His96-Tyr100 region has the most pronounced differences in the shape of the Leu26 pocket, but the position of 1-(4-chlorobenzyl) is not altered. A hydrogen bond is formed between the indole of WK2-3 and the Leu54 carbonyl oxygen of MDM2.

Interestingly, despite of the differences between MDM2 and MDMX pockets (RMSD for main chain atoms 1.22 Å) seen in the native and inhibitor bound structures, the

modes of the binding of those inhibitors to MDM2 and MDMX, remain virtually identical. The plane of the chloroindole ring in the MDMX structure, when viewed along the imidazole-chloroindole connecting bond, is rotated by only 14.8° relative to that in the MDM2 structure. The 4-chlorobenzyl substituents of these two compounds fill the Leu26 subpockets (for MDMX the 4-chlorobenzyl group is located 0.53 Å towards the α2' helix compared to that in MDM2). The 6-chloroindole ring, substituting the native tryptophan p53 side-chain, appears to be an efficient, interacting scaffold well suited for both proteins. While it requires a substantial, induced-fit adaptation of MDMX, it can effectively contribute to the MDMX binding by overcoming the energy cost of the protein adaptation, as is also shown by the even higher affinity of the 6-chloro-Trp peptide inhibitor.(Kallen, J. *et al.*, 2009) The Phe19 binding subpocket of both MDM2 and MDMX is similar, with the biggest differences located at the rim of the p53-binding cleft. As it was stated above, an effective inhibitor does not need to penetrate this space to the very bottom. Rather, it seems, that an enlarged hydrophobic surface is required for optimal interaction. Therefore, it should suffice to fill this subpocket with a nonpolar, aliphatic, but preferably aromatic moiety, which is universal to both proteins' pockets. The Leu26 pocket seems to present the major challenge for developing a dual action, and potent MDM2 and MDMX inhibitor. The major differences, clustered around the α2' helix, are most probably the cause for much weaker binding of the known MDM2 inhibitors to MDMX. Apparently, the chlorophenyl group, present in all known MDM2 inhibitors so far, is not optimal for the p53-binding pocket of MDMX. While position of Tyr100 in MDM2 varies greatly from structure to structure, the equivalent Tyr99 of MDMX remains in most cases in the "closed" conformation and this configuration must be accounted for as an important factor when optimizing the inhibitors towards MDMX. Certainly, this subpocket still requires the optimization of binding modules to obtain the nanomolar small molecular weight MDMX antagonists.

5. Summary

Cancer is the leading cause of death worldwide. Almost 50% of all human cancers are derived from mutations in the p53 gene, and the other 50% arise from the deregulation of the wt-p53 pathway - mostly through the activity of the p53 inhibitors MDM2 and MDMX. The small-molecule compounds that disrupt the p53-MDM2 and p53-MDMX interactions should be effective in a broad spectrum of cancer types and thus targeting the p53-MDM2 and p53-MDMX interactions have become a major subject of cancer research.

The work described in this thesis is part of a collaborative project on the development of new anticancer drugs that inhibit the p53-MDM2 and p53-MDMX interactions. The compounds were discovered by the computational screening using the AnchorQuery platform and were analyzed by fluorescent polarization and 1D AIDA-NMR assays to determine the affinity of each compound to MDM2 and MDMX. Compounds exhibiting high affinity (ca. sub μM) were optimized and further analyzed by 2D-HSQC-NMR spectroscopy and X-ray crystallography. Hundreds of compounds were synthesized and analyzed this way, leading to the discovery of the new high affinity P53-MDM2 antagonists. Their crystal structures lead to new insights in the p53-MDM2 and p53 MDMX protein-protein interaction that can be used for further development of drug-like compounds. Two ways of the small-molecule-MDM2 binding are described in this thesis: The already known and commonly used 3-point pharmacophore model and a novel 4-point pharmacophore model. All known small molecular antagonists of the p53-MDM2 interaction reported in the literature are based on the 3-point pharmacophore model, which targets the conformational state of the protein found in the p53-MDM2 complex. However, newly synthesized compounds described in this thesis induce an additional metastable hydrophobic pocket on the MDM2 surface, exploring non-native p53-MDM2 interactions. These compounds benefit from an extended hydrophobic contact interface and, in contrast to other small molecule p53-MDM2 inhibitors, exhibit a 4-point binding mode.

A “good” binding p53-MDM2 inhibitor was used in an exhaustive fluorination scan, aiming to investigate the biological activity of fluorine in small drug-like compounds. Previously fluorine had been reported to have a high value for drug development, as amongst others, it improves the binding affinity of small molecules to its target, target selectivity, the oral absorption and exposure and it prevents the drug from being

metabolized. The cocrystal structure of one of the fluorinated compounds with MDM2 reveals the structural basis of this compound interaction with MDM2. Due to the electrostatic interaction between the fluorine of the small molecule inhibitor and the receptor, the potency of the compound could be improved. Our findings may help medical chemists in successfully modulating molecular interactions with other types of targets.

6. Zusammenfassung

Krebs ist weltweit die führende Ursache für den Tod. Fast 50% aller humaner Krebsarten leiten sich von Mutationen im p53 Gen ab, die restlichen 50% entstehen durch Deregulation der wt-p53-Signaltransduktionskaskade - hauptsächlich durch die Aktivität der p53 Inhibitoren MDM2 und MDMX. Die niedermolekularen chemischen Verbindungen, die die p53-MDM2 and p53-MDMX Interaktion spalten, sollten für ein breites Spektrum von Krebsarten wirksam sein und sind folglich zu einem der wichtigsten Themen in der Krebsforschung geworden.

Die hier beschriebene Arbeit ist Teil eines Kollaborationsprojekts an der Entwicklung von neuen Antikrebs Arzneistoffen, die die Interaktion von p53-MDM2 und p53-MDMX inhibieren. Die chemischen Verbindungen, die durch computerbasiertes screening mittels der AnchorQuery Plattform entdeckt worden sind, wurden durch Fluoreszenz-Polarisations- und 1D AIDA-NMR Methoden auf deren Affinitäten zu MDM2 und MDMX hin untersucht. Die chemischen Verbindungen mit einer hohen Affinität (ca. sub µM) wurden optimiert und mittels 2D-HSQC-NMR Spektroskopie und Röntgenkristallographie weiter untersucht. Hunderte chemischer Verbindungen wurden so synthetisiert und analysiert, was zur Entdeckung neuer hochaffiner p53-MDM2 Antagonisten geführt hat. Deren Kristallstruktur führte zu neuen Einblicken in die p53-MDM2 bzw. p53-MDMX Protein-Protein Interaktion, welche für die weitere Entwicklung von Arzneimitteln verwendet werden kann. Zwei Bindungsarten dieser niedermolekularen Substanzen an MDM2 bzw. MDMX werden in dieser Arbeit beschrieben: Das bereits bekannte und übliche „3-point pharmacophore“ Modell und das neue „4-point pharmacophore“- Model. Alle bekannten niedermolekularen Antagonisten der p53-MDM2 Interaktion, die in der Literatur beschrieben sind, basieren auf einem “3-point pharmacophore” Modell, welches die Konformation wie im p53-MDM2 Komplex annimmt. Allerdings erzeugen neu synthetisierte chemische Verbindungen, die in dieser Arbeit beschrieben werden, eine zusätzliche metastabile hydrophobische Bindungstasche auf der MDM2 Oberfläche, wodurch auch neue nicht-native p53-MDM2 Verbindungen geknüpft werden. Diese Verbindungen profitieren von einer erweiterten hydrophoben Interaktionsgrenzfläche und weisen so, im Gegensatz zu allen anderen p53-MDM2 Inhibitoren, eine 4-Punkte Bindungsweise auf.

Ein „gut“ bindender p53-MDM2 Inhibitor wurde für eine umfassende Fluor Untersuchung benutzt, um die biologische Aktivität von Fluor in niedermolekularen Substanzen zu untersuchen. Fuorin wurde bereits als sehr nützlich in der Arzneimittelentwicklung beschrieben, unter anderem wegen der verbesserten Bindungsaffinitäten von chemischen Substanzen an deren Zielproteinen, der Zielproteinspezifität, der mündlichen Absorption und Aufnahme, sowie der Verhinderung vor Methabolisierung. Die Co-kristallstruktur einer der fluorinierten chemischen Verbindungen mit MDM2 enthüllt die strukurelle Grundlage dieser Interaktion. Durch die elekrostatische Interaktion zwischen dem Fluorin des niedermolekularen Moleküls und des Empfängers, konnte die Wirkung der Substanz verbessert werden. Diese Forschungsergebnisse können Pharmaforschern helfen, molekulare Interaktionen an weiteren Zielobjekten erfolgreich zu modifizieren.

7. References

Alberts, B., Johnson, A., Lewis J., Raff M., Roberts K., Walter P., (2008). “Molecular Biology of the Cell”. 5th ed., New York: Garland Science.

Allen, J. G.; M. P. Bourbeau; G. E. Wohlhieter; M. D. Bartberger; K. Michelsen; R. Hungate; R. C. Gadwood; R. D. Gaston; B. Evans; L. W. Mann; M. E. Matison; S. Schneider; X. Huang; D. Yu; P. S. Andrews; A. Reichelt; A. M. Long; P. Yakowec; E. Y. Yang; T. A. Lee and J. D. Oliner (2009). "Discovery and optimization of chromenotriazolopyrimidines as potent inhibitors of the mouse double minute 2-tumor protein 53 protein-protein interaction." J Med Chem 52(22): 7044-7053.

Ayed, A.; F. A. Mulder; G. S. Yi; Y. Lu; L. E. Kay and C. H. Arrowsmith (2001). "Latent and active p53 are identical in conformation." Nat Struct Biol 8(9): 756-760.

Backes, B. J.; K. Longenecker; G. L. Hamilton; K. Stewart; C. Lai; H. Kopecka; T. W. von Geldern; D. J. Madar; Z. Pei; T. H. Lubben; B. A. Zinker; Z. Tian; S. J. Ballaron; M. A. Stashko; A. K. Mika; D. W. A. Beno; A. J. Kempf-Grote; C. Black-Schaefer; H. L. Sham and J. M. Trevillyan (2007). "Pyrrolidine-constrained phenethylamines: The design of potent, selective, and pharmacologically efficacious dipeptidyl peptidase IV (DPP4) inhibitors from a lead-like screening hit." Bioorganic & Medicinal Chemistry Letters 17(7): 2005-2012.

Bailey, S. (1994). "The Ccp4 Suite - Programs for Protein Crystallography." Acta Crystallographica Section D-Biological Crystallography 50: 760-763.

Banin, S.; L. Moyal; S. Shieh; Y. Taya; C. W. Anderson; L. Chessa; N. I. Smorodinsky; C. Prives; Y. Reiss; Y. Shiloh and Y. Ziv (1998). "Enhanced phosphorylation of p53 by ATM in response to DNA damage." Science 281(5383): 1674-1677.

Bernal, F.; A. F. Tyler; S. J. Korsmeyer; L. D. Walensky and G. L. Verdine (2007). "Reactivation of the p53 tumor suppressor pathway by a stapled p53 peptide." J Am Chem Soc 129(9): 2456-2457.

Bissantz, C.; B. Kuhn and M. Stahl (2010). "A medicinal chemist's guide to molecular interactions." J Med Chem 53(14): 5061-5084.

Bista, M.; K. Kowalska; W. Janczyk; A. Domling and T. A. Holak (2009). "Robust NMR screening for lead compounds using tryptophan-containing proteins." J Am Chem Soc 131(22): 7500-7501.

Boettcher, A.; N. Buschmann; P. Furet; J. M. Groell; J. Kallen; J. Hergovich Lisztwan; K. Masuya; L. Mayr and A. Vaupel (2008). 3-imidazolyl-indoles for the treatment of proliferative diseases. WO.

Böhm, H.-J.; D. Banner; S. Bendels; M. Kansy; B. Kuhn; K. Müller; U. Obst-Sander and M. Stahl (2004). "Fluorine in Medicinal Chemistry." ChemBioChem 5(5): 637-643.

Bottger, V.; A. Bottger; C. Garcia-Echeverria; Y. F. Ramos; A. J. van der Eb; A. G. Jochemsen and D. P. Lane (1999). "Comparative study of the p53-mdm2 and p53-MDMX interfaces." Oncogene 18(1): 189-199.

Boyd, S. D.; K. Y. Tsai and T. Jacks (2000). "An intact HDM2 RING-finger domain is required for nuclear exclusion of p53." Nat Cell Biol 2(9): 563-568.

Braithwaite, A. W.; G. Del Sal and X. Lu (2006). "Some p53-binding proteins that can function as arbiters of life and death." Cell Death Differ 13(6): 984-993.

Burns, T. F. and W. S. El-Deiry (1999). "The p53 pathway and apoptosis." J Cell Physiol 181(2): 231-239.

Cai, L.; S. Lu and V. W. Pike (2008). "Chemistry with [18F]Fluoride Ion." European Journal of Organic Chemistry 2008(17): 2853-2873.

Canman, C. E. and D. S. Lim (1998). "The role of ATM in DNA damage responses and cancer." Oncogene 17(25): 3301-3308.

Chehab, N. H.; A. Malikzay; M. Appel and T. D. Halazonetis (2000). "Chk2/hCds1 functions as a DNA damage checkpoint in G(1) by stabilizing p53." Genes Dev 14(3): 278-288.

Cheok, C. F.; C. S. Verma; J. Baselga and D. P. Lane (2011). "Translating p53 into the clinic." Nat Rev Clin Oncol 8(1): 25-37.

Czarna, A.; B. Beck; S. Srivastava; G. M. Popowicz; S. Wolf; Y. Huang; M. Bista; T. A. Holak and A. Domling (2010). "Robust generation of lead compounds for protein-protein interactions by computational and MCR chemistry: p53/Hdm2 antagonists." Angew Chem Int Ed Engl 49(31): 5352-5356.

Czarna, A.; G. M. Popowicz; A. Pecak; S. Wolf; G. Dubin and T. A. Holak (2009). "High affinity interaction of the p53 peptide-analogue with human Mdm2 and Mdmx." Cell Cycle 8(8): 1176-1184.

D'Silva, L.; P. Ozdowy; M. Krajewski; U. Rothweiler; M. Singh and T. A. Holak (2005a). "Monitoring the effects of antagonists on protein-protein interactions with NMR spectroscopy." J Am Chem Soc 127(38): 13220-13226.

D'Silva, L.; P. Ozdowy; M. Krajewski; U. Rothweiler; M. Singh and T. A. Holak (2005b). "Monitoring the effects of antagonists on protein-protein interactions with NMR spectroscopy." Journal of the American Chemical Society 127(38): 13220-13226.

Dawson, R.; L. Muller; A. Dehner; C. Klein; H. Kessler and J. Buchner (2003). "The N-terminal domain of p53 is natively unfolded." J Mol Biol 332(5): 1131-1141.

Dömling, A. (2008). "Small molecular weight protein-protein interaction antagonists--an insurmountable challenge?" Current Opinion in Chemical Biology 12(3): 281-291.

Domling, A. and K. Khoury (2010). "Praziquantel and schistosomiasis." ChemMedChem 5(9): 1420-1434.

el-Deiry, W. S.; S. E. Kern; J. A. Pietenpol; K. W. Kinzler and B. Vogelstein (1992). "Definition of a consensus binding site for p53." Nat Genet 1(1): 45-49.

el-Deiry, W. S.; T. Tokino; V. E. Velculescu; D. B. Levy; R. Parsons; J. M. Trent; D. Lin; W. E. Mercer; K. W. Kinzler and B. Vogelstein (1993). "WAF1, a potential mediator of p53 tumor suppression." Cell 75(4): 817-825.

Fang, S.; J. P. Jensen; R. L. Ludwig; K. H. Vousden and A. M. Weissman (2000). "Mdm2 is a RING finger-dependent ubiquitin protein ligase for itself and p53." J Biol Chem 275(12): 8945-8951.

Ferreira, M. E.; S. Hermann; P. Prochasson; J. L. Workman; K. D. Berndt and A. P. Wright (2005). "Mechanism of transcription factor recruitment by acidic activators." J Biol Chem 280(23): 21779-21784.

Fersht, A. R. (1998). Structure and Mechanism in Protein Science: A Guide to Enzyme Catalysis and Protein Folding, W. H. Freeman.

Fields, S. and S. K. Jang (1990). "Presence of a potent transcription activating sequence in the p53 protein." Science 249(4972): 1046-1049.

Francoz, S.; P. Froment; S. Bogaerts; S. De Clercq; M. Maetens; G. Doumont; E. Bellefroid and J. C. Marine (2006). "Mdm4 and Mdm2 cooperate to inhibit p53 activity in proliferating and quiescent cells in vivo." Proc Natl Acad Sci U S A 103(9): 3232-3237.

Fry, D. C.; S. D. Emerson; S. Palme; B. T. Vu; C. M. Liu and F. Podlaski (2004). "NMR structure of a complex between MDM2 and a small molecule inhibitor." J Biomol NMR 30(2): 163-173.

Fry, D. C. and L. T. Vassilev (2005). "Targeting protein-protein interactions for cancer therapy." J Mol Med (Berl) 83(12): 955-963.

Garcia-Echeverria, C.; P. Chene; M. J. Blommers and P. Furet (2000). "Discovery of potent antagonists of the interaction between human double minute 2 and tumor suppressor p53." J Med Chem 43(17): 3205-3208.

Geyer, R. K.; Z. K. Yu and C. G. Maki (2000). "The MDM2 RING-finger domain is required to promote p53 nuclear export." Nat Cell Biol 2(9): 569-573.

Grasberger, B. L.; T. Lu; C. Schubert; D. J. Parks; T. E. Carver; H. K. Koblish; M. D. Cummings; L. V. LaFrance; K. L. Milkiewicz; R. R. Calvo; D. Maguire; J. Lattanze; C. F. Franks; S. Zhao; K. Ramachandren; G. R. Bylebyl; M. Zhang; C. L. Manthey; E. C. Petrella; M. W. Pantoliano; I. C. Deckman; J. C. Spurlino; A. C. Maroney; B. E. Tomczuk; C. J. Molloy and R. F. Bone (2005). "Discovery and cocrystal structure of benzodiazepinedione HDM2 antagonists that activate p53 in cells." J Med Chem 48(4): 909-912.

Hagmann, W. K. (2008). "The Many Roles for Fluorine in Medicinal Chemistry." Journal of Medicinal Chemistry 51(15): 4359-4369.

Hall-Jackson, C. A.; D. A. Cross; N. Morrice and C. Smythe (1999). "ATR is a caffeine-sensitive, DNA-activated protein kinase with a substrate specificity distinct from DNA-PK." Oncogene 18(48): 6707-6713.

Hartwell, L. H. and T. A. Weinert (1989). "Checkpoints: controls that ensure the order of cell cycle events." Science 246(4930): 629-634.

Haupt, Y.; R. Maya; A. Kazaz and M. Oren (1997). "Mdm2 promotes the rapid degradation of p53." Nature 387(6630): 296-299.

Hendlich, M.; A. Bergner; J. Gunther and G. Klebe (2003). "Relibase: design and development of a database for comprehensive analysis of protein-ligand interactions." J Mol Biol 326(2): 607-620.

Hirao, A.; Y. Y. Kong; S. Matsuoka; A. Wakeham; J. Ruland; H. Yoshida; D. Liu; S. J. Elledge and T. W. Mak (2000). "DNA damage-induced activation of p53 by the checkpoint kinase Chk2." Science 287(5459): 1824-1827.

Honda, R.; H. Tanaka and H. Yasuda (1997). "Oncoprotein MDM2 is a ubiquitin ligase E3 for tumor suppressor p53." FEBS Lett 420(1): 25-27.

Honda, R. and H. Yasuda (2000). "Activity of MDM2, a ubiquitin ligase, toward p53 or itself is dependent on the RING finger domain of the ligase." Oncogene 19(11): 1473-1476.

Hu, B.; D. M. Gilkes and J. Chen (2007). "Efficient p53 activation and apoptosis by simultaneous disruption of binding to MDM2 and MDMX." Cancer Res 67(18): 8810-8817.

Huang, X. (2003). "Fluorescence polarization competition assay: the range of resolvable inhibitor potency is limited by the affinity of the fluorescent ligand." J Biomol Screen 8(1): 34-38.

Huang, Y. and A. Domling (2010). "1,4-Thienodiazepine-2,5-diones via MCR (II): scaffold hopping by Gewald and Ugi-deprotection-cyclization strategy." Chem Biol Drug Des 76(2): 130-141.

Huang, Y.; S. Wolf; D. Koes; G. M. Popowicz; C. J. Camacho; T. A. Holak and A. Domling (2011). "Exhaustive Fluorine Scanning toward Potent p53-Mdm2 Antagonists." ChemMedChem.

Jackson, M. W. and S. J. Berberich (2000). "MdmX protects p53 from Mdm2-mediated degradation." Mol Cell Biol 20(3): 1001-1007.

Joerger, A. C. and A. R. Fersht (2008). "Structural biology of the tumor suppressor p53." Annu Rev Biochem 77: 557-582.

Jones, S. N.; A. E. Roe; L. A. Donehower and A. Bradley (1995). "Rescue of embryonic lethality in Mdm2-deficient mice by absence of p53." Nature 378(6553): 206-208.

Kabsch, W. (1993). "Automatic Processing of Rotation Diffraction Data from Crystals of Initially Unknown Symmetry and Cell Constants." Journal of Applied Crystallography 26: 795-800.

Kallen, J.; A. Goepfert; A. Blechschmidt; A. Izaac; M. Geiser; G. Tavares; P. Ramage; P. Furet; K. Masuya and J. Lisztwan (2009). "Crystal Structures of Human MdmX (HdmX) in Complex with p53 Peptide Analogues Reveal Surprising Conformational Changes." J Biol Chem 284(13): 8812-8821.

Kerekes, A. D.; S. J. Esposite; R. J. Doll; J. R. Tagat; T. Yu; Y. Xiao; Y. Zhang; D. B. Prelusky; S. Tevar; K. Gray; G. A. Terracina; S. Lee; J. Jones; M. Liu; A. D. Basso and E. B. Smith (2011). "Aurora Kinase Inhibitors Based on the Imidazo[1,2-a]pyrazine Core Fluorine and Deuterium Incorporation Improve Oral Absorption and Exposure." Journal of Medicinal Chemistry 54(1): 201-210.

Kim, C. Y.; P. P. Chandra; A. Jain and D. W. Christianson (2001). "Fluoroaromatic-fluoroaromatic interactions between inhibitors bound in the crystal lattice of human carbonic anhydrase II." J Am Chem Soc 123(39): 9620-9627.

Kim, C. Y.; J. S. Chang; T. T. Baird; J. B. Doyon; C. A. Fierke; A. Jain and D. W. Christianson (2000). "Contribution of Fluorine to Protein−Ligand Affinity in the Binding of Fluoroaromatic Inhibitors to Carbonic Anhydrase II." J Am Chem Soc 122(49): 12125–12134.

Krajewski, M.; U. Rothweiler; L. D'Silva; S. Majumdar; C. Klein and T. A. Holak (2007a). "An NMR-based antagonist induced dissociation assay for targeting the ligand-protein and protein-protein interactions in competition binding experiments." J Med Chem 50(18): 4382-4387.

Krajewski, M.; U. Rothweiler; L. D'Silva; S. Majumdar; C. Klein and T. A. Holak (2007b). "An NMR-Based antagonist induced dissociation assay for targeting the ligand-protein and protein-protein interactions in competition binding experiments." Journal of Medicinal Chemistry 50(18): 4382-4387.

Kubbutat, M. H.; S. N. Jones and K. H. Vousden (1997). "Regulation of p53 stability by Mdm2." Nature 387(6630): 299-303.

Kussie, P. H.; S. Gorina; V. Marechal; B. Elenbaas; J. Moreau; A. J. Levine and N. P. Pavletich (1996). "Structure of the MDM2 oncoprotein bound to the p53 tumor suppressor transactivation domain." Science 274(5289): 948-953.

Lai, Z.; K. V. Ferry; M. A. Diamond; K. E. Wee; Y. B. Kim; J. Ma; T. Yang; P. A. Benfield; R. A. Copeland and K. R. Auger (2001). "Human mdm2 mediates

multiple mono-ubiquitination of p53 by a mechanism requiring enzyme isomerization." J Biol Chem 276(33): 31357-31367.

Laurie, N. A.; C. S. Shih and M. A. Dyer (2007). "Targeting MDM2 and MDMX in retinoblastoma." Curr Cancer Drug Targets 7(7): 689-695.

Le Bars, D. (2006). "Fluorine-18 and medical imaging: Radiopharmaceuticals for positron emission tomography." Journal of Fluorine Chemistry 127(11): 1488-1493.

Lee, H.; K. H. Mok; R. Muhandiram; K. H. Park; J. E. Suk; D. H. Kim; J. Chang; Y. C. Sung; K. Y. Choi and K. H. Han (2000). "Local structural elements in the mostly unstructured transcriptional activation domain of human p53." J Biol Chem 275(38): 29426-29432.

Marine, J. C.; M. A. Dyer and A. G. Jochemsen (2007). "MDMX: from bench to bedside." J Cell Sci 120(Pt 3): 371-378.

Marine, J. C. and A. G. Jochemsen (2004). "Mdmx and Mdm2: brothers in arms?" Cell Cycle 3(7): 900-904.

Marine, J. C. and A. G. Jochemsen (2005). "Mdmx as an essential regulator of p53 activity." Biochem Biophys Res Commun 331(3): 750-760.

Marugan, J. J.; K. Leonard; P. Raboisson; J. M. Gushue; R. Calvo; H. K. Koblish; J. Lattanze; S. Zhao; M. D. Cummings; M. R. Player; C. Schubert; A. C. Maroney and T. Lu (2006). "Enantiomerically pure 1,4-benzodiazepine-2,5-diones as Hdm2 antagonists." Bioorg Med Chem Lett 16(12): 3115-3120.

McRee, D. E. (2004). "Differential evolution for protein crystallographic optimizations." Acta Crystallographica Section D-Biological Crystallography 60: 2276-2279.

Meyer, E. A.; R. K. Castellano and F. Diederich (2003). "Interactions with aromatic rings in chemical and biological recognition." Angew Chem Int Ed Engl 42(11): 1210-1250.

Migliorini, D.; D. Danovi; E. Colombo; R. Carbone; P. G. Pelicci and J. C. Marine (2002). "Hdmx recruitment into the nucleus by Hdm2 is essential for its ability to regulate p53 stability and transactivation." J Biol Chem 277(9): 7318-7323.

Morgenthaler, M.; E. Schweizer; A. Hoffmann-Röder; F. Benini; R. E. Martin; G. Jaeschke; B. Wagner; H. Fischer; S. Bendels; D. Zimmerli; J. Schneider; F.

Diederich; M. Kansy and K. Müller (2007). "Predicting and Tuning Physicochemical Properties in Lead Optimization: Amine Basicities." ChemMedChem 2(8): 1100-1115.

Mori, S.; C. Abeygunawardana; M. O. Johnson and P. C. van Zijl (1995). "Improved sensitivity of HSQC spectra of exchanging protons at short interscan delays using a new fast HSQC (FHSQC) detection scheme that avoids water saturation." J Magn Reson B 108(1): 94-98.

Müller, K.; C. Faeh and F. Diederich (2007). "Fluorine in Pharmaceuticals: Looking Beyond Intuition." Science 317(5846): 1881-1886.

Nakamura, S.; J. A. Roth and T. Mukhopadhyay (2000). "Multiple lysine mutations in the C-terminal domain of p53 interfere with MDM2-dependent protein degradation and ubiquitination." Mol Cell Biol 20(24): 9391-9398.

Oliner, J. D.; J. A. Pietenpol; S. Thiagalingam; J. Gyuris; K. W. Kinzler and B. Vogelstein (1993). "Oncoprotein MDM2 conceals the activation domain of tumour suppressor p53." Nature 362(6423): 857-860.

Parant, J.; A. Chavez-Reyes; N. A. Little; W. Yan; V. Reinke; A. G. Jochemsen and G. Lozano (2001). "Rescue of embryonic lethality in Mdm4-null mice by loss of Trp53 suggests a nonoverlapping pathway with MDM2 to regulate p53." Nat Genet 29(1): 92-95.

Park, B. K.; N. R. Kitteringham and P. M. O'Neill (2001). "METABOLISM OF FLUORINE-CONTAINING DRUGS." Annual Review of Pharmacology and Toxicology 41(1): 443-470.

Paulovich, A. G.; D. P. Toczyski and L. H. Hartwell (1997). "When checkpoints fail." Cell 88(3): 315-321.

Percival, A. (1991). "Impact of chemical structure on quinolone potency, spectrum and side effects." Journal of Antimicrobial Chemotherapy 28(suppl C): 1-8.

Perrakis, A.; R. Morris and V. S. Lamzin (1999). "Automated protein model building combined with iterative structure refinement." Nat Struct Biol 6(5): 458-463.

Perry, M. E. (2010) "The Regulation of the p53-mediated Stress Response by MDM2 and MDMX". Cold Spring Harb Perspect Biol 2:a000968

Phan, J.; Z. Li; A. Kasprzak; B. Li; S. Sebti; W. Guida; E. Schonbrunn and J. Chen (2010). "Structure-based design of high affinity peptides inhibiting the interaction of p53 with MDM2 and MDMX." J Biol Chem 285(3): 2174-2183.

Pietenpol, J. A.; T. Tokino; S. Thiagalingam; W. S. el-Deiry; K. W. Kinzler and B. Vogelstein (1994). "Sequence-specific transcriptional activation is essential for growth suppression by p53." Proc Natl Acad Sci U S A 91(6): 1998-2002.

Piotto, M.; V. Saudek and V. Sklenar (1992). "Gradient-tailored excitation for single-quantum NMR spectroscopy of aqueous solutions." J Biomol NMR 2(6): 661-665.

Popowicz, G.; A. Czarna and T. Holak (2008). "Structure of the human Mdmx protein bound to the p53 tumor suppressor transactivation domain." Cell Cycle 7(15): 2441-2443.

Popowicz, G. M.; A. Czarna and T. A. Holak (2008). "Structure of the human Mdmx protein bound to the p53 tumor suppressor transactivation domain." Cell Cycle 7(15): 2441-2443.

Popowicz, G. M.; A. Czarna; S. Wolf; K. Wang; W. Wang; A. Domling and T. A. Holak (2010a). "Structures of low molecular weight inhibitors bound to MDMX and MDM2 reveal new approaches for p53-MDMX/MDM2 antagonist drug discovery." Cell Cycle 9(6): 1104-1111.

Popowicz, G. M.; A. Czarna; S. Wolf; K. Wang; W. Wang; A. Dömling and T. A. Holak (2010b). "Structures of low molecular weight inhibitors bound to MDMX and MDM2 reveal new approaches for p53-MDMX/MDM2 antagonist drug discovery." Cell Cycle 9(6): 1104-1111.

Popowicz, G. M.; A. Domling and T. A. Holak (2011). "The structure-based design of Mdm2/Mdmx-p53 inhibitors gets serious." Angew Chem Int Ed Engl 50(12): 2680-2688.

Purser, S.; P. R. Moore; S. Swallow and V. Gouverneur (2008). "Fluorine in medicinal chemistry." Chemical Society Reviews 37(2): 320-330.

Rehm, T.; R. Huber and T. A. Holak (2002). "Application of NMR in structural proteomics: screening for proteins amenable to structural analysis." Structure 10(12): 1613-1618.

Rodriguez, M. S.; J. M. Desterro; S. Lain; D. P. Lane and R. T. Hay (2000). "Multiple C-terminal lysine residues target p53 for ubiquitin-proteasome-mediated degradation." Mol Cell Biol 20(22): 8458-8467.

Roth, J.; M. Dobbelstein; D. A. Freedman; T. Shenk and A. J. Levine (1998). "Nucleo-cytoplasmic shuttling of the hdm2 oncoprotein regulates the levels of

the p53 protein via a pathway used by the human immunodeficiency virus rev protein." EMBO J 17(2): 554-564.

Rothweiler, U.; A. Czarna; L. Weber; G. M. Popowicz; K. Brongel; K. Kowalska; M. Orth; O. Stemmann and T. A. Holak (2008). "NMR screening for lead compounds using tryptophan-mutated proteins." Journal of Medicinal Chemistry 51(16): 5035-5042.

Sablina, A. A.; A. V. Budanov; G. V. Ilyinskaya; L. S. Agapova; J. E. Kravchenko and P. M. Chumakov (2005). "The antioxidant function of the p53 tumor suppressor." Nat Med 11(12): 1306-1313.

Salonen, L. M.; M. Ellermann and F. Diederich (2011). "Aromatic rings in chemical and biological recognition: energetics and structures." Angew Chem Int Ed Engl 50(21): 4808-4842.

Schon, O.; A. Friedler; M. Bycroft; S. M. Freund and A. R. Fersht (2002). "Molecular mechanism of the interaction between MDM2 and p53." J Mol Biol 323(3): 491-501.

Shangary, S. and S. Wang (2009). "Small-molecule inhibitors of the MDM2-p53 protein-protein interaction to reactivate p53 function: a novel approach for cancer therapy." Annu Rev Pharmacol Toxicol 49: 223-241.

Sharp, D. A.; S. A. Kratowicz; M. J. Sank and D. L. George (1999). "Stabilization of the MDM2 oncoprotein by interaction with the structurally related MDMX protein." J Biol Chem 274(53): 38189-38196.

Shieh, S. Y.; J. Ahn; K. Tamai; Y. Taya and C. Prives (2000). "The human homologs of checkpoint kinases Chk1 and Cds1 (Chk2) phosphorylate p53 at multiple DNA damage-inducible sites." Genes Dev 14(3): 289-300.

Shvarts, A.; W. T. Steegenga; N. Riteco; T. van Laar; P. Dekker; M. Bazuine; R. C. van Ham; W. van der Houven van Oordt; G. Hateboer; A. J. van der Eb and A. G. Jochemsen (1996). "MDMX: a novel p53-binding protein with some functional properties of MDM2." EMBO J 15(19): 5349-5357.

Srivastava, S.; B. Beck; W. Wang; A. Czarna; T. A. Holak and A. Domling (2009). "Rapid and efficient hydrophilicity tuning of p53/mdm2 antagonists." J Comb Chem 11(4): 631-639.

Stad, R.; N. A. Little; D. P. Xirodimas; R. Frenk; A. J. van der Eb; D. P. Lane; M. K. Saville and A. G. Jochemsen (2001). "Mdmx stabilizes p53 and Mdm2 via two distinct mechanisms." EMBO Rep 2(11): 1029-1034.

Stad, R.; Y. F. Ramos; N. Little; S. Grivell; J. Attema; A. J. van Der Eb and A. G. Jochemsen (2000). "Hdmx stabilizes Mdm2 and p53." J Biol Chem 275(36): 28039-28044.

Stoll, R.; C. Renner; S. Hansen; S. Palme; C. Klein; A. Belling; W. Zeslawski; M. Kamionka; T. Rehm; P. Muhlhahn; R. Schumacher; F. Hesse; B. Kaluza; W. Voelter; R. A. Engh and T. A. Holak (2001). "Chalcone derivatives antagonize interactions between the human oncoprotein MDM2 and p53." Biochemistry 40(2): 336-344.

Stommel, J. M.; N. D. Marchenko; G. S. Jimenez; U. M. Moll; T. J. Hope and G. M. Wahl (1999). "A leucine-rich nuclear export signal in the p53 tetramerization domain: regulation of subcellular localization and p53 activity by NES masking." EMBO J 18(6): 1660-1672.

Sturzbecher, H. W.; R. Brain; C. Addison; K. Rudge; M. Remm; M. Grimaldi; E. Keenan and J. R. Jenkins (1992). "A C-terminal alpha-helix plus basic region motif is the major structural determinant of p53 tetramerization." Oncogene 7(8): 1513-1523.

Su, H.; Y. Xie; W.-B. Liu and S.-L. You (2011). "Methyl-monofluorination of ibuprofen selectively increases its inhibitory activity toward cyclooxygenase-1 leading to enhanced analgesic activity and reduced gastric damage in vivo." Bioorganic & Medicinal Chemistry Letters 21(12): 3578-3582.

Sur, S.; R. Pagliarini; F. Bunz; C. Rago; L. A. Diaz, Jr.; K. W. Kinzler; B. Vogelstein and N. Papadopoulos (2009). "A panel of isogenic human cancer cells suggests a therapeutic approach for cancers with inactivated p53." Proc Natl Acad Sci U S A 106(10): 3964-3969.

Tanimura, S.; S. Ohtsuka; K. Mitsui; K. Shirouzu; A. Yoshimura and M. Ohtsubo (1999). "MDM2 interacts with MDMX through their RING finger domains." FEBS Lett 447(1): 5-9.

Tao, W. and A. J. Levine (1999). "Nucleocytoplasmic shuttling of oncoprotein Hdm2 is required for Hdm2-mediated degradation of p53." Proc Natl Acad Sci U S A 96(6): 3077-3080.

Thrower, J. S.; L. Hoffman; M. Rechsteiner and C. M. Pickart (2000). "Recognition of the polyubiquitin proteolytic signal." EMBO J 19(1): 94-102.

Tibbetts, R. S.; K. M. Brumbaugh; J. M. Williams; J. N. Sarkaria; W. A. Cliby; S. Y. Shieh; Y. Taya; C. Prives and R. T. Abraham (1999). "A role for ATR in the DNA damage-induced phosphorylation of p53." Genes Dev 13(2): 152-157.

Tokalov, S. V. and N. D. Abolmaali (2010). "Protection of p53 wild type cells from taxol by Nutlin-3 in the combined lung cancer treatment." BMC Cancer 10: 57.

Toledo, F.; C. J. Lee; K. A. Krummel; L. W. Rodewald; C. W. Liu and G. M. Wahl (2007a). "Mouse mutants reveal that putative protein interaction sites in the p53 proline-rich domain are dispensable for tumor suppression." Mol Cell Biol 27(4): 1425-1432.

Toledo, F. and G. M. Wahl (2006). "Regulating the p53 pathway: in vitro hypotheses, in vivo veritas." Nat Rev Cancer 6(12): 909-923.

Toledo, F. and G. M. Wahl (2007b). "MDM2 and MDM4: p53 regulators as targets in anticancer therapy." Int J Biochem Cell Biol 39(7-8): 1476-1482.

Vassilev, L. T. (2007). "MDM2 inhibitors for cancer therapy." Trends Mol Med 13(1): 23-31.

Vassilev, L. T.; B. T. Vu; B. Graves; D. Carvajal; F. Podlaski; Z. Filipovic; N. Kong; U. Kammlott; C. Lukacs; C. Klein; N. Fotouhi and E. A. Liu (2004). "In vivo activation of the p53 pathway by small-molecule antagonists of MDM2." Science 303(5659): 844-848.

Venot, C.; M. Maratrat; C. Dureuil; E. Conseiller; L. Bracco and L. Debussche (1998). "The requirement for the p53 proline-rich functional domain for mediation of apoptosis is correlated with specific PIG3 gene transactivation and with transcriptional repression." EMBO J 17(16): 4668-4679.

Waga, S.; G. J. Hannon; D. Beach and B. Stillman (1994). "The p21 inhibitor of cyclin-dependent kinases controls DNA replication by interaction with PCNA." Nature 369(6481): 574-578.

Waga, S. and B. Stillman (1998). "Cyclin-dependent kinase inhibitor p21 modulates the DNA primer-template recognition complex." Mol Cell Biol 18(7): 4177-4187.

Walker, K. K. and A. J. Levine (1996). "Identification of a novel p53 functional domain that is necessary for efficient growth suppression." Proc Natl Acad Sci U S A 93(26): 15335-15340.

Wang, L.; G. He; P. Zhang; X. Wang; M. Jiang and L. Yu (2011). "Interplay between MDM2, MDMX, Pirh2 and COP1: the negative regulators of p53." Mol Biol Rep 38(1): 229-236.

Wang, Z. X. (1995). "An exact mathematical expression for describing competitive binding of two different ligands to a protein molecule." FEBS Lett 360(2): 111-114.

Warren, G. L.; C. W. Andrews; A. M. Capelli; B. Clarke; J. LaLonde; M. H. Lambert; M. Lindvall; N. Nevins; S. F. Semus; S. Senger; G. Tedesco; I. D. Wall; J. M. Woolven; C. E. Peishoff and M. S. Head (2006). "A critical assessment of docking programs and scoring functions." J Med Chem 49(20): 5912-5931.

Wells, J. A. and C. L. McClendon (2007). "Reaching for high-hanging fruit in drug discovery at protein-protein interfaces." Nature 450(7172): 1001-1009.

Wells, M.; H. Tidow; T. J. Rutherford; P. Markwick; M. R. Jensen; E. Mylonas; D. I. Svergun; M. Blackledge and A. R. Fersht (2008). "Structure of tumor suppressor p53 and its intrinsically disordered N-terminal transactivation domain." Proc Natl Acad Sci U S A 105(15): 5762-5767.

Wlodek, S.; A. G. Skillman and A. J. Nicholls (2010). "Ligand Entropy in Gas-Phase, Upon Solvation and Protein Complexation. Fast Estimation with Quasi-Newton Hessian." J Chem Theory Comput 6(7): 2140–2152.

Wolf, S.; Y. Huang; G. M. Popowicz; S. Goda; T. A. Holak and A. Dömling. "Ugi Multicomponent Reaction Derived p53-Mdm2 Antagonists" in preparation

Wüthrich, K. (1986). NMR of proteins and nucleic acids. New York, Wiley.

Xiong, Y. (1996). "Why are there so many CDK inhibitors?" Biochim Biophys Acta 1288(1): 01-05.

Yanamala, N.; A. Dutta; B. Beck; B. Van Fleet; K. Hay; A. Yazbak; R. Ishima; A. Doemling and J. Klein-Seetharaman (2010). "NMR-Based Screening of Membrane Protein Ligands." Chemical Biology & Drug Design 75(3): 237-256.

Zheng, T.; J. Wang; X. Song; X. Meng; S. Pan; H. Jiang and L. Liu (2010). "Nutlin-3 cooperates with doxorubicin to induce apoptosis of human hepatocellular carcinoma cells through p53 or p73 signaling pathways." J Cancer Res Clin Oncol 136(10): 1597-1604.

Zondlo, S. C.; A. E. Lee and N. J. Zondlo (2006). "Determinants of specificity of MDM2 for the activation domains of p53 and p65: proline27 disrupts the MDM2-binding motif of p53." Biochemistry 45(39): 11945-11957.